Ministry of Higher Education and Scientific Research

وزارة التعليم العالي والبحث العلمي

University Badji Mokhtar – Annaba
Faculty of Sciences

Departement of chemistry

جامعة باجي مختار – عنابـــة

كـلـيـة العلوم

قســـم االكيمياء

Thesis

Submitted to obtain the diploma of

PhD In-Sciences

Speciality : Organic Chemistry

Par :

MESSAADIA Sabir

Title :

Modélisation moléculaire de l'influence de la polarité et de la nature électronique des substituants sur la réactivité et le mécanisme des réactions organiques

Composition of the jury :

N°	Name	Grade	Establishment	Quality
01	**Noureddine Dadda**	MCA	University Badji Mokhtar -Annaba	President
02	**Abdelmalek Khorief Nacereddine**	Prof	ENSET Skikda	Supervisor
03	**Abdelhafid Djerourou**	Prof	University Badji Mokhtar -Annaba	Co-supervisor
04	**Hacene Bendjeffal**	Prof	ENSET Skikda	Examinator
05	**Fouad Chafaa**	MCA	University of Batna 2	Examinator
06	**Mourad Boukachabia**	MCA	University Badji Mokhtar -Annaba	Examinator

Dedication

To my dearest parents: Father and Mother

To my wife

To my dear brothers and sisters

To all my friends and colleagues

Acknowledgements

This work was carried out in the Laboratory of Synthesis and Organic Biocatalysis (LSBO) at Badji Mokhtar University Annaba-Algeria.

First of all, I would like to thank Pr. KHORIEF NACEREDDINE Abdelmalek, Thank you for monitoring and supporting me during these years. Thank you for your great availability, for your encouragement and for your kindness and wise advice.

It was a real and immense pleasure to work alongside you.

All my thanks also go to Pr. DJEROUROU Abdelhafid who co-supervised this thesis. Thank you for your great availability, for your encouragement and for your assistance in LSBO.

My sincere thanks also go to Professor Noureddine Dada for having done me the honor of presiding over my thesis jury.

I express my humble thanks to all the members of my thesis jury: *Pr. Hacene Bendjeffal, Dr. Fouad Chafaa and Dr. Mourad Boukachabia.*

Abstract

Exploration des facteurs contrôlant le mécanisme et la stéréosélectivité élevée de la réaction de cycloaddition polaire [3+2] de l'azométhine imine N, N'-cyclique avec le 3-nitro-2-phényl-2H chromène. Une étude de la théorie de la densité électronique moléculaire

Abstract:

In this work we performed a computational investigation based on molecular electron density theory study of the [3+2] cycloaddition reaction of 5-oxo-2-(phenylmethylidene)pyrazolidin-2-ium-1-ide, a simple azomethine imine, with 3-nitro-2-phenyl-2H-chromene at the B3LYP/6-311G(d,p) computational level in order to find out the origin of the stereoselectivity experimentally observed. Analysis of reagents with electron localization function foresees a polar process; the energy profiles of the possible reactive pathways in gas phase and in solution of isopropanol confirm the high exo stereoselectivity and the complete ortho regioselectivity of the reaction experimentally observed. study of the most preferred pathway using some quantum chemistry tools such as quantum theory of atoms in molecules and the independent gradient model based on Hirshfeld distribution shows that the existance of several hydrogen bonds and van der Waals intermolecular noncovalent interactions are the factors favoring the ortho-exo selectivity. The bonding evolution theory study of the most favorable pathway reveals a two-stage one-step molecular mechanism.

Keywords: regioselectivity, stereoselectivity, azomethine imine, chromenes, [3+2] cycloaddition reaction, DFT, MEDT, regioselectivity, stereoselectivity

Modélisation moléculaire de l'influence de la polarité et de la nature électronique des substituants sur la réactivité et le mécanisme des réactions organiques

Resumé:

Dans ce travail, une étude de la théorie de la densité électronique moléculaire de la réaction de cycloaddition [3+2] de la 5-oxo-2-(phénylméthylidène)pyrazolidin-2-ium-1-ide, une simple azométhine imine, avec le 3-nitro-2-phényl-2H-chromène a été réalisée au niveau theorique B3LYP/6-311G(d,p) afin d'explorer l'origine de la stéréosélectivité observée expérimentalement. Alors que l'analyse ELF de l'analyse et l'analyse de la population naturelle s'attendent à un processus polaire entre les réactifs ; les profils énergétiques des voies réactives possibles en phase gazeuse et en solvant indiquent une exo stéréosélectivité élevée et une ortho régiosélectivité complète de la réaction en excellent accord avec les résultats expérimentaux. L'analyse de la voie la plus favorisée à l'aide de la théorie quantique des atomes dans les molécules et d'un modèle de gradient indépendant basé sur la distribution de Hirshfeld indique que la présence de plusieurs liaisons hydrogène et les interactions intermoléculaires non covalentes de van der Waals sont les facteurs favorisant la sélectivité ortho-exo. L'étude de la théorie de l'évolution des liaisons de la voie la plus favorable révèle un mécanisme moléculaire en deux étapes en une étape.

Mot clé : azométhine imine, chromènes, réaction de cycloaddition [3+2], DFT, théorie de la densité électronique moléculaire, régiosélectivité, stéréosélectivité.

محاكاة جزيئية لتأثير القطبية والطبيعة الإلكترونية للجذور على التفاعلية الكيميائية وآليات تفاعل المركبات العضوية

ملخص:

في هذا العمل، تم إجراء دراسة نظرية حسب كثافة الإلكترون الجزيئية لـ [3+2] تفاعل الإضافة الحلقية لـ 5-أوكسو-2-(فينيل ميثيليدين) بيرازوليدين-2-إيوم-1-بيئة تطوير متكاملة ، أزوميثين إيمين بسيط ، مع 3-نيترو-2-فينيل-2 ح-كرومين على ((B3LYP/6-311G(d,p) المستوى الحسابي من أجل استكشاف أصل الانتقائية التي تمت ملاحظتها تجريبيا. بينما يتوقع تحليل دالة تموضع الإلكترون عملية قطبية بين الكواشف; تشير ملامح الطاقة للمسارات التفاعلية المحتملة في الطور الغازي وفي محلول الأيزوبروبانول إلى انتقائية exo عالية وانتقائية ortho كاملة للتفاعل باتفاق ممتاز مع النتائج التجريبية. يشير تحليل المسار المفضل باستخدام نظرية الكم للذرات في الجزيئات، ونموذج التدرج المستقل القائم على توزيع هيرشفيلد إلى أن وجود العديد من الروابط الهيدروجينية والتفاعلات غير الاساسية بين الجزيئات هي العوامل المسؤولة عن الانتقائية. تكشف دراسة نظرية تطور الترابط للمسار المفضل عن آلية جزيئية من مرحلتين من خطوة واحد.

الكلمات المفتاحية: أزوميثين إيمين ، كروميتيس ، [3+2] تفاعل إضافة حلقي, نظرية الكثافة الوظيفية, نظرية كثافة الإلكترون الجزيئي,الانتقائية, الانتقائية الفراغية

Table of Contents

List of Figures

List of Schemes

List of Tables

List of Abbreviations

CA	Cyclo addition
DA	Diels-Alder
TAC	Three atom components
EWG	Electron withdrawing group
ERG	Electron releasing group
VBT	Valence bond theory
FMO	Frontier molecular orbital
HOMO	Highest occupied molecular orbital
LUMO	Lowest unoccupied molecular orbital
MO	Molecular orbital
NED	Normal electron demand
IED	Inversed electron demand
TST	Transition state theory
TS	Transition State
QC	Quantum chemistry
MNDO	Modified neglect of diatomic overlap
MSCF	Multi configuration self-consistent field
CI	Configuration interaction
B3LYP	Becke, 3-parameter, lee–yang–parr
MEDT	Molecular electron density theory
AIM	Atom in molecule
ELF	Electron localization function
CT	Catastroph theory
GS	Ground state
QTAIM	Quantum Theory of Atoms in Molecules
NCI	Non-Covalentes Interactions
DNA	Deoxyribonucleic acid
RNA	Rebonucleic acid
DFT	Density Functional Theory
LDA	Local density approximation
LSDA	Local spin density approximation
GGA	Generalized Gradient Approximation
HF	Hatree-Fock
SCRF	model (Self Consistent Reaction Field)
PCM	Polarizable Continuum Model
CDFT	Conceptual Density Theory
BCP	Bond Critical Point
RCP	Ring Critical Point
RDG	Reduced density gradient
IGMH	Independent gradient model Hirshfeld

ASD	Atomic Spin Density
GEDT	Global Electron Density Transfer
IBSIW	internal bond strength index for weak interactions
IRC	Intrinsic Reaction Coordinate

General Introduction

Computational chemistry, alternatively sometimes called theoretical chemistry or molecular modelling is the field where quantum mechanics is used to explain phenomena associated to chemical structures and reactions.

Historically; the application of quantum mechanics to organic chemistry dates back to1930. Approximate quantum mechanical treatments for organic molecules continued throughout the 1950s and 1960s [1]. Uses of ab initio approaches, such as Hartree–Fock theory [2], started in earnest in the 1970s and really bloomed in the mid-1980's, with the development of computer codes that allowed for automated optimization of ground and transition states and incorporation of electron correlation using configuration interaction or perturbation techniques. [3],[4]

This success combination between computers and theoretical models can be seen by the number of the paper published at this period of time; which showed to computational chemist the importance of the using theoretical models to explain chemical properties of some structures. After the development of the computing capabilities of computers in the last decades; the number of theoretical papers published in increased dramatically with the appearance of new theoretical model and soft wares explaining the experimental findings not only of simple systems but also for macro molecules such as proteins and other biological systems.

The study of reactions from the point of view of their mechanism and the relationship between structure and reactivity has always been at the core of this field and has taken advantage of this progress in computational tools, which allowed the development of different theoretical models and theories used successfully to get information and understand the chemical structures and reactions never been achievable by normal experimental procedures such us reactive centers of molecules, transition state structures...

Studying chemical reactions requires accurate quantification of energies and deep understanding of chemical bonding patterns; to this end we chose the density functional theory (DFT)[5] for its accuracy results and reasonable computing time to join theoretical calculations and experimental findings in order to explain and clarify the regioselectivity and the stereoselectivity of cycloaddition reactions; a reaction extensively theoretically studied and reported in literature.

In this work we report a theoretical investigation on the stereoselectivity of the (3+2) cycloaddition reaction between 3-nitro-2-phenyl-2H-chromene and 5-oxo-2-(phenylmethylidene)pyrazolidin-2-ium-1-ide reported by Alexey and coworkers in 2017 [6].

This manuscript is divided on two parties

Part 1: includes three chapters:

- Bibliographic research about cycloaddition reactions and pyrazols/N,N-bicyclic pyrazolidinones derivatives.
- Density functional theory [7].
- Descriptions the different theories used to study the reactivity and selectivity of cycloaddition reactions namely, the frontier molecular orbitals theory[8], transition state theory [9] and conceptual density functional theory.

Part 2: in this part we introduce the results theoretical results explaining the regioselectivity and the factors controlling the stereoselectivity of the 32 CA reaction between N,N'cyclic azomethine imine with a 3-nitro-2-phenyl-2H-chromene within molecular electron density theory perspective.

References

[1] J. D. Bolcer and R. B. Hermann, “The Development of Computational Chemistry in the United States,” in *Reviews in Computational Chemistry*, 1994, pp. 1–63.

[2] E. H. Lieb and B. Simon, “The Hartree-Fock theory for coulomb systems,” *Commun. Math. Phys.*, vol. 53, no. 3, pp. 185–194, 1977.

[3] E. Hückel, “Grundzüge der Theorie ungesättigter und aromatischer Verbindungen,” *Zeitschrift für Elektrochemie und Angew. Phys. Chemie*, vol. 43, no. 9, pp. 752–788, 1937.

[4] E. Hückel, “Quantentheoretische Beiträge zum Problem der aromatischen und ungesättigten Verbindungen. III,” *Zeitschrift für Phys.*, vol. 76, no. 9, pp. 628–648, 1932.

[5] W. Kohn, A. D. Becke, and R. G. Parr, “Density Functional Theory of Electronic Structure,” *J. Phys. Chem.*, vol. 100, no. 31, pp. 12974–12980, Jan. 1996, doi: 10.1021/jp960669l.

[6] A. Y. Barkov, N. S. Zimnitskiy, I. B. Kutyashev, V. Y. Korotaev, and V. Y. Sosnovskikh, “Highly stereoselective [3+2]-cycloaddition reaction of stabilised N,N′-cyclic azomethine imines with 3-nitro-2-phenyl-2H-chromenes: Synthesis of tetrahydrochromeno[4,3-c]pyrazolo[1,2-a]pyrazol-11-ones,” *Tetrahedron Lett.*, vol. 58, no. 42, 2017, doi: 10.1016/j.tetlet.2017.09.015.

[7] R. S. Mulliken, “Spectroscopy, molecular orbitals, and chemical bonding,” *Science (80-.).*, vol. 157, no. 3784, pp. 13–24, 1967.

[8] K. N. Houk, “Frontier molecular orbital theory of cycloaddition reactions,” *Acc. Chem. Res.*, vol. 8, no. 11, pp. 361–369, 1975.

[9] P. Pechukas, “Transition state theory,” *Annu. Rev. Phys. Chem.*, vol. 32, no. 1, pp. 159–177, 1981.

Chapter 1: [3+2] cycloaddition reactions

1.1 Introduction

In organic synthesis; cycloaddition reactions are considered among the most powerful and elegant ways to form bonds in a single step along with the capability of generating several stereogenic centres at the accurate prediction of stereo chemical outcomes [1].

Cycloaddition describes the union of two independent π systems through a concerted process involving a cyclic movement of electrons and resulting in the formation of new ring.

A cycloaddition reaction is categorized as a [m+n] cycloaddition when a system of m conjugated atoms combines with a system of n conjugated atoms to form a new ring. These reactions are classified according to the number of π electrons involved in each reacting molecules. The major classes are [π2+π2], [π4+π2], [π6+π2], [π8+π2], and [π6+π4]. These are simply known as [2+2], [4+2], [3+2], [6+2], [8+2], and [6+4]-cycloaddition reactions and are illustrated in the scheme below.

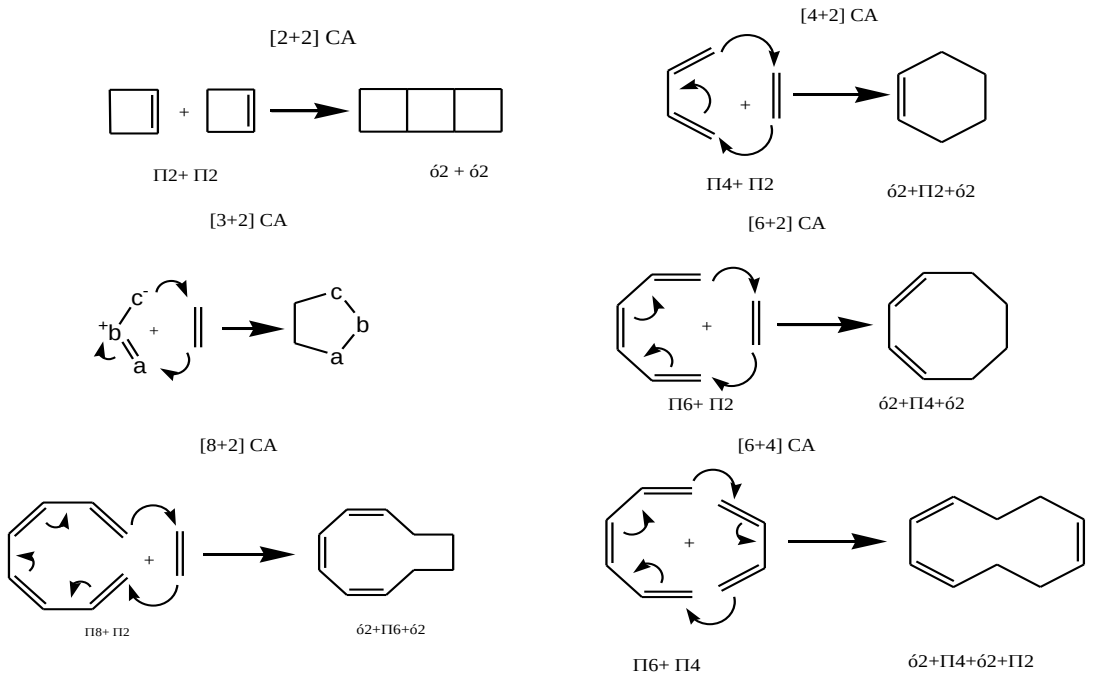

Scheme 1-1: different types of cycloaddition reactions

In this chapter we focus only at [3+2] cycloaddition reactions and its characteristics in organic synthesis.

1.2 1, 3-dipolar cycloaddition reactions (32CA)

[3+2] reactions, is a form of cycloaddition reactions consists of the reaction between a compound presenting an unsaturation called dipolarophile with to a three-atom component (TAC), i.e. an a-b-c compounds representing zwitterionic species whose core framework is constituted by three continued heavy nuclei sharing an electron density of at least 4 e; During this process, two σ bonds are formed by involving four electrons from the dipole and two π electrons from the dipolarophile. [2]–[4]

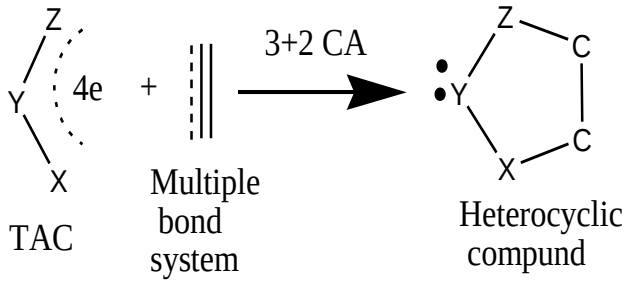

Scheme 1-2: Construction of five-membered heterocyclic compounds by 32CA reaction

1.3 History

The reaction was initially reported in the first time 1883 by Curtius [4]; five years later Büchner reported the reaction of the diazo acetic ester with the α,β-unsaturated esters; it was considered as the birth of 1,3 dipolar cycloaddition reactions [5]. After five years he suggested that the 1-pyrazoline is produced by rearrangement of and 1-pyrazoline and 2-pyrazoline resulting from reaction of methyl diazoacetate with methyl acrylate[6]. Five years later i.e. in 1898 Beckmann discovered nitrones and nitrile oxides. Diels Alder reactions were discovered in 1928 [7] giving to organic chemistry community new synthetic way to produce six membered heterocycle compounds in stereoselective and enantioselective manner.

Despite, the 32CA reactions did not receive considerable attention as Diels Alder reactions on its the first decade; they mark a continuous evolution over last 70 years specially since 1961 after the systematic works of Huisgen [8] who knew after that as that father of 32CA reaction for the efforts he made with his coworkers for the development of this reactions. Meantime Woodward and Hoffman established the new concept of conservation of orbital symmetry [9] [10] making a significant idea for the comprehension of the mechanism of cycloaddition reactions. It is the principle that hook used to predict the regeoselectivity of 32Ca reactions [11],[12].

1.4 1.3 dipoles

1,3 dipoles are chemical compounds containing 4 electrons delocalized on three atoms a-b-c (see scheme 1), for this reason they are called also three atom components (TAC);They are able to react with compounds containing conjugated systems called depolarophiles [4],[7] and form two δ bonds by participation of two π electrons of the dipolarophile and four electrons of the dipole.

1,3 dipoles are classified according their structure into two main groups: bent (B-TAC) and linear (L-TAC) structures (see scheme).

1.4.1 Allelic TACs:

This type of TAC is characterized by bent structure and the presence of four electrons in three Pz orbitals, parallel and perpendicular to the plane of the dipole. They have two possible resonance structures in which the three centers have an octet electron, and two structures in which a or c atoms have an electron sextet. The central atom is N, O or sulfur S

1.4.2 Propargylic TACs:

This type of TAC has linear structure and an additional orbital located in the orthogonal plane to the molecular orbital (OM), so this last orbital is not directly involved in the resonance structure and thus in the cycloaddition reactions. The central atom b is limited to nitrogen.

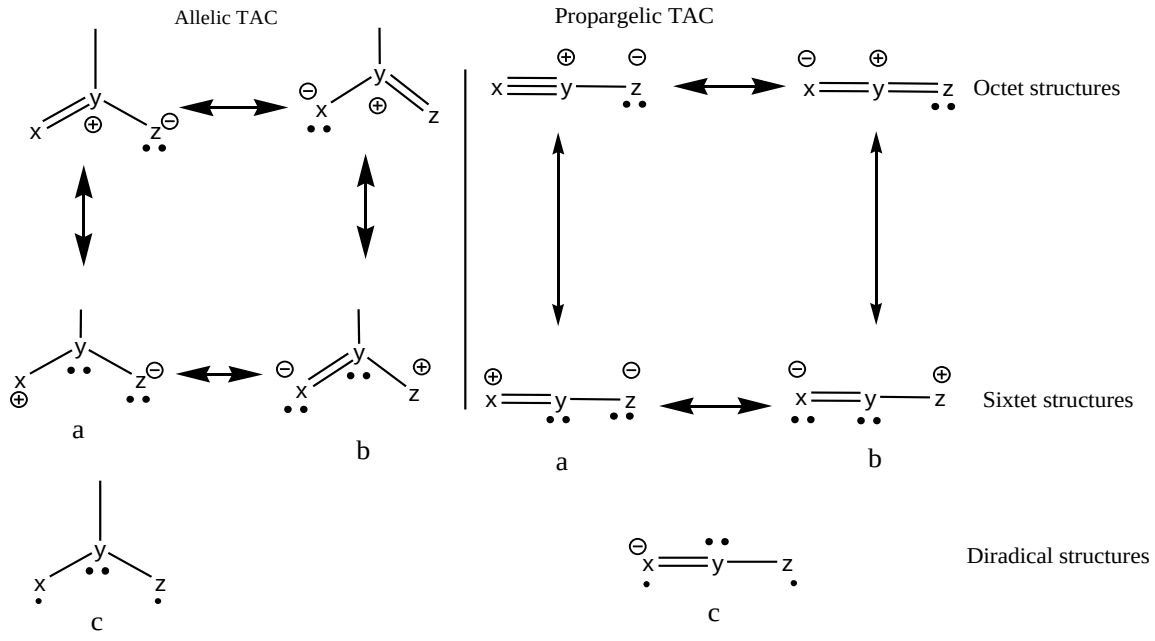

Scheme 1-3: Representation of resonance structures of TACs

Consequently, many allylic and propargylic dipoles can be obtained; most important of them are shown in the figures below:

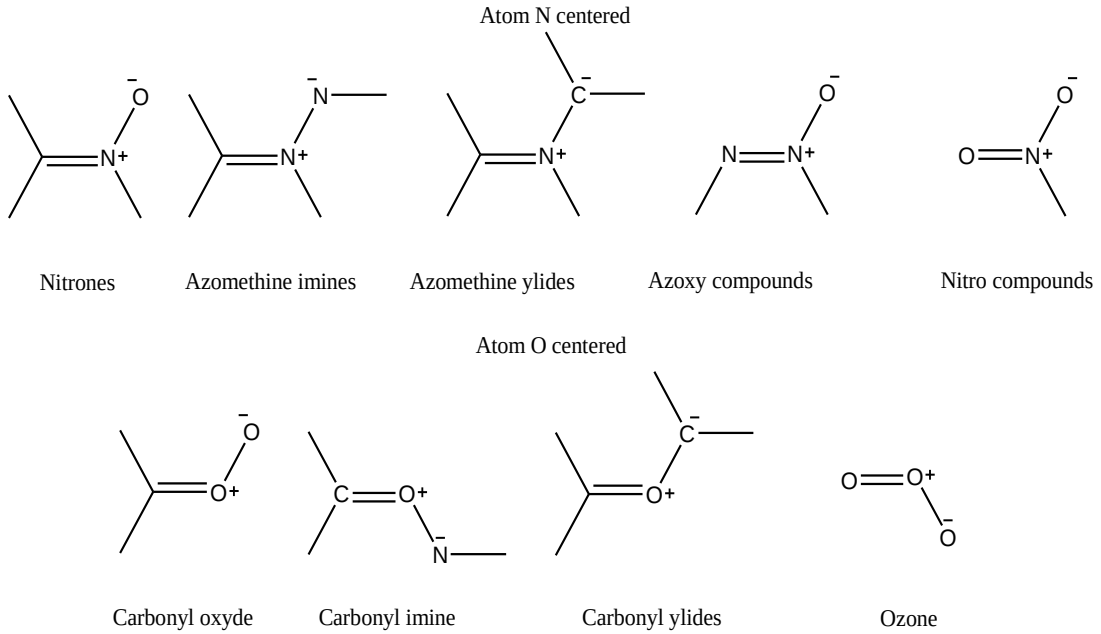

Scheme 1-4: Allelic TAC

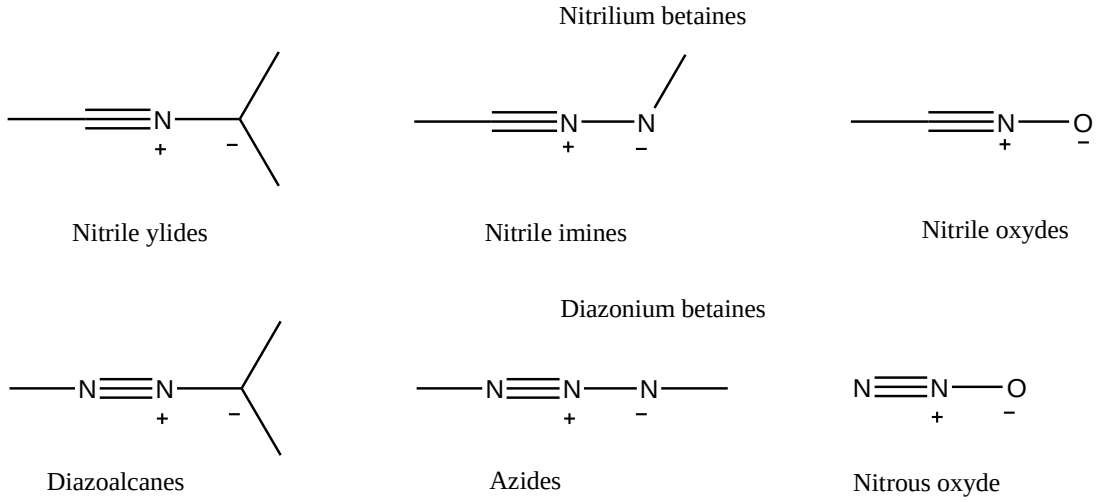

Scheme 1-5: Propargylic TACs

1.5 Selectivity of 32CA reactions

It is well known that the 32CA reaction present high selectivity to form a specific product or a mixture of two isomers while four products are theoretically possible when approaching reagents to each other's; on the literature the majority of number of 32CA reactions do not deviate from this rule and furnish one product or mixture of tow isomers where one is dominant over the other instead of four possible products; Indeed, the preferable product is depending on how reagents approach to each other.

1.5.1 Regioselectivity

When the action of a reagent can a priori be oriented on several sites of a molecule, by providing several different structural isomers, the reaction is said to be regioselective if it takes place preferentially on one of these sites by producing predominantly only one of these structural isomers.

On 32CA reactions the regioselectivity depends on which atom of the dipole will be linked to the substituted atom or the atom bearer of the main function of the dienophile. This is correct when the dienophile and the dipole are asymmetric [13] and two pathways are possible *ortho* and *meta*.

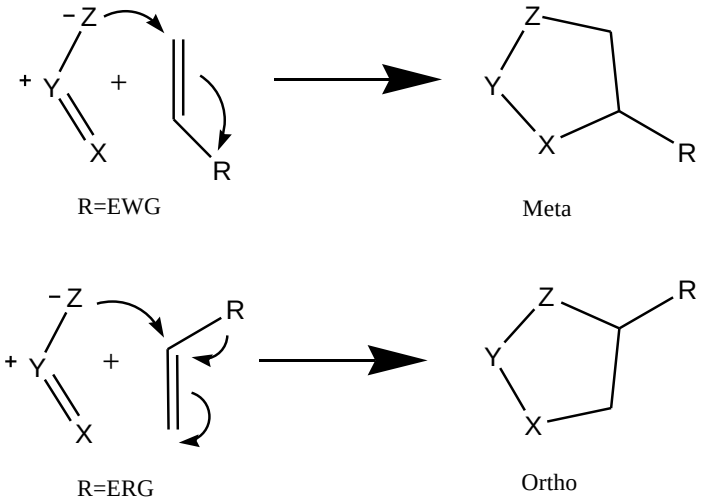

Scheme 1-6: the regioselectivity of 32CA reactions

The regioselectivity depends to the electronic characteristics of reagents such the nature of the substitution linked to the interacting atoms, the electrophilicity and the nucleophilicity of the dipole and the dienophile.

1.5.2 Stereoselectivity

The stereoselectivity depends on the oncoming way of the reagents toward each other in the space and the planar structure of the dipole and the dienophile. There are two kinds of oncoming methods the *endo* and the *exo* resulting respectively to two possible diastereomers cycloadducts trans and cis.

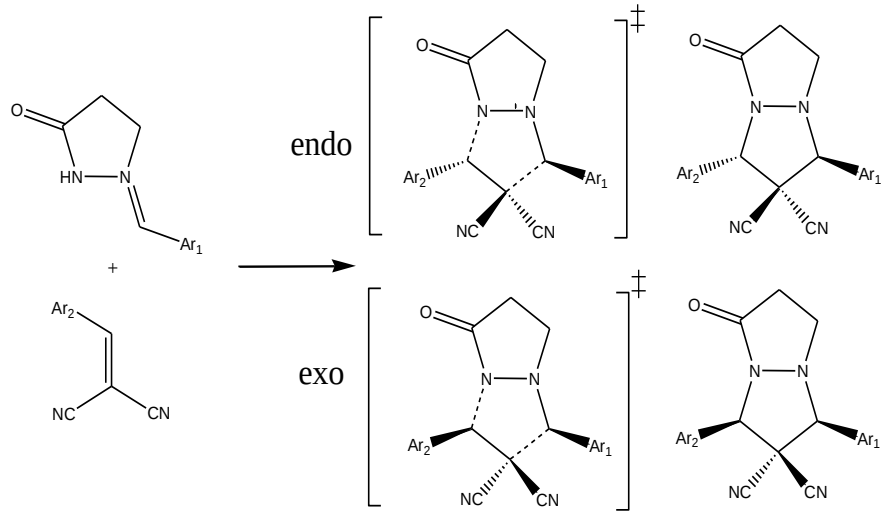

Scheme 1-7: Endo and exo approaches in 32CA reaction of azomithine imine with pnitrobenzylidenemalononitrile [14]

Note that while the exo approach is when the outside group on the dipole is on the opposite side of the new ring as the EWG on the dienophile; the endo one is when the outside group on the dipole are on the same face of the new five membered ring as the EWG on the dienophile. This later is most cases stabilized by interactions between the secondary p orbitals of the atoms which are not concerned by interactions [12], [15], [16]. Nevertheless, many other factors can affect the endo/exo stereoselectivity such as steric hindrance which might favors the formation of the exo cycloadduct. Moreover, some studies showed that non covalent interactions such as hydrogen bonds can make an approach is preferred compared to the other [17], [18]

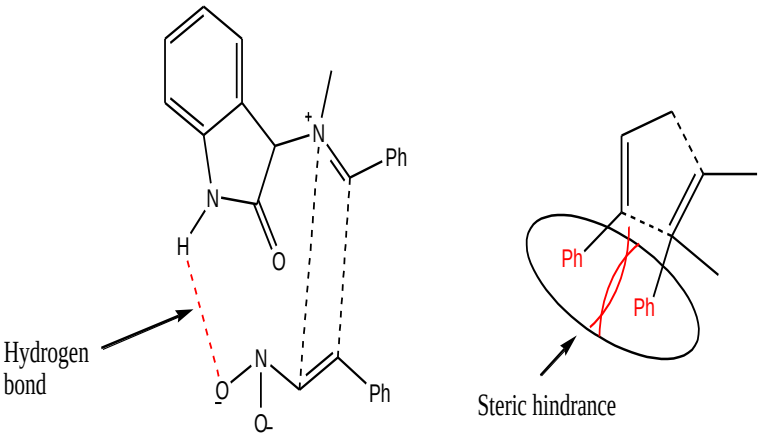

Scheme 1-8: representation of factors affecting endo/exo stereoselectivity [19]

It is worth to mention that while cis/trans are used mostly for alkenes and cyclic systems which are locked and cannot change the orientation of the groups; the terms syn/anti are more appropriate for describing a system where a rotation about a single bond is possible.

1.6 Molecular mechanism of 32CA reactions

Since its appear in the end of the 19th century the 32CA reaction attracted the interest of the organic chemists and become one of the most attracting subjects in the field of chemistry especially with exhaustive development of the computational chemistry tools that offered a performant tool to understand the mechanistic aspect of these reactions witch was for a long time a debate between scientist in this field and have changed with time and this is because when the nature of the mechanism changes the stereospecificity is lost and undesirable stereoisomers might appear.

1.6.1 Proposition of Huisgen and Firestone

Since the TAC cannot be represented by single Lewis structure according the resonance concept developed within the Valence Bond Theory (VBT) [20] by Pauling in 1928 [21]. Two models were proposed separately:

The first one was by Huisgen in 1961 and stated that “1,3-dipoles could be mainly represented by octet and sextet resonance Lewis structures; and this because while the sextet structure represent the dipolar character of the 1,3 dipoles (see Scheme 1-3);the octet resonance structures were recommended to be the major contributors to the electronic structure of the “1,3-dipoles“ and, hence, these species were thus considered “hetero allyl anion“ systems whose termini are both nucleophilic and electrophilic (ambivalent) [13].

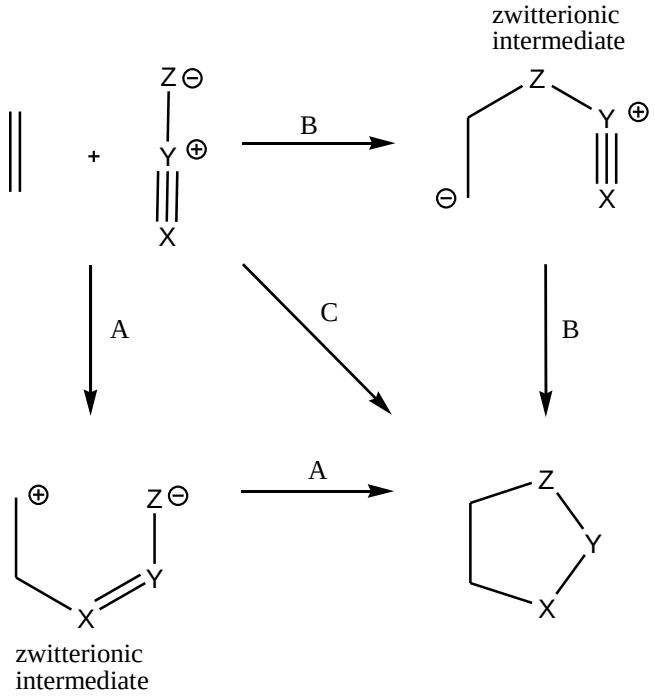

Scheme 1-9: The three Huisgen’s proposed mechanisms for 32CA reactions

Based on that; Huisgen proposed that 32CA reactions of TAC takes three possible concerted mechanisms through a zwitterionic TS according to either the positive or the negative centre of the TAC will attack first the double bond of the dienophile or both charge centers attack the at the same time (see scheme 1-9).

In other words; the dipole and the dipolarophile are added according to a concerted mechanism where the two σ bonds are formed simultaneously but not necessarily at the same speed.

Seven years later and after some experimental contradiction with Huisgen suggestion; Firestone proposed a two-step mechanism via the formation of a diradical intermediate without the rejection of Huisgen's mechanism [22] .

His suggestion comes from the idea that a diradical resonance structure c equivalent to a↔b may usually be accepted as the principal representation of these species (see c in Scheme 1-3). Nowadays the Firestone's stepwise mechanism still exist after gathering proves about the existence of the diradical spaces along the pathway of several cycloaddition reactions [23]

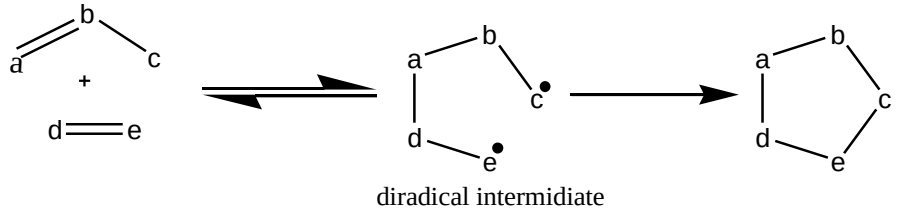

Scheme 1-10: firestone proposed mechanism for 32CA reactions

In 1985, Firestone and Hook after working on 32CA reaction of benzonitrile oxide with styrene and methyle acrylate accepted the concerted mechanism proposed by Huisgen [24],[25]; this later who reported his first two step zwitterionic mechanism later in 1986 [26],[27].

1.6.2 Proposition of Fukui based on FMO theory

The FMO is well known chemical reactivity model proposed by Fukui in 1964 [28] ; indeed, while Fukui was studying reactivity of aromatic compounds, he observed that the pair of π orbitals occupying the energetically the highest molecular orbitals play a decisive role in chemical reactivity of these compounds. In 1964 he proposed the his famous theory which states that '' *a majority of chemical reactions should take place at the position and in the direction of maximum overlapping of the HOMO and the LUMO of the reacting species''* [29]–[31], therefore; the HOMO and the LUMO will interact in such wise that the rate of reaction is inversely related to

the energy gap and thus MOs do not only control the reactivity, but also the regioselectivity.

After that; its Sustmann who applied the FMO to the 32CA reactions for the first time, and depending on the disposition of the HOMO and LUMO in the MO energy diagram he divided the 32CA reaction into three types:

Type I or NED: (normal electron demand), the prevailing interaction is that of $HOMO_{TAC}$ with $LUMO_{ethylene}$; they are accelerated by the presence of ERGs in the TAC and EWGs in the ethylene derivative.

Type II or IED: (inverse electron demand), the prevailing interactions are between $LUMO_{TAC}$ and $HOMO_{ethylene}$; ERGs on the ethylene derivative and EWGs on the TAC will accelerate the reaction.

Type III: FMO energies of TAC and ethylene derivative are similar, so both are to be considered; adding either an ERG or EWG to the TAC or ethylene derivative can accelerate these reactions.

It is noteworthy to add that despite the plethora of data that could be explained as a unified model; Sustmann emphasized to do not overdraw this model because molecules are not just HOMO and LUMO and thus; do not overdraw this model based on oversimplified one electron treatment of the Hückel type [32].

In 1973 and on the aim to predict the relative rates and regeoselectivity of 32CA reactions [14]; Houk calculated the energies of the FMO [11] and coefficients using semi empirical methods for ten parent and some substituted nitrilium betaine, diazonium betaines, azomethinium betaines and carbonyl betaines, and for a series of substituted alkenes and he stated that the regeoselectivity can be predicted based on the most favorable interaction which occurs between the centers that have the greatest FMO coefficients. He renamed the three Sustmann's types [15] of 32CA reaction as follow:

HO controlled when the interaction HOMO dipole - LUMO dienophile is the greatest, LU controlled when the LUMO dipole – HOMO dienophile is the greatest dipole and HO, LU controlled when the HOMO dipole and LUMO dienophile are equal as depicted in scheme below

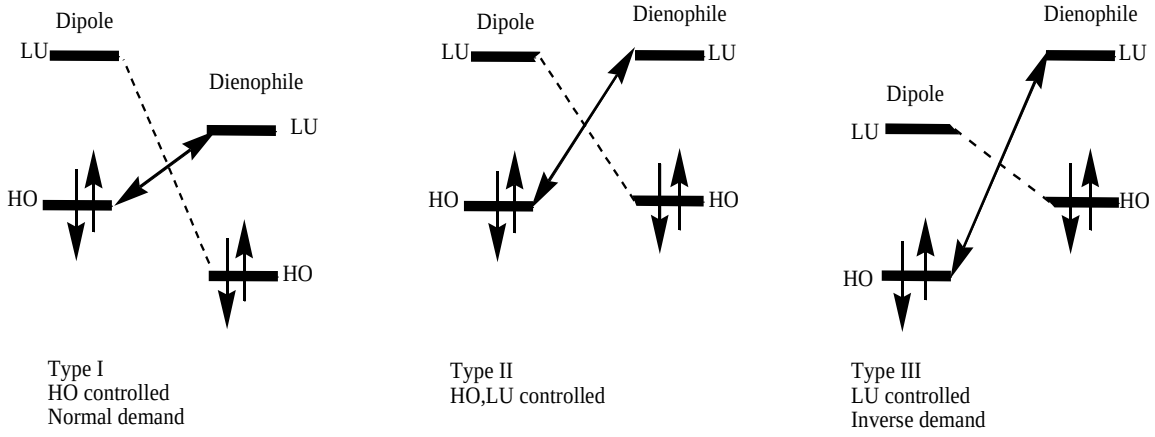

Scheme 1-11: Hook nomenclature and Soustman's classification of 32CA reactions

1.6.3 Mechanistic studies based on TST

It in 1970 when the first geometry optimization of transition state using quantum chemistry calculation which enabled the first studies of molecular mechanisms based on the TS theory [33]. Within this theory the concept of the activation complex or TS permitted the foundation of a relationship between the experimental activation energy and the energy of the TS associated to an organic reaction.

Based on TST, Dewar was one of the first in performing molecular geometry optimizations along a reaction path [34]–[36]. He obtained approximate geometries for reactants, TSs and products involved in the cope rearrangement and electrocyclic processes [34]–[36].

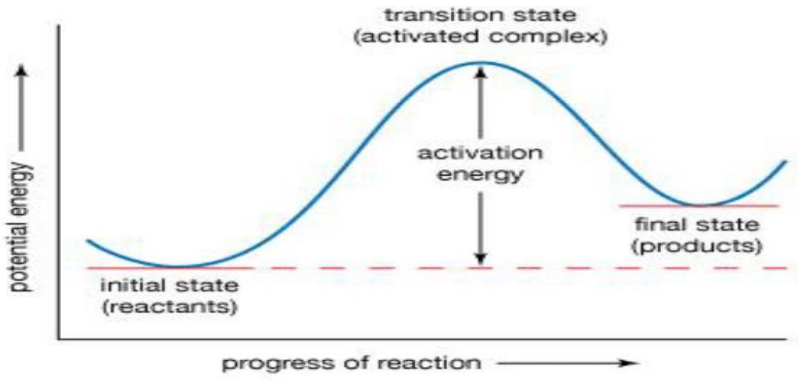

Figure 1-1: classical transition state theory

The development of QC methods powered the debate about the mechanism of the 32CA reactions for example; the reaction of NO with acetylene was subjected to many studies at different level of theory, i.e. Poppinger reported one step mechanism through a concerted TS using Ab initio calculation [37], while MNDO calculation predict two step via diradical intermediate [38]; After that , another Ab initio calculation was performed and suggested concerted process through asynchronous TS [39]. On the other hand, a calculation at MSCF plus CI predicted a stepwise diradical mechanism [40] and MCSCF calculations by McDouall showed that the "concerted "one-step mechanism is favored [41].

Based on QC calculations based on TST and experimental observations, 32CA reactions were mechanistically classified into three categories: (i) the "concerted" mechanism where the two new bonds are formed simultaneously; (ii) a stepwise diradical mechanism involving a diradical intermediate; and (iii) a stepwise dipolar mechanism via a zwitterionic intermediate. In general, QC theoretical studies of 32C reactions allowed establishing that most of them take place through a one-step mechanism in which the formation of the two single bonds is more or less asynchronous.

1.6.4 The Woodward and Hoffmann pericyclic mechanism.

In the aim to study the stereochemistry and the feasibility of some simple reactions Woodward and Hoffmann introduced the orbital symmetry rules in 1965

[42] [43] [10]; which are a simpler version of the Longuet-Higgins and Abrahamson's approach based on the symmetry of the wave function of the molecules have some element of symmetry [43]. Three years later, i.e. in 1968 they generalized the conservation of orbitals symmetry for every concerted reactions and it was in 1969 when they introduced the definition of pericyclic reactions as *"reactions in which all first-order changes in bonding relationships take place in concert on a closed curve and must obey the selection rules".* [44],[45]

In parallel of these efforts Dewar suggested in 1966 that cyclic TS are either aromatic, non-aromatic or anti-aromatic and by formulating the Evan's principle [46] he stated that '' "thermally induced "pericyclic" reactions proceed preferentially via aromatic TSs'' [47].

In this regard and due to the spread of the "pericyclic mechanism within the chemistry scientist; in 1995 Hook classified 32CA reaction as pericyclic reactions taking place through aromatic TSs.

1.6.5 The Houk's model based on Distortion/Interaction Energy (DIEM)

Based on Morokuma's energy decomposition model [48]; Hook proposed in 2007 the distortion/interaction model [49], [50] in which the activation barrier is divided to two parties namely the distortion energy and the interaction energy.

It is noteworthy to mention that; while interaction energy is the attractive and repulsive forces, the distortion energy is the energy needed to distort reagents into TS without allowing interactions.

In fact, this model was verified by studying many 32CA reaction involving six propargylic TACs and three allelic TACs at the B3LYP/6-31G(d) level of theory. He concluded that "*the distortion energy of the reagents towards the TS is the major factor controlling the reactivity differences of TACs*". [49],[50]

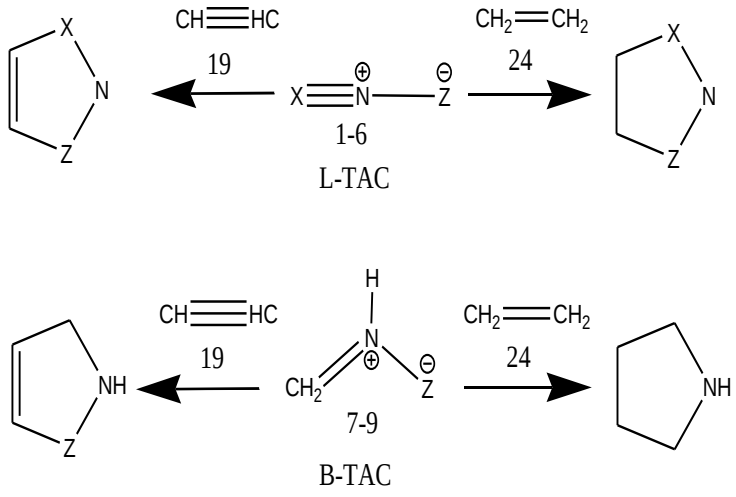

Scheme 1-12: Hook studied reactions

Three years later Braida [51] added the contribution of the diradical structure c (see scheme 3) to the same molecules studied by Hook. He found a good and linear relationship and good correlation between the contribution of the diradical structure c to the resonance hybrid of the TAC and their activation enthalpies in the studied 32CA reactions. Thus he concluded that *" the diradical character of the reactive state, albeit important, is still very far from that of a pure diradical state"* [51] and *" could by no means be interpreted as a support for a diradical mechanism, being as good as a concerted reaction".* [51]

1.6.6 Mechanistic Studies Based on the Analysis of Electron Density: Birth of the MEDT

Despite several models developed since the thirties of the 20th century, the characterization of chemical bonds and the bond forming/breaking pattern in organic chemistry still ambiguous [52] as it is microscopic phenomena and not consistent with quantum mechanical principals. To this end; and in order to adjust the chemical concepts with the quantum chemical postulates; new mathematical approaches and model have been appeared. One of the most influencing theories is the theory of dynamical systems introduced by Bader within atom in molecule theory (AIM) [53] that allowed the partition of the electron density within the molecular space into basins associated with atoms has become quickly a performant tool for analysis of

chemical species. The development of the AIM theory conducted to significant concepts such as bond critical points [54],[55].

Another procedure that gave a link between the chemical structure and the electron density distribution is the analysis of the ELF of Becke and Edgecombe [56] introduced in 1990 which constitute a relative measure of the electron pair localization characterizing the corresponding electron density. One year later i.e. in 1991 this procedure was presented by Silvi and Savin in an attractive chemical fashion [57]–[59] offering a good graphical representation of the molecular system.

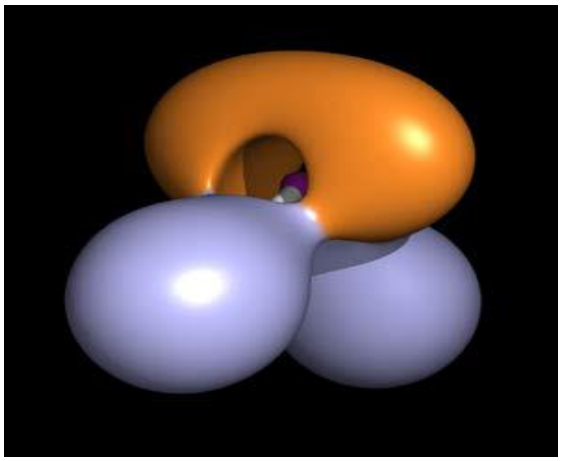

Figure 1-2: ELF basins of the water molecule

After that on 1997 Krokidis proposed BET [60] as a joint use of the ELF and Thom's Catastrophe Theory (CT) [61],[62] to check the bonding changes along a reaction path, this theory becomes powerful tool for analyzing electronic changes along chemical processes and thus defining reactional mechanisms.

Recently Domingo proposed a new reactivity model named Molecular Electron density theory MEDT [63] in which the changes in electron density along a chemical process are responsible the feasibility of chemical reaction and not interaction of MO as the FMO stated [64] . it should be emphasized that the MEDT is a joint-use of CDFT reactivity indices for the ground states (GSs) of reagents [65] and

tools based on electron density such as FLF and QTAIM and NCI [66] to study the change in energy and analyses the reorganization of electron density which give a complete understanding of thermodynamics and kinetics along a reaction process.

The early applications of the MEDT on some cycloaddition reactions [14], [67], [68] revolutionize the field of organic chemistry and rejected the old reactivity models based on the analysis of MO and ruled out the "concerted" and "pericyclic" mechanisms for DA reactions [67].

1.7 Non covalent interactions

The non-covalent interactions are ubiquitous present in nature and contribute to the cohesion on all chemical, proteins and biologicals systems. In general, these interactions are weak in energy compared to covalent interactions but they play an important role on the stability of structures as well as in organic synthesis. Non covalent interactions are classified into many types as follow:

1.7.1 Hydrogen bonds:

Hydrogen bonds are interactions occur between hydrogen atom bonded to an electronegative entity such as oxygen, nitrogen fluorine and lone pair electrons of oxygen, nitrogen or fluorine atom of the neighbouring molecule.

Usually they are depicted as dotted lines in chemical structures between the group that provides the hydrogen proton known as *hydrogen bond donor* and the group providing the lone pair kwon as the *hydrogen bond acceptor*.

The length of the hydrogen bon is around 0.25nm and is its strength is between the covalent bond and the Van der Waals bonds [69],[70].

A-T base pair:

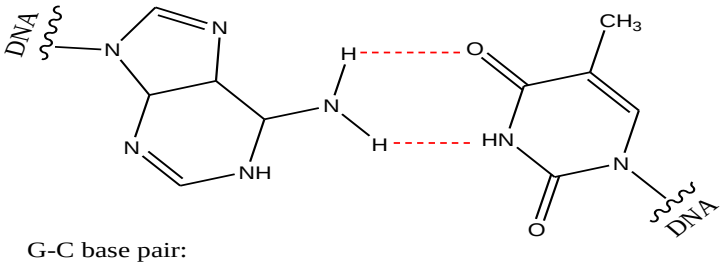

G-C base pair:

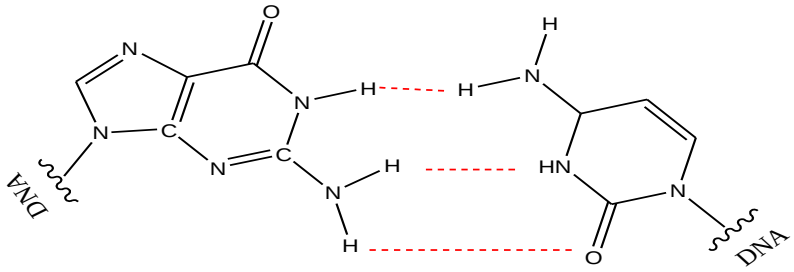

Scheme 1-13: Hydrogen bonds

1.7.2 Halogen bonds

The halogen bond was recognized by Colin over one and a half centuries ago [71] they correspond to an attractive interaction between an electrophilic region in a halogen (X) and a nucleophile (B) yielding a R–X···B contact.

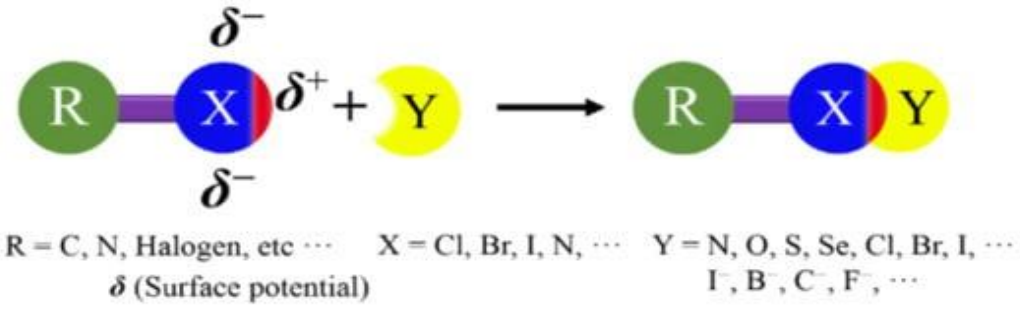

Figure 1-3: Halogen bond (XB)

A halogen bond (halogen interaction) basically refers to a non-covalent interaction where the halogen atom acts as an electrophilic entity [72].The halogen bond is related to the presence of a sigma hole on the carbon-halogen axis due to the polarizability of halogen atoms, in particular iodine and bromine.

1.7.3 Electrostatic interactions:

There are two kinds of electrostatic interactions depending of the of electric charges of the two interacting atoms; while electrostatic attractions occur between opposite charges such as ionic bonds and partial charges or dipoles, electrostatic repulsions occur between molecules that have the same partial charges.

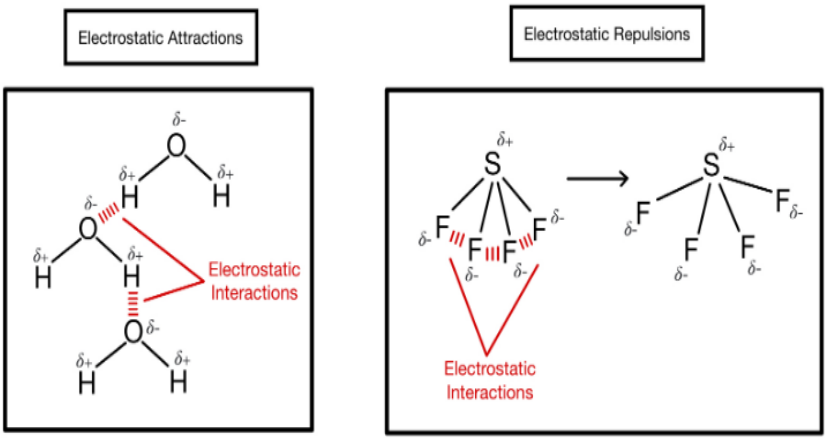

Figure 1-4: Example of electrostatic interactions

1.7.3.1 Π-interactions

Non covalent π-interactions are one of the most significant interactions in biological systems such as DNA and RNA and proteins. An in-depth understanding of this interaction can help in designing more efficient functional materials and drugs. There are many types of π interactions the most important are:

Cation-π interactions: are a noncovalent molecular interaction between the face of an electron-rich π system (e.g. benzene, ethylene, acetylene) and an adjacent cation (e.g. Li+, Na+). This interaction is an example of noncovalent bonding between a monopole (cation) and a quadrupole (π system).

The characteristics of the formed complexes are as follows: an increase of cation atomic number leads to a decrease of interaction energy and an increase of cation

charge leads to an increase of interaction energy. Aromatic amino acids bind with metal cations mainly through interactions with their main chain. Nevertheless, cation-π interaction with a hydrophobic side chain significantly enhances binding energy. Cation-π interactions can have a stabilizing role on the secondary, tertiary and quaternary structure of proteins. These interactions play an important role in substrate or ligand binding sites in many proteins. Cation-π interactions are abundant and play an important role in many biological processes. [72]

Anion-π interactions: are non-covalent contacts between an electron deficient (π-acidic) aromatic system and an anion.[72] Elegant studies have divulged that the anion-π interaction is, in general, dominated by electrostatic and anion-induced polarization contributions [73] .

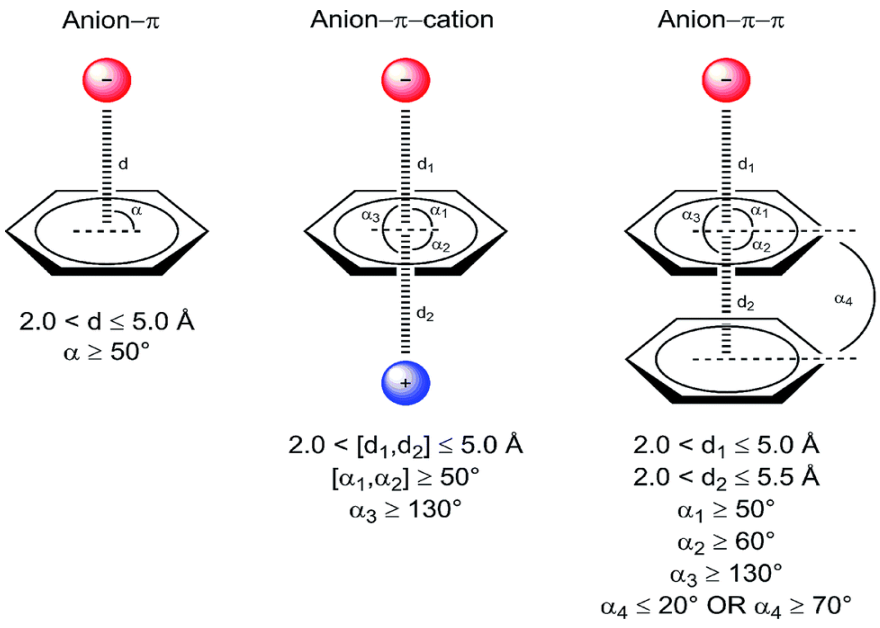

Figure 1-5: Anion-π, Cation-π and π-π interactions

1.8 References

[1] W. H. Pearson, "Alkaloid synthesis via [3+ 2] cycloadditions," *Pure Appl. Chem.*, vol. 74, no. 8, pp. 1339–1347, 2002.

[2] W. Carruthers and I. Coldham, *Some modern methods of organic synthesis*. Cambridge University Press, 1986.

[3] A. Padwa, *1, 3-Dipolar cycloaddition chemistry*. Wiley-interscience, 1984.

[4] A. Padwa and W. H. Pearson, *Synthetic Applications of 1, 3-Dipolar Cycloaddition Chemistry Toward Heterocycles and Natural Products, Volume 59*, vol. 59. John Wiley & Sons, 2003.

[5] E. Buchner, "Einwirkung von Diazoessigäther auf die Aether ungesättigter Säuren," *Berichte der Dtsch. Chem. Gesellschaft*, vol. 21, no. 2, pp. 2637–2647, 1888.

[6] E. Bechmann. Ber, "Dtsch. Chem. Ges," p. 23 :3331, 1890.

[7] O. Diels and K. Alder, "Justus Liebigs Ann," *Chem*, vol. 460, p. 98, 1928.

[8] R. Huisgen, "Kinetics and mechanism of 1, 3-dipolar cycloadditions," *Angew. Chemie Int. Ed. English*, vol. 2, no. 11, pp. 633–645, 1963.

[9] R. B. Woodward and R. Hoffmann, "The conservation of orbital symmetry," *Angew. Chemie Int. Ed. English*, vol. 8, no. 11, pp. 781–853, 1969.

[10] R. Hoffmann and R. B. Woodward, "Selection rules for concerted cycloaddition reactions," *J. Am. Chem. Soc.*, vol. 87, no. 9, pp. 2046–2048, 1965.

[11] K. N. Houk, J. Sims, R. E. Duke, R. W. Strozier, and J. K. George, "Frontier molecular orbitals of 1,3 dipoles and dipolarophiles," *J. Am. Chem. Soc.*, vol. 95, no. 22, pp. 7287–7301, Oct. 1973, doi: 10.1021/ja00803a017.

[12] K. N. Houk, J. Sims, C. R. Watts, and L. J. Luskus, "Origin of reactivity, regioselectivity, and periselectivity in 1, 3-dipolar cycloadditions," *J. Am. Chem. Soc.*, vol. 95, no. 22, pp. 7301–7315, 1973.

[13] R. Huisgen, "1, 3-Dipolar cycloadditions. 76. Concerted nature of 1, 3-dipolar cycloadditions and the question of diradical intermediates," *J. Org. Chem.*, vol. 41, no. 3, pp. 403–419, 1976.

[14] M. Ríos-Gutiérrez, L. Nasri, A. Khorief Nacereddine, A. Djerourou, and L. R. Domingo, "A molecular electron density theory study of the [3 + 2] cycloaddition reaction between an azomethine imine and electron deficient ethylenes," *J. Phys. Org. Chem.*, vol. 31, no. 6, 2018, doi: 10.1002/poc.3830.

[15] M. T. Rispens, E. Keller, B. de Lange, R. W. J. Zijlstra, and B. L. Feringa,

"Asymmetric 1, 3-dipolar cycloadditions to 5-(R)-menthyloxy-2 (5H)-furanone," *Tetrahedron: Asymmetry*, vol. 5, no. 4, pp. 607–624, 1994.

[16] R. Sustmann, "A simple model for substituent effects in cycloaddition reactions. I. 1, 3-dipolar cycloadditions," *Tetrahedron Lett.*, vol. 12, no. 29, pp. 2717–2720, 1971.

[17] L. Nasri, M. Ríos-Gutiérrez, A. K. Nacereddine, A. Djerourou, and L. R. Domingo, "A molecular electron density theory study of [3 + 2] cycloaddition reactions of chiral azomethine ylides with β-nitrostyrene," *Theor. Chem. Acc.*, vol. 136, no. 9, pp. 1–12, 2017, doi: 10.1007/s00214-017-2133-8.

[18] C. Sobhi, A. Khorief Nacereddine, A. Djerourou, M. Ríos-Gutiérrez, and L. R. Domingo, "A DFT study of the mechanism and selectivities of the [3+ 2] cycloaddition reaction between 3-(benzylideneamino) oxindole and trans-β-nitrostyrene," *J. Phys. Org. Chem.*, vol. 30, no. 6, p. e3637, 2017.

[19] L. Nasri, "Etude computationnelle de l'effet du solvant sur le mecanisme et la selectivite des reactions de cycloaddition," University Badji Mokhtar Annaba, 2018.

[20] J. C. Slater, "Directed valence in polyatomic molecules," *Phys. Rev.*, vol. 37, no. 5, p. 481, 1931.

[21] K. S. Pitzer, "The nature of the chemical bond and the structure of molecules and crystals: an introduction to modern structural chemistry.," *J. Am. Chem. Soc.*, vol. 82, no. 15, p. 4121, 1960.

[22] R. A. Firestone, "Mechanism of 1, 3-dipolar cycloadditions," *J. Org. Chem.*, vol. 33, no. 6, pp. 2285–2290, 1968.

[23] R. A. Firestone, "The Low Energy of Concert in Many Symmetry-Allowed Cycloadditions Supports a Stepwise-Diradical Mechanism," *Int. J. Chem. Kinet.*, vol. 45, no. 7, pp. 415–428, 2013.

[24] K. N. Houk, R. A. Firestone, L. L. Munchausen, P. H. Mueller, B. H. Arison, and L. A. Garcia, "Stereospecificity of 1, 3-dipolar cycloadditions of p-nitrobenzonitrile oxide to cis-and trans-dideuterioethylene," *J. Am. Chem. Soc.*, vol. 107, no. 24, pp. 7227–7228, 1985.

[25] K. N. Houk, J. Gonzalez, and Y. Li, "Pericyclic reaction transition states: passions and punctilios, 1935-1995," *Acc. Chem. Res.*, vol. 28, no. 2, pp. 81–90, 1995.

[26] R. Huisgen, G. Mloston, and E. Langhals, "The first two-step 1, 3-dipolar cycloadditions: interception of intermediate," *J. Org. Chem.*, vol. 51, no. 21, pp. 4085–4087, 1986.

[27] R. Huisgen, G. Mloston, and E. Langhals, "The first two-step 1, 3-dipolar

cycloadditions: non-stereospecificity," *J. Am. Chem. Soc.*, vol. 108, no. 20, pp. 6401–6402, 1986, doi: 10.1021/ja00280a053.

[28] K. Fukui, T. Yonezawa, and H. Shingu, "A molecular orbital theory of reactivity in aromatic hydrocarbons," *J. Chem. Phys.*, vol. 20, no. 4, pp. 722–725, 1952.

[29] K. Fukui, "An MO-theoretical illumination for the principle of stereoselection," *Bull. Chem. Soc. Jpn.*, vol. 39, no. 3, pp. 498–503, 1966.

[30] K. Fukui and H. Fujimoto, "Sigma-Pi Interaction Accompanied by Stereoselection," *Bull. Chem. Soc. Jpn.*, vol. 39, no. 10, pp. 2116–2126, 1966.

[31] K. Fukui, "Recognition of stereochemical paths by orbital interaction," *Acc. Chem. Res.*, vol. 4, no. 2, pp. 57–64, 1971.

[32] R. Sustmann, "Orbital energy control of cycloaddition reactivity," in *Physical Organic Chemistry–2*, Elsevier, 1974, pp. 569–593.

[33] H. Eyring, "The activated complex in chemical reactions," *J. Chem. Phys.*, vol. 3, no. 2, pp. 107–115, 1935.

[34] A. Brown, M. J. S. Dewar, and W. Schoeller, "MINDO [modified intermediate neglect of differential overlap]/2 study of the Cope rearrangement," *J. Am. Chem. Soc.*, vol. 92, no. 18, pp. 5516–5517, 1970.

[35] M. J. S. Dewar and S. Kirschner, "MINDO [modified intermediate neglect of differential overlap]/2 study of aromatic (' allowed') electrocyclic reactions of cyclopropyl and cyclobutene," *J. Am. Chem. Soc.*, vol. 93, no. 17, pp. 4290–4291, 1971.

[36] M. J. S. Dewar and S. Kirschner, "Classical and nonclassical potential surfaces. Significance of antiaromaticity in transition states," *J. Am. Chem. Soc.*, vol. 93, no. 17, pp. 4292–4294, 1971.

[37] D. Poppinger, "Ab initio molecular orbital study of simple 1, 3-dipolar reactions," *Aust. J. Chem.*, vol. 29, no. 3, pp. 465–478, 1976.

[38] M. J. S. Dewar, S. Olivella, and H. S. Rzepa, "Ground States of Molecules. 49. MINDO/3 Study of the Retro-Diels-Alder Reaction of Cyclohexene," *J. Am. Chem. Soc.*, vol. 100, no. 18, pp. 5650–5659, 1978, doi: 10.1021/ja00486a013.

[39] A. Komornicki, J. D. Goddard, and H. F. Schaefer III, "Reaction of acetylene with fulminic acid. The prototype 1, 3-dipolar cycloaddition," *J. Am. Chem. Soc.*, vol. 102, no. 6, pp. 1763–1769, 1980.

[40] P. C. Hiberty, G. Ohanessian, and H. B. Schlegel, "Theoretical ab initio study of 1, 3-dipolar cycloaddition of fulminic acid to acetylene. Support for Firestone's mechanism," *J. Am. Chem. Soc.*, vol. 105, no. 4, pp. 719–723, 1983.

[41] J. J. W. McDouall, M. A. Robb, U. Niazi, F. Bernardi, and H. B. Schlegel, “An MC-SCF study of the mechanisms for 1, 3-dipolar cycloadditions,” *J. Am. Chem. Soc.*, vol. 109, no. 15, pp. 4642–4648, 1987.

[42] R. B. Woodward and R. Hoffmann, “Stereochemistry of electrocyclic reactions,” *J. Am. Chem. Soc.*, vol. 87, no. 2, pp. 395–397, 1965.

[43] R. B. Woodward and R. Hoffmann, “Selection rules for sigmatropic reactions,” *J. Am. Chem. Soc.*, vol. 87, no. 11, pp. 2511–2513, 1965.

[44] H. C. Longuet-Higgins and E. W. Abrahamson, “The electronic mechanism of electrocyclic reactions,” *J. Am. Chem. Soc.*, vol. 87, no. 9, pp. 2045–2046, 1965.

[45] R. B. Woodward and R. Hoffmann, “A ngew. Chem. 1969, 81, 797,” *Angew. Chem. Int. Ed. Engl*, vol. 8, p. 781, 1969.

[46] M. J. S. Dewar, “Tetrahedron Suppl. 8,” *Part*, vol. 1, p. 75, 1966.

[47] M. J. S. Dewar, “Tetrahedron Suppl. 1966, 8, 75.(b) Dewar. MJS Angew,” *Chem.. Int. Ed. Engl*, vol. 10, p. 761, 1971.

[48] S. Nagase and K. Morokuma, “An ab initio molecular orbital study of organic reactions. The energy, charge, and spin decomposition analyses at the transition state and along the reaction pathway,” *J. Am. Chem. Soc.*, vol. 100, no. 6, pp. 1666–1672, 1978.

[49] D. H. Ess and K. N. Houk, “Distortion/interaction energy control of 1, 3-dipolar cycloaddition reactivity,” *J. Am. Chem. Soc.*, vol. 129, no. 35, pp. 10646–10647, 2007.

[50] D. H. Ess and K. N. Houk, “Theory of 1, 3-dipolar cycloadditions: distortion/interaction and frontier molecular orbital models,” *J. Am. Chem. Soc.*, vol. 130, no. 31, pp. 10187–10198, 2008.

[51] B. Braida, C. Walter, B. Engels, and P. C. Hiberty, “A clear correlation between the diradical character of 1, 3-dipoles and their reactivity toward ethylene or acetylene,” *J. Am. Chem. Soc.*, vol. 132, no. 22, pp. 7631–7637, 2010.

[52] B. T. Sutcliffe, “The development of the idea of a chemical bond,” *Int. J. Quantum Chem.*, vol. 58, no. 6, pp. 645–655, 1996.

[53] R. F. W. Bader, “Molecular fragments or chemical bonds,” *Acc. Chem. Res.*, vol. 8, no. 1, pp. 34–40, Jan. 1975, doi: 10.1021/ar50085a005.

[54] R. F. W. Bader, S. G. Anderson, and A. J. Duke, “Quantum topology of molecular charge distributions. 1,” *J. Am. Chem. Soc.*, vol. 101, no. 6, pp. 1389–1395, 1979.

[55] R. F. W. Bader, T. T. Nguyen-Dang, and Y. Tal, “Quantum topology of molecular

charge distributions. II. Molecular structure and its change," *J. Chem. Phys.*, vol. 70, no. 9, pp. 4316–4329, 1979.

[56] A. D. Becke and K. E. Edgecombe, "A simple measure of electron localization in atomic and molecular systems," *J. Chem. Phys.*, vol. 92, no. 9, pp. 5397–5403, 1990, doi: 10.1063/1.458517.

[57] B. Silvi and A. Savin, "Classification of chemical bonds based on topological analysis of electron localization functions," *Nature*, vol. 371, no. 6499, pp. 683–686, 1994.

[58] A. Savin, B. Silvi, and F. Colonna, "Topological analysis of the electron localization function applied to delocalized bonds," *Can. J. Chem.*, vol. 74, no. 6, pp. 1088–1096, 1996.

[59] A. Savin, R. Nesper, S. Wengert, and T. F. Fässler, "ELF: The electron localization function," *Angew. Chemie Int. Ed. English*, vol. 36, no. 17, pp. 1808–1832, 1997.

[60] X. Krokidis, S. Noury, and B. Silvi, "Characterization of elementary chemical processes by catastrophe theory," *J. Phys. Chem. A*, vol. 101, no. 39, pp. 7277–7282, 1997.

[61] R. Thom, *Structural stability and morphogenesis*. CRC press, 2018.

[62] A. E. R. Woodcock and T. Poston, *A geometrical study of the elementary catastrophes*, vol. 373. Springer, 2006.

[63] L. R. Domingo, "Molecular electron density theory: A modern view of reactivity in organic chemistry," *Molecules*, vol. 21, no. 10, pp. 1–15, 2016, doi: 10.3390/molecules21101319.

[64] R. S. Mulliken, "Spectroscopy, molecular orbitals, and chemical bonding," *Science (80-.).*, vol. 157, no. 3784, pp. 13–24, 1967.

[65] P. Geerlings, F. De Proft, and W. Langenaeker, "Conceptual density functional theory," *Chem. Rev.*, vol. 103, no. 5, pp. 1793–1874, 2003.

[66] E. R. Johnson, S. Keinan, P. Mori-Sánchez, J. Contreras-García, A. J. Cohen, and W. Yang, "Revealing noncovalent interactions," *J. Am. Chem. Soc.*, vol. 132, no. 18, pp. 6498–6506, 2010.

[67] L. R. Domingo, "A new C-C bond formation model based on the quantum chemical topology of electron density," *RSC Adv.*, vol. 4, no. 61, pp. 32415–32428, 2014, doi: 10.1039/c4ra04280h.

[68] M. Ríos-Gutiérrez, L. R. Domingo, and P. Pérez, "Understanding the high reactivity of carbonyl compounds towards nucleophilic carbenoid intermediates generated from carbene isocyanides," *RSC Adv.*, vol. 5, no. 103,

pp. 84797–84809, 2015, doi: 10.1039/c5ra15662a.

[69] A. D. Buckingham and P. W. Fowler, “A model for the geometries of van der Waals complexes,” *Can. J. Chem.*, vol. 63, no. 7, pp. 2018–2025, 1985.

[70] A. D. Buckingham, P. W. Fowler, and A. J. Stone, “Electrostatic predictions of shapes and properties of van der Waals molecules,” *Int. Rev. Phys. Chem.*, vol. 5, no. 2–3, pp. 107–114, 1986.

[71] M. Colin, “Note sur quelques combinaisons de l’iode,” *Ann. Chim*, vol. 91, pp. 252–272, 1814.

[72] P. Metrangolo and G. Resnati, “Halogen bonding: a paradigm in supramolecular chemistry,” *Chem. Eur. J.*, vol. 7, no. 12, pp. 2511–2519, 2001.

[73] D. Quiñonero *et al.*, “Anion–π interactions: do they exist?,” *Angew. Chemie*, vol. 114, no. 18, pp. 3539–3542, 2002.

Chapter 2: Density functional theory and theoretical aspect of the chemical reactivity

2.1 Introduction

On the beginning of the twentieth century; physicians discovered that the lows of Newtonian mechanics do not explain correctly the phenomena associated to microscopic particles. Thus; these lows are not applicable on microscopic scale since many accumulated proves confirmed that limitation [1].

To understand the physical and chemical properties of such particles scientists should apply another low called quantum mechanics which computes and describes the electronic and atomic systems by solving equations of molecular dynamics, statistical mechanics and structural electronics calculations. These latter use mathematical formalism to solve equations of quantum mechanics.

For a system containing many particles there are many methods of quantum calculations such Hartree Fock approximation and electronic correlation and density functional theory (DFT).

In this chapter we focus on only on DFT and the most important principals that DFT stands on as well as the theoretical calculations and parameters used to study the chemical reactivity.

2.2 Density functional theory

2.2.1 Fundamentals of DFT

In-depth understanding of chemical and physical characteristic of molecular system requires the inclusion of some electronic effects especially on systems contains metal atoms. It has been noticed that on Post Hartree Fock approximations take that effects on consideration but calculations are so slowly and require enormous memory size and computing time when studying large size chemical structures. For that the DFT has appeared and developed in the last fourteen years

as a performant alternative for studying chemical systems which gather the accuracy of results within reasonable computing time.

Initially use for solids; The DFT has been rapidly become more and more popular for the following:

- Includes within its formalism the most important electronic correlations.
- Less computing cost for large chemical and biological structures.
- The formalism of the wave function can be interpreted chemically.

The DFT is based on the Thomas and Fermi postulate stated that “Electrical properties can be described in terms of the electron density functional, by locally applying appropriate relations to a homogeneous electronic system” [2]. This postulate was too simple and not able to describe molecular systems.

It is Hohenberg et Kohn on 1964 [3] the first who described the energy as a function of electronic density by showing that the external potential where interacting particles moves can be determined by electronic density:

$$\mathbf{elec} = \mathbf{E}[\boldsymbol{\rho}(\mathbf{r})] \qquad \textbf{Eq. 1}$$

Where ρ is the electronic density, it describes the probability of presence of the cloud of electrons at a volume of space r.

Note that ρ is a positive function depending only on the three coordinates (x,y,z) of space. This quantity vanishes at infinity and is equal to N - total number of electrons - when it is integrated over all space.

And the functional is a function of a function. i, e he notation of a functional is $[f(r)]$, where r is a variable of the function f.

$$\begin{cases} \boldsymbol{\rho(r \to \infty) = 0} \\ \boldsymbol{\int \rho(r) dr = N} \end{cases}$$ **Eq. 2**

Due to ability of density functional to describe the characteristics of the electronics system; many formalisms based on it have been proposed but the most exact was presented by Hohenberg et Kohn on two theories:

2.2.1.1 First theory of Hohenberg and Kohn

This theory is a justification of the idea that; a given electron density corresponds to a unique external potential. The potential $V(r)_{ext}$ is, in fact, determined, up to a constant, by the electron density $\rho(r)$.

Therefore; The total ground state energy E is a unique functional of the particles density $\rho(\overrightarrow{r})$ a given external potential This theory means that it is enough to know only the electron density to determine all the wave functions and the electronic characteristics for a given system. Accordingly, the total energy E of a system of interacting electrons in an external potential is represented as a functional of the ground state electron density ρ_0 as follows:

$$\boldsymbol{E = <\varphi|H|\varphi> = F[\rho] + \int V_{ext}(\overrightarrow{r})\ \rho(\overrightarrow{r})\, dr}$$ **Eq. 3**

$$\mathbf{F[\rho] = <\varphi|U + T\ |\varphi>}$$ **Eq. 4**

Where U and T are the kinetic energy and the interaction inter particles which is not dependent of the external potential [3].

The Hamiltonian operator could be uniquely determined and this the wave functions Y (of all states) and all material properties computed.

$$\hat{H} = -\frac{1}{2}\sum_{i}^{n}\Delta i + \sum_{i>j}^{n}\frac{1}{r\,ij} + V_{ext}(r_i) \qquad \textbf{Eq. 5}$$

With

$$V_{ext}(r_i) = -\sum_{K=1}^{N}\frac{Z_K}{R_{Ki}} \qquad \textbf{Eq. 6}$$

$V_{ext}(r_i)$ external potential of electron i.

2.2.1.2 Second theory of Hohenberg and Kohn

This second theorem states that the density functional that provides access to the ground state energy gives the lowest energy if the density is that of the ground state. This theory is based on the variational principle analogous to that proposed in the Hartree-Fock approach for a functional of the wave function, but applied this time to a functional of the electronic density

$$\frac{\partial E[\rho(r)]}{\partial \rho(r)} = 0 \qquad \textbf{Eq. 7}$$

In summary: all properties of a system defined by an external potential V_{ext} can be determined from the ground state electron density. The energy of the system E(r) reaches its minimum value if and only if the electron density is that of the ground state. The use of this variational approach is limited to finding the ground state

energy and, to be more precise, this reasoning is limited to the ground state for a given symmetry [4].

$$E[\rho] \geq E_0[\rho_0] = E_0 \qquad \text{Eq. 8}$$

2.2.1.3 The equations of Kohn- Sham

On 1965 Kohn-sham [5] proposed a set of equations similar to the equations of Hartree Fock by replacing the real system made up of interacting particles by gas composed of non-interacted particles. consequently; it is possible to obtain more accurately the kinetic energy of system of N non interacting electrons as a functional of the density ρ(r).

The idea was to use a fictitious system of n electron but they have the same density as the real system and to solve Schrödinger mono electronic equations.

While the Hamiltonian can be expressed as:

$$\hat{H} = \sum_{i=1}^{n} \left[-\frac{1}{2} \nabla_i^2 + V_i(r) \right] = \sum_{i=1}^{n} h_i^{ks} \qquad \text{Eq. 9}$$

With

$$h_i^{ks} = -\frac{1}{2} \nabla_i^2 + V_S(r_i) \qquad \text{Eq. 10}$$

The Kohn- Sham equations for the electron I can be written as follow:

$$h_i^{ks}\,\theta_i^{ks} = \varepsilon_i^{ks}\,\theta_i^{ks}$$ **Eq. 11**

knowing that ε_i^{ks} is the Kohn- Sham orbital of the electron i.

To make DFT and Kohn- Sham equations practically useful we need some approximations for calculating exchange correlation energy.

2.3 Some approximations used on DFT

2.3.1 Local density approximation LDA

The idea of this approximation is based on the local treatment of the density. On LDA the electronic density of a reel system is substituted by one of homogenous gas; it presents a good physical model when studying molecule with density varies slightly like metals but some characters are overestimated such as bond energies and some other are underestimated such as bond lengths.

This approximation is the base of all modern exchange correlation approximations which can be written as:

$$E_{XC}^{LDA}[\rho] = \int \rho(r)\varepsilon_{XC}(\rho)dr$$ **Eq. 12**

Note that the exchange term is defined by Bloch and Dirac relation [6]:

$$\varepsilon_X(\rho(r)) = -\frac{3}{4}\sqrt[3]{\frac{3\rho(r)}{\pi}}$$ **Eq. 13**

The term $\varepsilon_X\big(\rho(r)\big)$ is done by Vosko, Wilk, et Nusair formula [7]

2.3.2 Local spin density approximation LSDA

This approximation takes in consideration the spin polarization. While on LDA the electron having opposed spin have the same spatial KS; LSDA distinguish between the orbitals of electrons with opposite spins.

The electron density is written as:

$$\boldsymbol{\rho(r) = \rho_{\alpha}(r) + \rho_{\beta}(r)} \qquad \textbf{Eq. 14}$$

Thus:

$$\boldsymbol{E_{XC}^{LSDA}[\rho_{\alpha} + \rho_{\beta}] = \int \rho(r)\varepsilon_{XC}\left(\rho_{\alpha}(r) + \rho_{\beta}(r)\right) dr} \qquad \textbf{Eq. 15}$$

This approximation suits the systems in which the electronic density variation is slow compared which make its use more frequent.

2.3.3 Generalized Gradient Approximation GGA

This approximation is introduced to overcome the problem of electronic density that change slowly with the position from atom to another in a homogenous gas system. This improvement is known as *Generalized Gradient Approximation (GGA)* [8]*;* it consists to express the functional of exchange energy correlation functional as a function of the electron density and its gradient in order to defeat the heterogeneity of the electronic density.

$$E_{XC}^{GGA}[\rho_\alpha, \rho_\beta] = \int (\rho_\alpha, \rho_\beta, \nabla\rho_\alpha, \nabla\rho_\beta) dr$$ **Eq. 16**

Where E_{XC}^{GGA} density of exchange correlation energy.

$$E_{xc}^{GGA} = E_X^{GGA} + E_C^{GGA}$$ **Eq. 17**

$$E_X^{GGA} = E_X^{LDA} + \sum_\sigma \int F(S_\rho)\rho_\sigma^{\frac{3}{4}}(r) dr$$ **Eq. 18**

And

$$\sigma = \alpha \text{ or } \beta \text{ and } S_\sigma = \frac{|\nabla\rho_\sigma(r)|}{\rho_\sigma^{\frac{3}{4}}(r)}$$ **Eq. 19**

S: parameter of local inhomogeneity

It worth to mention that the use of the GGA significantly increases the accuracy of calculation compared to LDA especially for binding energy of molecules. it was this feature which lead to the very wide spread acceptance of DFT in the chemistry community during the early 1990's

2.3.4 The functionals meta-GGA

Meta-GGA functionals are extension of GGA, they depend on the Laplacian of the spin density or of the local the kinetic energy [9],[10].

$$\boldsymbol{\tau_\sigma(r) = \frac{1}{2}\sum_i |\nabla \psi_i(r)|^2} \qquad \textbf{Eq. 20}$$

2.3.5 Hybrid functional B3LYP

Hybrid functionals are introduced in order to correct the self-interaction error and to fix the non-local correlation of the traditional LDA and GGA approximations. To this end On 1993; Becke [11] suggested to mix exchange energy with the traditional exchange correlation energy of HF and local one and He proposed for this purpose an expression with three parameters which will be designated by B3

$$\boldsymbol{E_{xc} = E_{xc}^{LDA} + a_0(E_x^{exact} - E_x^{LDA}) + a_x \Delta E_x^{B\,88} + a_c \Delta E_c^{PW\,91}} \qquad \textbf{Eq. 21}$$

Where a_0, a_x and a_c are defined by means of semi empirical calculations and adjusted according to experimental findings, they equal 0.20, 0.72 and 0.81 respectively [12].

E_x^{exact} is the exchange energy exact obtained from HF calculations.

B3LYP [13] is most popular hybrid functional, it defer from the above expression by the replacement of the PW91 correlation energy functional by the LYP (Lee-Yang-Parr) correlation functional; it combines the local exchange functional, functional exchange of Becke and of HF with the local correlation functional (VWN) and the corrected gradient of Lee Young Parr and gives better results than B3PW91 of Perdew and Wang [13] and other GGA functionals for organic molecules.

$$\mathbf{E}_{xc}^{B3LYP} = (\mathbf{1} - \boldsymbol{a_0} - \boldsymbol{a_x})\boldsymbol{E_x^{LDA}} + \boldsymbol{a_0}\boldsymbol{E_x^{HF}} + \boldsymbol{a_x}\boldsymbol{E_x^{B\,88}} + (\mathbf{1} - \boldsymbol{a_c})\boldsymbol{E_c^{VWN}} + \boldsymbol{a_c}\boldsymbol{E_c^{LYP}} \quad \textbf{Eq. 22}$$

2.4 Solvent effect

Most of organic reactions are performed experimentally on solvents which eases the interactions between reagents by creating hydrophobic-hydrophilic interactions and hydrogen bonds. Consequently, it appears essential to properly represent the solvent around solutes in computational studies and do not only settle on gas phase structure for better understanding the bonding phenomena and chemical processes.

Two major strategies are distinguished for representing the solvent in computational calculations, the explicit methods, which represent the solvent in a microscopic way, and the implicit one where the solvent effect represented in macroscopic way.

2.4.1 The explicit model

This model provides more realistic picture of the system solvent-solute; within this model more parameters are used to model the atoms such as hydrogen bond, hydrophobic interaction, and viscosity, resulting in more accuracy and therefore more computing time. In general, molecular mechanics (force field) are utilized for the computation of physical and chemical properties including motion of the large molecular systems. This model is applicable in of molecular mechanics (MM) and dynamics (MD) or Monte Carlo (MC) simulations, although some quantum chemical calculations.

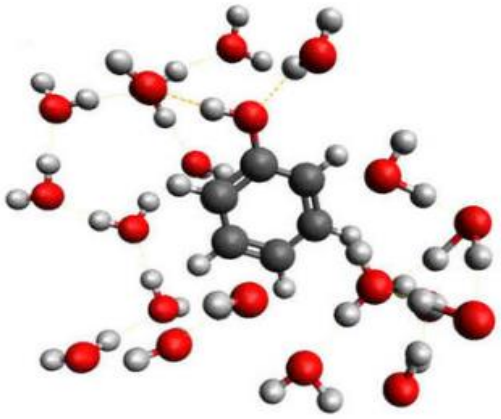

Figure 2-1: example of explicit solvation model by water molecules

The expensiveness and long computational time limit the use of this model and encourage researches to evolve another models based on a continuous distribution of solvent, e.g., an implicit solvent model.

2.4.2 The implicit model

This model enables better calculations of thermodynamic data [14] by calculating average quantities and allowing the direct treatment directly the solute/solvent interactions in terms of free energy . The implicit model is based mainly on the idea that the effect of water on the solute molecules is electrostatic. The solvent is then represented as a continuous medium, without microscopic structure.

The first works on this model were presented by Born 1912 and Onsager 1936 [15] where the solute is immersed in a cavity of the solvent of low dielectric constant with fixed partial charges.

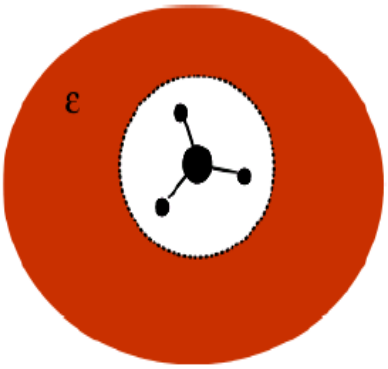

Figure 2-2: representation of implicit solvation model

2.4.2.1 SCRF model (Self Consistent Reaction Field)

The cavity is constructed by a set of spheres centered on the nuclei and having a radius of van der Waals. The built of the cavity costs some free positive energy [16] [17],[18] which depends on solvent nature and the cavity topology. Within this solvation model we figure out three types of interactions: interactive, repulsive and electrostatic.

The charge distribution of the solute polarizes the surface of the cavity of the continuum allowing charges to appear at the solute continuum interface and modifies the electronic density of the solute. Then the continuum has to adapt and there is a new change in the distribution of charges at the solute-continuum interface…and so on until electrostatic convergence is achieved between the distribution of charges specific to the solute and that of the surface of the cavity. This energy term, always negative, is the electrostatic contribution (ΔG_{elec}).

The total energy of interactions is expressed as follow:

$$\Delta \boldsymbol{G_{sol}} = \Delta \boldsymbol{G_{cav}} + \Delta \boldsymbol{G_{elec}} + \Delta \boldsymbol{G_{disp}} + \Delta \boldsymbol{G_{rep}} \qquad \textbf{Eq. 23}$$

Where the term dispersion/repulsion ($\Delta G_{disp} + \Delta G_{rep}$) implies the interaction of the solute with the solvent at the cavity interface, and gives a negative/positive contribution to the energy variation.

2.4.2.2 PCM model (Polarizable Continuum Model)

The Polarizable Continuum Model (PCM) by Tomasi and coworkers is one of the most frequently used solvation methods because of the continuous improvements, both in terms of computational efficiency and generality [19],[20] and has seen numerous variations over the years.

Within this model, the solute which is embedded into a cavity is treated as a polarizable charge distribution and solvent (surrounded by the solute) is represented with a dielectric continuum medium that is polarized by the solute. The induced charge on the solvent affects the charge distribution of solutes as well as their geometry. The solvent reaction field found because of induced solvent charge can be acquired with the self-consistent method by solving the non-homogeneous Poisson equation, which is coupled to the quantum mechanical electron density of the solute molecule.

The PCM model calculates the molecular free energy in solution as the sum over three terms.

Eq. 24

$$\boldsymbol{G_{sol} = G_{dr} + G_{es} + G_{cav}}$$

Where: G_{es} , G_{dr} , G_{cav} are the dispersion-repulsion, electrostatic and cavitation free energies respectively.

While calculation of the cavitation energy G_{cav} uses the surface defined by the van der Waals-spheres, the solvent accessible surface is used to calculate the dispersion-repulsion contribution G_{dr} to the solution free energy. The latter differs

from the former through additional consideration of the (idealized) solvent radius. The electrostatic contribution to the free energy in solution G_{es} uses an approximate version of the solvent excluding surface constructed through scaling all radii by a constant factor (e.g. 1.2 for water) and then adding some more spheres not centered on atoms in order to arrive at a somewhat smoother surface.

The polarizable continuum model is a well-known and verified solvent model, which is often used to predict the electrolyte structure/stability and to understand the chemical properties in a practical environment.

Two types of PCMs have been popularly used: the dielectric PCM (D-PCM) in which the continuum is polarizable and the conductor-like PCM (C-PCM) in which the continuum is conductor-like similar to COSMO Solvation Model.

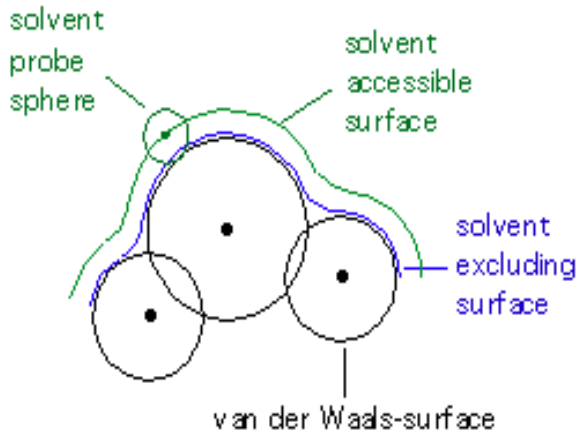

Figure 2-3: representation of PCM model

2.5 The chemical reactivity

2.5.1 Introduction

The chemical reactivity is the chemistry field that uses the computational tools to understand the characteristics of chemical structures, its ability to react between each other, the electronic changes that occurs at the atomic level, how bonds are formed and broken during the transformation from reagents to products and the parameters that control that structural changes.

Influenced by the continuous rapid growth of the computational tools and methods on the last decades; the chemical reactivity knew the appearance of a lot of development and models that took it from the interest in simple molecules and processes to the study of complex chemical reactions and systems and widen its use to other fields such as biology and medicines. Such as transition state theory, MO and CDF Theory.

As we discussed TST and FMO theories on the previous chapter; we focus in the following on the CDFT indices and their use on the description on the chemical reactivity.

2.5.2 Conceptual density functional theory (CDFT) indices

Since its first appearance on 1965 by Hohenberg and Kohn [21] the DFT theory revolutionized the computational chemistry by the smart idea based on using the electric density ρ (r) to understand molecular structures instead the wave function Ψ as carrier of information through two famous theorems (see previous chapter) i,e they allowed the characterization in a formally exact way the total energy E of the ground state through a variational principle with respect to the electronic density ρ (r)

$$\frac{\delta(\mathbf{E} - \mu\mathbf{N})}{\delta\rho} = \mathbf{0}$$ **Eq. 25**

Later Parr and his collaborators [22] proved that the density is compatible with a single external potential v(**r**), i.e. ρ determines v. As ρ also determines N by integration, it also determines the Hamiltonian. Through the variational procedure (the second theorem) the ρ results from solving the Euler equation of the problem:

$$V(r) + \frac{\delta F_{HK}}{\delta\rho(r)} = \mu =$$ **Eq. 26**

Where F_{HK} is the Hohenberg Kohn functional which is solved by Kohn and Sham transforming the variational equation into a series of pseudo one-electron eigenvalue equations, similar to the Hartree–Fock equations [23] and tis this considered from the wave function to the density as the basic holder of information. In this context calculations proved that the chemical potential can be written as a function of the energy with respect to system`s number of electron [24].

$$\mu = \left(\frac{\partial E}{\partial N}\right)_V$$ **Eq. 27**

2.5.3 Global reactivity indices

2.5.3.1 The electronegativity and the chemical potential

The previous expression is similar to the early expression of electronegativity presented in 1960 [25]. It is a global property that does not change from one point of space to another and defined as the derivative of the energy relative to a number of

number of electrons. It can be expressed depending on ionization and electron affinity.

$$\mu = -\chi = -{}^{1}/_{2}\,(I + A) \qquad \textbf{Eq. 28}$$

Where: μ is the electronic chemical potential; it is thus the local slope of the energy curve as a function of the electron number [25].

Upon employing further approximation by making use of Koopmans' theorem, one can arrive at the following expression:[26],[27]

$$\mu = -\chi = -{}^{1}/_{2}\,(E_{HOMO} + E_{LUMO}) \qquad \textbf{Eq. 29}$$

This expression built a link between the DFT and chemistry, i.e. atoms and molecules can be ranked on the basis of their ability to attract or lose electrons in the presence of atoms of another chemical species. it is therefore of fundamental importance in problems of chemical reactivity, even though historically it was introduced in an ‘empirical’ way and has been nowadays recovered within a well-founded theoretical framework.

2.5.3.2 The chemical hardness and softness

The chemical hardness is a qualitative indication of the polarizability of a chemical space, i.e. of the tendency of its electron cloud to get distorted by an external electrical field. It was introduced in 1963 by Pearson and Parr [28] in the context of studying acid base reactions.

Later they defined the expressed the hardness η as with the second-order derivative of electronic energy E with respect to the electron number N ad the softness as the inverse of it [29]:

$$\eta = \frac{1}{2}\frac{\partial^2 E}{\partial N^2} = \frac{1}{2}\frac{\partial \mu}{\partial N} \qquad \textbf{Eq. 30}$$

$$\eta = \left(\frac{\partial^2 E}{\partial N^2}\right)_{v(r)} = \left(\frac{\partial \mu}{\partial N}\right)_{v(r)} = I - A = -(E_{HOMO} - E_{LUMO}) \qquad \textbf{Eq. 31}$$

$$S = \frac{1}{\eta} = \frac{\partial N}{\partial \mu} \qquad \textbf{Eq. 32}$$

2.5.3.3 The electrophilicity index

The electrophilicity ω [28],[30] is defined as energy stabilization due to charge transfer when the system acquires an ΔN electronic charge. the approximate expression of ω in the basic state is:

$$\omega = \frac{\mu^2}{2\eta} \qquad \textbf{Eq. 33}$$

2.5.3.4 La nucleophilicity

The nucleophilicity measures the ability of a molecule to loss its electronic density when reacting electron-deficient center [31]. They and be defined it as the oposite of the ionization potential and used the energy of the HOMO orbital to calculated by the Kohn Sham to obtain the empiric formulas of the nucleophilicity.

$$\mathbf{N} = \boldsymbol{\varepsilon_{HOMO}} - \boldsymbol{\varepsilon_{LUMO}} \qquad \textbf{Eq. 34}$$

it is worth to mention that in 2002 Domingo and coworkers have demonstrated that complexes molecules containing many functional groups can be classified as strong nucleophiles and electrophiles at the same time [32], hence systematic classification of a strong nucleophile as a weak electrophiles is no longer correct

in this context we not that the tetracyanoetheylene (TCE) is the reference of the nucleophilicity scale as he has the lowest HOMO energy among many organic compounds in participating in cycloaddition reactions.

2.5.4 Local reactivity indices

2.5.4.1 Fukui indices

The term of local reactivity saw the light on 1984 when Parr [33] described his first local descriptor which made a link between the FMO theory and chemical reactivity.

$$\boldsymbol{f}(\mathbf{r}) = \left(\boldsymbol{\partial^2 E}/_{\boldsymbol{\partial N}}\ \boldsymbol{\delta V(r)}\right) \qquad \textbf{Eq. 35}$$

By applying the perturbation theory [23], the above expression can be written as:

$$f(\mathbf{r}) = \left(\partial\rho(r)/\partial N\right)_V$$ **Eq. 36**

This second order derivative highlighted the role of the frontier orbitals in chemical reactivity. In honor of Fukui, this local descriptor f(r) was termed the Fukui function.

The evaluation of f(r) is very complicated; Yang and Mortier [34] gave a simple process for calculating f(K) (Fukui condensed function), based on the Mulliken population analysis (MPA) and the finite difference approximation of Fukui function in a finite difference approximation, for a system of N electrons, f (K) values for the atom K are given by:

$$f_k^+ = [q_k(N+1) - q_k(N)]$$ **Eq. 37**

$$f_k^- = [q_k(N) - q_k(N-1)]$$ **Eq. 38**

$$f_k^0 = [q_k(N+1) - q_k(N-1)]/2$$ **Eq. 39**

q_K represents the electron population of the atom within a molecule while f_k^+ and f_k^- represent the ability of the k atom to react with a nucleophilic and electrophilic, respectively. A high value of f_k^+ indicates that the k atom has an electrophilic character, on the other hand, a high value of f_k^- means that site k is

more nucleophilic and available for electronic attacks. A high value of f_k^0 at site k indicates a high probability of a radical attack.

2.5.4.2 Local harness and local softness

Yang and Parr [29] estimated that the concepts of hardness and softness are intimately related to the Fukui functions. Therefore, they provided local definitions thereof. Actually, the Fukui function f (r) and the local softness s(r) are very often used as local reactivity parameters. Yang and Parr (1985) then define local softness as:

$$\mathbf{s}(\boldsymbol{r}) = \left(\frac{\boldsymbol{\partial \rho(r)}}{\boldsymbol{\partial N}}\right)_{\boldsymbol{V}} \left(\frac{\boldsymbol{\partial N}}{\boldsymbol{\partial \mu}}\right)_{\boldsymbol{V}} = \mathbf{f}(\mathbf{r})\boldsymbol{S} \qquad \textbf{Eq. 40}$$

where S is the global softness. The local softness is the inverse of the local hardness [35] and enables to locate the specific reaction sites between two reactants.

Thus, condensed local softness S_k^+can be easily calculated from condensed Fukui functions $f_k^{\pm}$ and S global softness:

$$\mathbf{S}_{\boldsymbol{K}}^{-} = \mathbf{S}\,[\boldsymbol{q_k(N)} - \boldsymbol{q_k(N-1)}\,] = \boldsymbol{S}\,\mathbf{f}_{\boldsymbol{K}}^{-} \qquad \textbf{Eq. 41}$$

$$\mathbf{S}_{\boldsymbol{K}}^{+} = \mathbf{S}\,[\boldsymbol{q_k(N+1)} - \boldsymbol{q_k(N)}\,] = \boldsymbol{S}\,\mathbf{f}_{\boldsymbol{K}}^{+} \qquad \textbf{Eq. 42}$$

2.5.4.3 Local electrophilicity

The most electrophilic center within a chemical structure as ben defined in 2003 by Chattarajet and coworkers [36]depending the global electrophilic index and the Fukui index f_k^+

$$\omega_k^+ = \omega\, f_k^+$$ **Eq. 43**

2.5.4.4 Local nucleophilicity

Similarely; the most nucleophilic site can be easily identified by the local nucleophilic index, N_k defined as the product of the global nucleophilic index N and the nucleophilic Fukui index f_k^- .

$$N_k = N\, f_k^-$$ **Eq. 44**

2.5.4.5 The Parr function

The Parr function proposed by Domingo in 2013 [37] properly characterizes the most reactive sites along polar chemical process, it is based on the change of the electronic spin density observed during transferring electron density between the most reactive centres in a reacting process.

$$P^-(r) = \rho_S^{rc}(r) \quad for\ electrophilic\ attacks$$ **Eq. 45**

$$P^+(r) = \rho_S^{ra}(r) \quad for\ nucleophilic\ attacks$$ **Eq. 46**

Where ρ_{ks}^{rc} and ρ_{ks}^{ra} are the atomic spin density of the radical cation and the radical anion respectively.

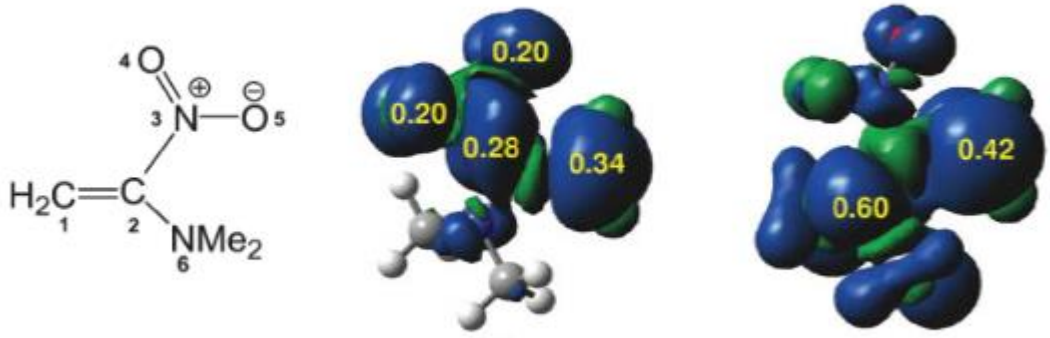

Figure 2-4: representation of: (b) ASD of the radical anion and the local electrophilic Parr function values, (c) ASD of the radical cation and the local nucleophilic Parr function values

2.6 Topological analysis of the electron localization function (ELF)

In the last decade of the last century, Becke and Edgecombe [38] proposed a quantum tools allowing the topological analysis of the electron density, named Electron Localization Function (ELF); This function measures the probability of finding the electron and assess the electron pair localization characterizing the corresponding electron density.

Originally ELF is defined as follow:

$$\mathbf{D}(\boldsymbol{r}) = \boldsymbol{\tau}_{\boldsymbol{\sigma}}(\mathbf{r}) - \frac{\mathbf{1}}{\mathbf{4}} \frac{(\boldsymbol{\nabla}\boldsymbol{\rho}_{\boldsymbol{\sigma}}(\boldsymbol{r}))^{\mathbf{2}}}{\boldsymbol{\rho}_{\boldsymbol{\sigma}}(\boldsymbol{r})} = \mathbf{f}(\mathbf{r})\boldsymbol{S} \qquad \textbf{Eq. 47}$$

where ρ is the electron spin density and τ the kinetic energy density.

Within the context of DFT, ELF is a density-based property that can be interpreted in terms of the positive-definite local Pauli and Thomas Fermi kinetic energy densities in a given system. The Pauli repulsion between two like-spin electrons, described by the size of D(r), is taken as a measure of the electron localization. Using the corresponding factor found for a uniform electron gas, Becke and Edgecombe, defined ELF as:

$$ELF = \frac{1}{1 + \chi^2}$$ **Eq. 48**

$$\chi = \frac{D_s(r)}{D_0(r)}$$ **Eq. 49**

Note that X is the ‘’kernel’’ of the ELF and can expressed depending to the excess of local kinetic energy due to the repulsion of Pauli DS and a reference value of the homogeneous gas of electrons D_0 (constant density) [39]

After that; Silvi and Savin [40] presented the ELF in a very chemical fashion, using their topological analysis as an appealing model of chemical bonding. Indeed, they introduced the notion of basins which correspond to domains where the possibility of finding electron pair is maximal, thereafter these basins are classified into cores basin and valence basins. While core basins are located around the nuclei (except for hydrogen) and are labeled C(A), where A represents the symbol of the atom; the valence basins are divided to monosynaptic, disynaptic, trisynaptic basins according to their connectivity to the core basins i, e there are monosynaptic labelled V(A) correspond to lone pairs or non-bonding regions, disynaptic labelled V(A,B) correspond bonding region A-B, trisynaptic basins and so on. There are also higher synaptic orders but Hydrogen is a particular case because it does not have core electrons.

Table 2-1: classification of basins according to their synaptic order

Name	symbole	Chemical interpretation
Monosynaptic	V (A)	lone pairs or non-bonding regions
disynaptic	V(X,Y)	Connection between two nuclei A ad B (Covalent bond)
polysynaptic	V(X, Y,…)	multicentre bonding

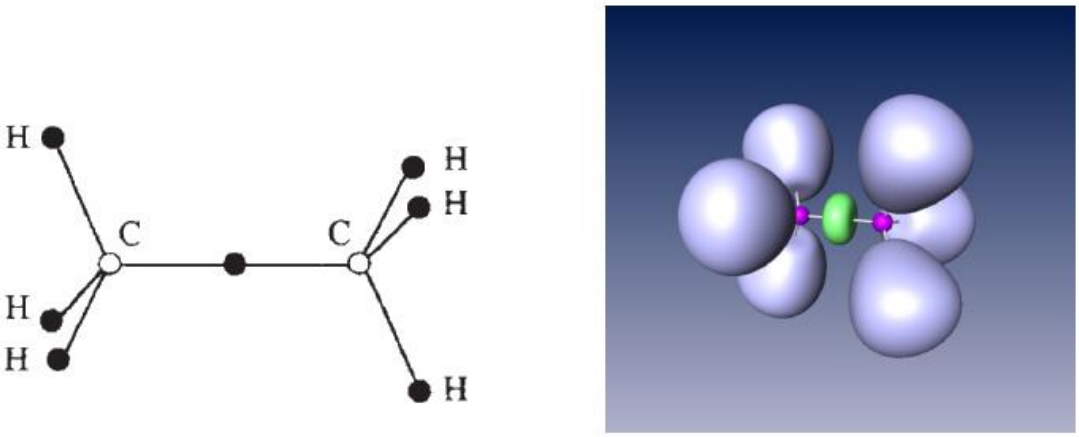

Figure 2-5: Illustration of attractors on the ethane molecule (left) and 3D representation of the isosurface ELF isosurface =0.8 (right)

The topological analysis of the ELF of the ethane molecule shows that the core basins of the carbon atom are represented in magenta, the valence basin of the C-C

covalent bond is represented in green while the basin of hydrogen are represented in blue [40],[41] .

As shown in the previous figure the ELF provides a qualitative representation of the chemical structure; a quantitative estimation of the basins electronic populations is achievable by integrating the electronic density.

$$\boldsymbol{N(x) = \int \rho(r)\ dr^3} \qquad \textbf{Eq. 50}$$

In this context we note that the atom valence population is the sum of the population of the basins surrounding its core and the population of the entire system is the sum of populations of the basin of atoms.

$$\boldsymbol{N_V(x) = \sum_i \left(V(A) + \sum_{A \neq B} \sum [V_i(A, B, \dots)] \right)} \qquad \textbf{Eq. 51}$$

2.7 QTAIM analysis

This theory is introduced by Bader and his group [42],[43] whose greatly contributed on the development of this theory and widen its application on reviling chemical bonding and physico-chemical properties of chemical systems. [44]. It based on the local maximum exhibited by the electron density only on nuclei positions, i.e. the first derivative $\rho(r)$ die out; these points are called critical points.

$$\boldsymbol{\nabla \rho(r_c) = i\frac{\partial \rho}{\partial x} + j\frac{\partial \rho}{\partial y} + k\frac{\partial \rho}{\partial z} = 0} \qquad \textbf{Eq. 52}$$

Note that under some circumstances some exceptions are observed.

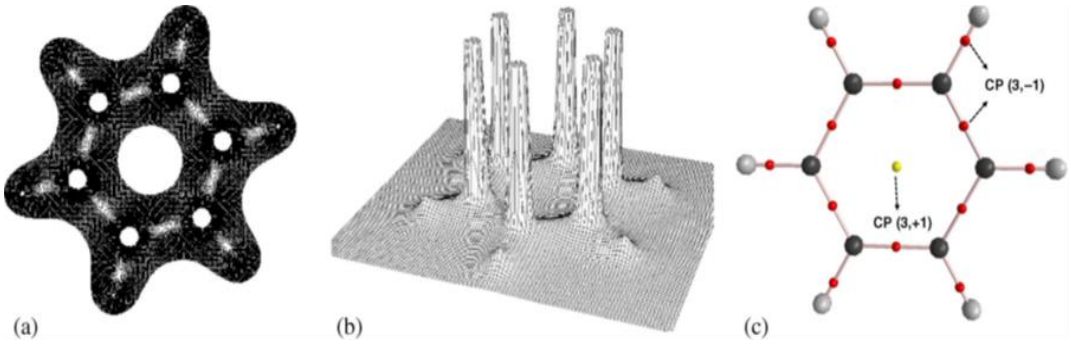

Figure 2-6: (a) Electron density contour map; (b) Relief map; (c) Molecular graph of Benzene

The exploration the second derivative of the electron density to define the sign of minimum or the maximum lead to a matrix of nine components known as the Hessian of $\rho(r_c)$

$$\nabla^2\rho(r_c) = \frac{\partial^2\rho(r_c)}{dx'^2} + \frac{\partial^2\rho(r_c)}{dy'^2} + \frac{\partial^2\rho(r_c)}{dz'^2} = \lambda_1 + \lambda_2 + \lambda_3 \qquad \textbf{Eq. 53}$$

$$H(r) = \begin{pmatrix} \frac{\partial^2\rho}{\partial x^2} & 0 & 0 \\ 0 & \frac{\partial^2\rho}{\partial y^2} & 0 \\ 0 & 0 & \frac{\partial^2\rho}{\partial z^2} \end{pmatrix} = \begin{pmatrix} \lambda_1 & 0 & 0 \\ 0 & \lambda_2 & 0 \\ 0 & 0 & \lambda_3 \end{pmatrix} \qquad \textbf{Eq. 54}$$

Where: λ1, λ2 and λ3 are represent the principal axes of curvature

On topological analysis language, CPs can be classified into four types according to how many eigenvalues of Hessian matrix of real space function are negative, these are Cps are:

(3,-3): All three eigenvalues of Hessian matrix of function are negative (-,-,-), namely the local maximum. For electron density analysis and for heavy atoms, the position of (3,-3) are nearly identical to nuclear positions, hence (3,-3) is also called *nuclear critical point (NCP).*

(3,-1): Two eigenvalues of Hessian matrix of function are negative (-,-,+), namely the second order saddle point. For electron density analysis, (3,-1) generally appears between attractive atomic pairs and hence commonly called as *bond critical point (BCP).*

The value of real space functions at BCP have great significance, for example the value of ρ and the sign of $\nabla^2\rho$ at BCP are closely related to bonding strength and bonding type respectively for analogous bonds [45] and used to predict hydrogen bond binding energies [46]

(3,+1): Only one eigenvalue of Hessian matrix of function is negative (+,+,-), namely first order saddle point (like transition state in potential energy surface). For electron density analysis, (3,+1) generally appears in the center of ring system and displays steric effect, hence (3,+1) is often named as *ring critical point (RCP).*

(3,+3): None of eigenvalues of Hessian matrix of function are negative (+,+,+) , namely the local minimum. For electron density analysis, (3,+3) generally appears in the center of cage system, hence is often referred to as *cage critical point (CCP).*

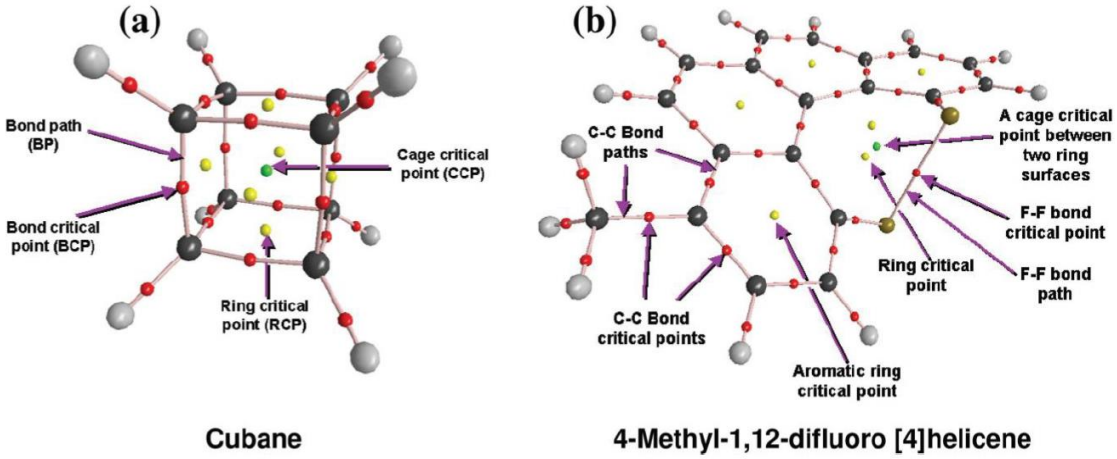

Figure 2-7: different types of CP

QTAIM analysis not just enough identify BCP and covalent bonds based on electron density but surpass it to characterize and assess the strength of system`s bond such as hydrogen ones and weak interactions by employing other parameters such as Laplacian of electron density, the energy density (H_{bcp}), the gradient of the electronic density (ρ_{bcp}), and its Laplacian $(\nabla^2 \rho_{bcp})$ [47] [48].

The Laplacian of the electron density in a critical point cp, $(\nabla^2 \rho_{bcp})$, is a very captivating parameter that determines where ρ_{bcp} is locally accumulated, $(\nabla^2 \rho_{bcp}) < 0$, and locally depleted, $(\nabla^2 \rho_{bcp}) > 0$. Thus, the sign of $(\nabla^2 \rho_{bcp})$ determines which of these two competing effects is dominant, allowing the characterization of (3, − 1) bcps associated with covalent bonds, $(\nabla^2 \rho_{bcp}) < 0$ and high ρ_{bcp}values, and those associated with ionic bonds or weak non-covalent interactions such as hydrogen bonds

As proposed by Rosas et al [47] , HBs interactions could be classified according to three types, in which strong HBs are characterized by a Laplacian $(\nabla^2 \rho_{bcp}) < 0$ and a total electron energy density, $(H_{bcp}) < 0$. A medium strength HBs are characterized by a, $(\nabla^2 \rho_{bcp}) < 0$ and $(H_{bcp}) > 0$, while weak strength HBs are defined by, $(\nabla^2 \rho_{bcp}) > 0$ and $(H_{bcp}) > 0$.

2.8 NCI analysis

Also known as Reduced density gradient (RDG) [49] , NCI analysis is a tool used to locate the weak non covalent interactions such as van der Waals interactions, hydrogen bonds and steric clashes in a chemical system, this technique is based on the on the idea of using the density and its first derivative.

$$\boldsymbol{RDG(r) = \frac{1}{2(3\pi^2)^{1/3}} \frac{|\nabla \rho(r)|}{\rho(r)^{4/3}}} \qquad \textbf{Eq. 55}$$

The RDG describes the deviation from a homogeneous electron distribution. In regions far from the molecule, in which the density decays to zero exponentially,

the reduced gradient will have very large positive values. In regions of covalent bonding and non-covalent interactions, the reduced gradient has very small values, close to zero.

On the other hand to distinguish between types of non-covalent interactions in a chemical system; the sign of the Laplacian of the density, $\nabla^2\rho(r)$ can be used. To do so, the three eigenvalues λ_i of the Hessian (second derivative) of the electron-density are calculated ($\lambda_1 \leq \lambda_2 \leq \lambda_3$). At the nuclei, all eigenvalues are negative, since the density is at a local maximum. In covalent bonds, the Hessian has one positive eigenvalue and two negative eigenvalues ($\lambda_1 < 0, \lambda_2 < 0, \lambda_3 > 0$) On the other hand, in regions of steric clashes or strain in the interatomic region, the second eigenvalue will be positive. Therefore, the sign of the second eigenvalue of the Hessian, λ_2 can be used to distinguish between bonded $\lambda_2 < 0$ and non-bonded $\lambda_2 > 0$ interactions. The strength of the interaction can be assessed by the density itself: higher density values at the location of the non-covalent interactions indicate a stronger interaction. For this reason, the NCI method relies on the inspection of the reduced density gradient versus sign $\lambda_2\ \rho(r)$ plots:

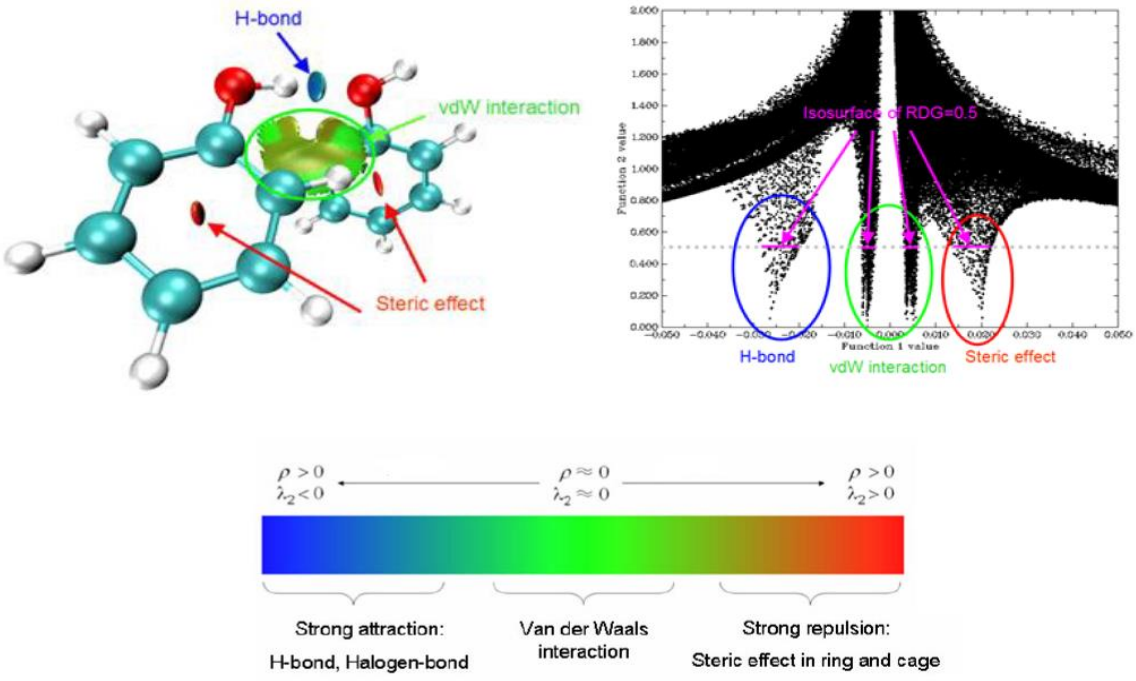

Figure 2-8: representation of NCI plots of the phenol dimer

2.9 References

[1] W. Heisenberg, “W. heisenberg, z. phys. 43, 172 (1927),” *Z. Phys*, vol. 43, p. 172, 1927.

[2] W. Kohn, “Nobel Lecture: Electronic structure of matter—wave functions and density functionals,” *Rev. Mod. Phys.*, vol. 71, no. 5, p. 1253, 1999.

[3] P. Hohenberg and W. Kohn, “No Title,” *Phys. Rev. B*, vol. 136, p. 864, 1964.

[4] P. Chaquin, *Manuel de chimie théorique: application à la structure et à la réactivité en chimie moléculaire*. Ellipses, 2006.

[5] W. Kohn and L. J. Sham, “Phys. Rev. 140, A1133.” 1965.

[6] P. A. M. Dirac, “Note on exchange phenomena in the Thomas atom,” in *Mathematical proceedings of the Cambridge philosophical society*, Cambridge University Press, 1930, pp. 376–385.

[7] S. H. Vosko, L. Wilk, and M. Nusair, “Accurate spin-dependent electron liquid correlation energies for local spin density calculations: a critical analysis,” *Can. J. Phys.*, vol. 58, no. 8, pp. 1200–1211, 1980.

[8] J. A. White and D. M. Bird, “Implementation of gradient-corrected exchange-correlation potentials in Car-Parrinello total-energy calculations,” *Phys. Rev. B*, vol. 50, no. 7, p. 4954, 1994.

[9] T. Van Voorhis and G. E. Scuseria, “A novel form for the exchange-correlation energy functional,” *J. Chem. Phys.*, vol. 109, no. 2, pp. 400–410, 1998.

[10] J. P. Perdew, S. Kurth, A. Zupan, and P. Blaha, “Accurate density functional with correct formal properties: A step beyond the generalized gradient approximation,” *Phys. Rev. Lett.*, vol. 82, no. 12, p. 2544, 1999.

[11] A. D. Becke, “A new mixing of Hartree–Fock and local density-functional theories,” *J. Chem. Phys.*, vol. 98, no. 2, pp. 1372–1377, 1993.

[12] K. Raghavachari, “Perspective on ‘Density functional thermochemistry. III. The role of exact exchange’ Becke AD (1993) J Chem Phys 98: 5648–52,” *Theor. Chem. Acc.*, vol. 103, pp. 361–363, 2000.

[13] P. J. Stephens, F. J. Devlin, C. F. Chabalowski, and M. J. Frisch, “Ab initio calculation of vibrational absorption and circular dichroism spectra using density functional force fields,” *J. Phys. Chem.*, vol. 98, no. 45, pp. 11623–11627, 1994.

[14] B. Roux and T. Simonson, “Implicit solvent models,” *Biophys. Chem.*, vol. 78, no. 1–2, pp. 1–20, 1999.

[15] L. Onsager, “Electric moments of molecules in liquids,” *J. Am. Chem. Soc.*, vol. 58, no. 8, pp. 1486–1493, 1936.

[16] E. Cances, B. Mennucci, and J. Tomasi, “A new integral equation formalism for the polarizable continuum model: Theoretical background and applications to isotropic and anisotropic dielectrics,” *J. Chem. Phys.*, vol. 107, no. 8, pp. 3032–3041, 1997.

[17] M. Cossi, V. Barone, R. Cammi, J. T.-C. P. Letters, and undefined 1996, “Ab initio study of solvated molecules: a new implementation of the polarizable continuum model,” *Elsevier*, Accessed: Jul. 25, 2021. [Online]. Available: https://www.sciencedirect.com/science/article/pii/0009261496003491

[18] V. Barone, M. Cossi, and J. Tomasi, “Geometry optimization of molecular structures in solution by the polarizable continuum model,” *J. Comput. Chem.*, vol. 19, no. 4, pp. 404–417, 1998, doi: 10.1002/(SICI)1096-987X(199803)19:4<404::AID-JCC3>3.0.CO;2-W.

[19] S. Miertuš, E. Scrocco, and J. Tomasi, “Electrostatic interaction of a solute with a continuum. A direct utilizaion of AB initio molecular potentials for the prevision of solvent effects,” *Chem. Phys.*, vol. 55, no. 1, pp. 117–129, 1981.

[20] R. Cammi and J. Tomasi, “Remarks on the use of the apparent surface charges (ASC) methods in solvation problems: Iterative versus matrix-inversion procedures and the renormalization of the apparent charges,” *J. Comput. Chem.*, vol. 16, no. 12, pp. 1449–1458, 1995.

[21] P. Hohenberg and W. Kohn, “Inhomogeneous electron gas,” *Phys. Rev.*, vol. 136, no. 3B, p. B864, 1964.

[22] R. G. Parr and W. Yang, “Density-Functional Theory of Atoms and Molecules: Oxford Science Publications,” *New York*. 1989.

[23] W. Kohn and L. J. Sham, “Self-consistent equations including exchange and correlation effects,” *Phys. Rev.*, vol. 140, no. 4A, p. A1133, 1965.

[24] M. B. Einhorn and R. Blankenbecler, “Bounds on scattering amplitudes,” *Ann. Phys. (N. Y).*, vol. 67, no. 2, pp. 480–517, 1971.

[25] R. P. Iczkowski and J. L. Margrave, “Electronegativity,” *J. Am. Chem. Soc.*, vol. 83, no. 17, pp. 3547–3551, 1961.

[26] R. G. Pearson, “Absolute electronegativity and hardness correlated with molecular orbital theory,” *Proc. Natl. Acad. Sci.*, vol. 83, no. 22, pp. 8440–8441, 1986.

[27] A. J. Cohen, P. Mori-Sánchez, and W. Yang, “Challenges for density functional theory,” *Chem. Rev.*, vol. 112, no. 1, pp. 289–320, 2012.

[28] R. G. Parr and R. G. Pearson, “Absolute hardness: companion parameter to absolute electronegativity,” *J. Am. Chem. Soc.*, vol. 105, no. 26, pp. 7512–7516, 1983.

[29] W. Yang and R. G. Parr, “Hardness, softness, and the fukui function in the electronic theory of metals and catalysis.,” *Proc. Natl. Acad. Sci.*, vol. 82, no. 20, pp. 6723–6726, 1985.

[30] A. T. Maynard, M. Huang, W. G. Rice, and D. G. Covell, “Reactivity of the HIV-1 nucleocapsid protein p7 zinc finger domains from the perspective of density-functional theory,” *Proc. Natl. Acad. Sci.*, vol. 95, no. 20, pp. 11578–11583, 1998.

[31] L. R. Domingo, E. Chamorro, and P. Pérez, “Understanding the reactivity of captodative ethylenes in polar cycloaddition reactions. A theoretical study,” *J. Org. Chem.*, vol. 73, no. 12, pp. 4615–4624, Jun. 2008, doi: 10.1021/JO800572A.

[32] L. R. Domingo, M. J. Aurell, P. Pérez, and R. Contreras, “Quantitative characterization of the global electrophilicity power of common diene/dienophile pairs in Diels–Alder reactions,” *Tetrahedron*, vol. 58, no. 22, pp. 4417–4423, 2002.

[33] R. G. Parr and W. Yang, “No Title,” *J. Am. Chem. Soc.*, vol. 106, p. 4049, 1984.

[34] W. Yang and W. J. Mortier, “The use of global and local molecular parameters for the analysis of the gas-phase basicity of amines,” *J. Am. Chem. Soc.*, vol. 108, no. 19, pp. 5708–5711, 1986.

[35] M. Berkowitz and R. G. Parr, “Molecular hardness and softness, local hardness and softness, hardness and softness kernels, and relations among these quantities,” *J. Chem. Phys.*, vol. 88, no. 4, pp. 2554–2557, 1988.

[36] P. K. Chattaraj, B. Maiti, and U. Sarkar, “Philicity: a unified treatment of chemical reactivity and selectivity,” *J. Phys. Chem. A*, vol. 107, no. 25, pp. 4973–4975, 2003.

[37] E. Chamorro, P. Pérez, and L. R. Domingo, “On the nature of Parr functions to predict the most reactive sites along organic polar reactions,” *Chem. Phys. Lett.*, vol. 582, pp. 141–143, 2013, doi: 10.1016/j.cplett.2013.07.020.

[38] A. D. Becke and K. E. Edgecombe, “A simple measure of electron localization in atomic and molecular systems,” *J. Chem. Phys.*, vol. 92, no. 9, pp. 5397–5403, 1990.

[39] A. Savin, A. D. Becke, J. Flad, R. Nesper, H. Preuss, and H. G. Von Schnering, “A new look at electron localization,” *Angew. Chemie Int. Ed. English*, vol. 30, no. 4, pp. 409–412, 1991.

[40] B. Silvi and A. Savin, “Classification of chemical bonds based on topological analysis of electron localization functions,” *Nature*, vol. 371, no. 6499, pp. 683–686, 1994.

[41] Y. Grin, A. Savin, and B. Silvi, “The ELF perspective of chemical bonding,” *Chem. Bond Fundam. Asp. Chem. Bond.*, pp. 345–382, 2014.

[42] R. F. W. Bader, “Atoms in molecules,” *Acc. Chem. Res.*, vol. 18, no. 1, pp. 9–15, 1985.

[43] R. F. W. Bader, “A quantum theory,” *Clarendon Oxford, UK*, 1990.

[44] R. F. W. Bader and D.-C. Fang, “Properties of atoms in molecules: caged atoms and the Ehrenfest force,” *J. Chem. Theory Comput.*, vol. 1, no. 3, pp. 403–414, 2005.

[45] A. Becke, *The quantum theory of atoms in molecules: from solid state to DNA and drug design*. John Wiley & Sons, 2007.

[46] R. D. Bach and H. B. Schlegel, “Bond dissociation energy of peroxides revisited,” *J. Phys. Chem. A*, vol. 124, no. 23, pp. 4742–4751, 2020.

[47] I. Rozas, I. Alkorta, and J. Elguero, “Behavior of ylides containing N, O, and C atoms as hydrogen bond acceptors,” *J. Am. Chem. Soc.*, vol. 122, no. 45, pp. 11154–11161, 2000.

[48] S. J. Grabowski, W. A. Sokalski, E. Dyguda, and J. Leszczyński, “Quantitative classification of covalent and noncovalent H-bonds,” *J. Phys. Chem. B*, vol. 110, no. 13, pp. 6444–6446, 2006.

[49] E. R. Johnson, S. Keinan, P. Mori-Sánchez, J. Contreras-García, A. J. Cohen, and W. Yang, “Revealing noncovalent interactions,” *J. Am. Chem. Soc.*, vol. 132, no. 18, pp. 6498–6506, 2010.

Chapter 3: Pyrazolidinones and their derivatives in organic chemistry

3.1 Introduction

Pyrazolidinones; sometimes called pyrazolidin-3-ones or 3-Pyrazolidinones and their derivatives represent a fascinating class of compounds that have garnered considerable interest in the field of medicinal chemistry. [1],[2 These compounds are characterized by a pyrazole ring fused with a four-membered cyclic lactam, forming the pyrazolidinone core structure. The unique combination of these two heterocycles imparts distinct chemical and biological properties, making pyrazolidinone derivatives versatile compounds in many fields.

The first studies of pyrazolidinones back to 1940 [3], [4] after that and due to the importance of these compounds in chemical processes; the number of studies have raised significantly. Up to now the evolution of the 3-Pyrazolidinone and its derivatives has been reported by Dorn 1981 [5] Claramunt and Elguero in 1991 [6] and in part by Svete in 2008 [7].

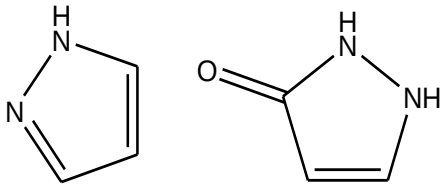

Pyrazole ring Pyrazolidinone

Scheme 3-1: Pyrazolidinones core structure

3.2 Importance of pyrazolidinones and derivatives

The unique structural features of pyrazolidinone derivatives contribute to their remarkable biological activities. Both mono and bi-cyclic derivatives, have demonstrated potential across a wide range of therapeutic areas.

In the antimicrobial field [8]–[10], pyrazolidinone derivatives have shown promising activity against both Gram-positive and Gram-negative bacteria [1].They often function by inhibiting key enzymes or disrupting crucial metabolic pathways, making them valuable candidates for combating antibiotic-resistant strains.

Moreover, some pyrazolidinone derivatives have shown anticancer, anti-inflammatory, and antiviral potential [8],[11], i.e. as anti-cancer Several compounds have demonstrated the ability to inhibit cancer cell proliferation, induce apoptosis, or interfere with specific signaling pathways involved in tumor growth. Their diverse mechanisms of action make them promising candidates for further development in cancer therapy.

In the inflammation treatment; pyrazolidinone derivatives have shown analgesic and antipyretic effects as well as anti-inflammatory by modulating key inflammatory mediators, including cytokines and enzymes such as cyclooxygenase (COX). Such compounds hold potential for the treatment of chronic inflammatory disorders, including rheumatoid arthritis and inflammatory bowel disease [8],[11].

Furthermore, and in the context of antiviral activity, pyrazolidinone derivatives have been explored for their inhibitory effects against various viral infections, including HIV, hepatitis B, and influenza. These compounds often target specific viral enzymes or proteins, interfering with viral replication or entry into host cells.

Addionally some bicyclic pyrazolidinones are used, among others, as drugs to relieve Alzheimer's disease [10].

Out of the medicinal area; pyrazolidinone derivatives are used as scaffolds in organocatalysis [12],[13] and as dyes in food and other industries [5], [14], [15].

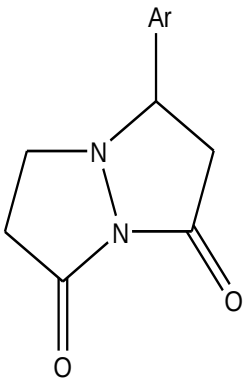

Herbicides, Pesticides

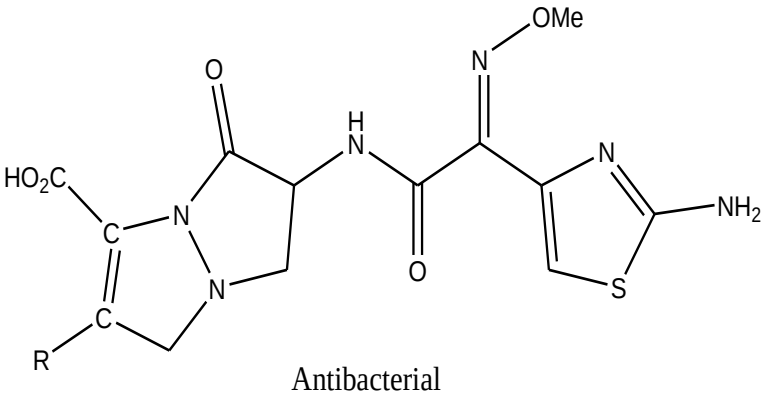

Antibacterial
LY173013: R= COOMe
Antibiotics
LY186826: R=COMe
LY193239: R=SO2Me
LY255262: R= CN

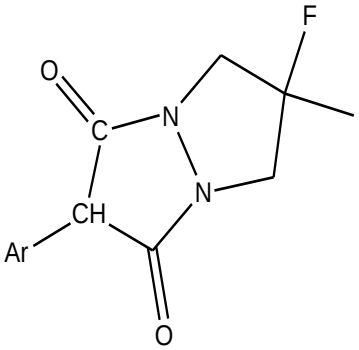

Anti-alzhaimer

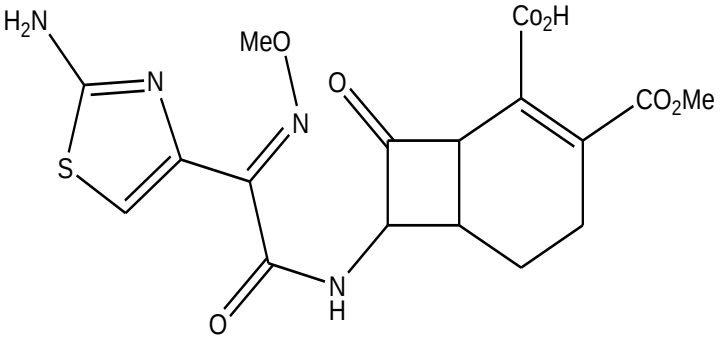

LY212280

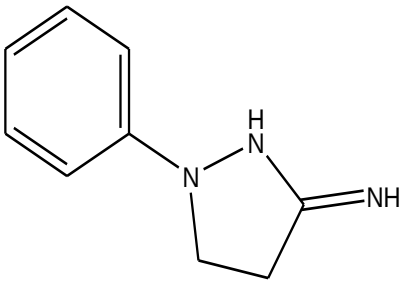

Phenidone

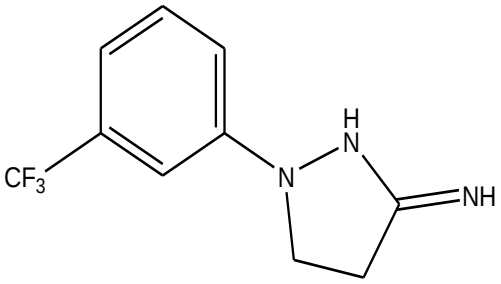

Inhibitors
BW755C

Scheme 3-2: some biologically active pyrazolidinones

3.3 Synthesis of pyrazolidinones and derivatives

3.3.1 Synthesis from α, β unsaturated esters

One of the most known ways for obtaining the pyrazolidinones is the heat of α, β esters (acrylates) with excess hydrazine hydrates [5],[16] however the use of excess of hydrazine hydrates makes sensitive functional groups also react. This limitation cannot be avoided by the incorporation of nucleophile resistant protecting groups in the process because they are usually difficult to remove.

The example below shows an alternative way to overcome this disadvantage; it consists of Wittig-Horner condensation of methyl 2-(benzyloxycarbonylamino)-2 (dimethoxyphosphoryl) acetate (**1**) with aldehydes and ketones following a slightly modified procedure by Schmidt and co-workers [17]. Acrylates (**2a–i**) were then treated with excess of N2H4·H2O in an alcohol (MeOH, EtOH, or nPrOH) at 20–100 °C to afford the corresponding 3-pyrazolidinones (**3a–i)** in 23–100% yields (Scheme 3.3). [18],[19]

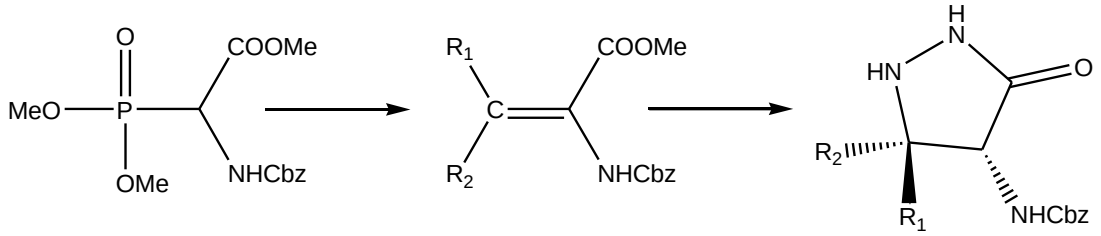

1 2a-i 3a-i

I) R1R2CO, DBU, CH2Cl2, r.t; II) N2H4.H2O, ROh r.t or reflux

Compound	R1	R2	Compound	R1	R2
3a	1-propyl	H	3f	3-nitrophenyl	H
3b	2-propyl	H	3g	4-nitrophenyl	H
3c	Me	Me	3h	4-chlorophenyl	H
3d	-(CH2)5-		3i	2-hydroxyphenyl	H
3e	Ph	H			

Scheme 3-3: synthesis of pyrazolidinones 4a-i

A recent example of utilization of α,β-unsaturated esters in the synthesis of 3- pyrazolidinones is a 'ring switching' transformation of commercially available 5,6-dihydro-2*H*pyran-2-one (**4**) with hydrazine hydrate in ethanol at room temperature. This reaction gave 5-(2-hydroxyethyl)pyrazolidin-3-one (**6a**) [20] in quantitative yield. It is also noteworthy, that 2-substituted analogues of (**6a)** could not be prepared in this way. For example, treatment of **(4)** with phenylhydrazine afforded the 1,4-addition intermediate (**5)**, which could not be converted into the corresponding pyrazolidinone (**6b)**, even under forcing conditions.

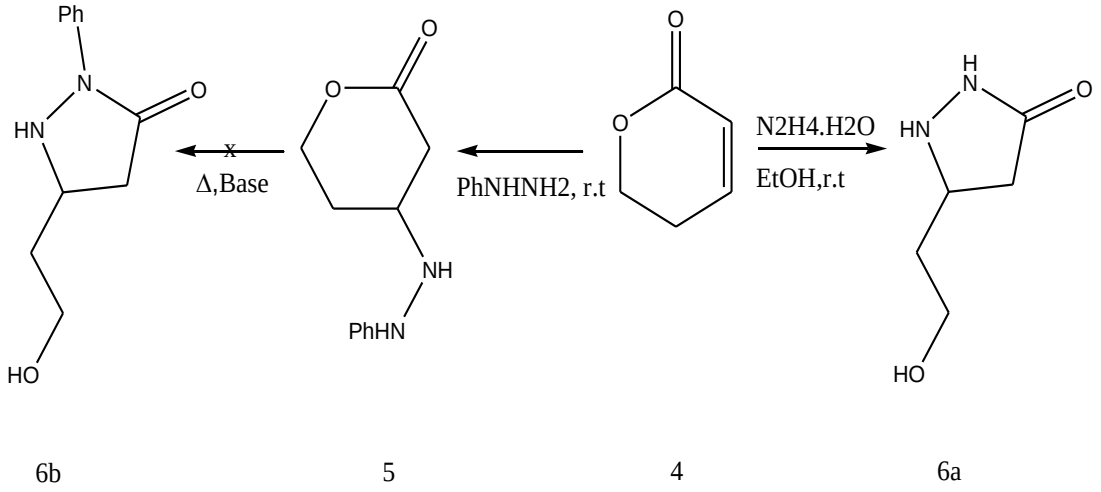

Scheme 3-4: synthesis of 5-(hydroxyethyl) pyrazolidinone (7a)

In summary, the formation of pyrazolidinones from hydrazines and α, β - unsaturated acids and their derivatives proceeds generally through a Michael addition followed by a exo-trisonal ring closure.

3.3.2 Synthesis from β-hydroxy esters

β-hydroxy esters are also suitable compounds for the preparation of pyrazolidinones. Jungheim and co-workers [21] reported in 1987 the preparation of 4-benzyloxycarbonylamino-3-pyrazolidinone (**8)** from methyl N-benzyloxycarbonyl-O-tosylserinate **(7)**

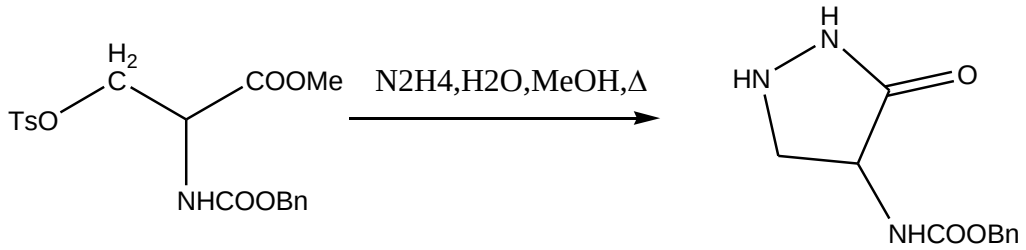

7 8

Scheme 3-5: synthesis of 4-benzyloxycarbonylamino-3-pyrazolidinone (8)

An example of non-racemic mixtures of pyrazolidinones prepared from ester has been reported also [22] by the conversion of S phenylalanine **(9)** into β-keto ester (**10**), this later was subjected to reduction reaction with NABH4 and chromatographic separation and recrystallization to give (3R,4S)-β-hydroxy ester (**11**) [23] and later the ester (**12**) after mesylation in pyridine which was in turn treated with excess hydrazine hydrate in dichloromethane to obtain the pyrazolidinones (**13**) and (**13**') as inseparable mixtures 62:38; 57% yield.

Another process is also possible from the ester (**12**); the cyclization with methylhydrazine gives two regioizomeric pyrazolidinones each as a mixture of epimers in 100% conversion. The products **14**, **14'**, **15**, and **15'** were formed in a ratio of 35:26:26:13.

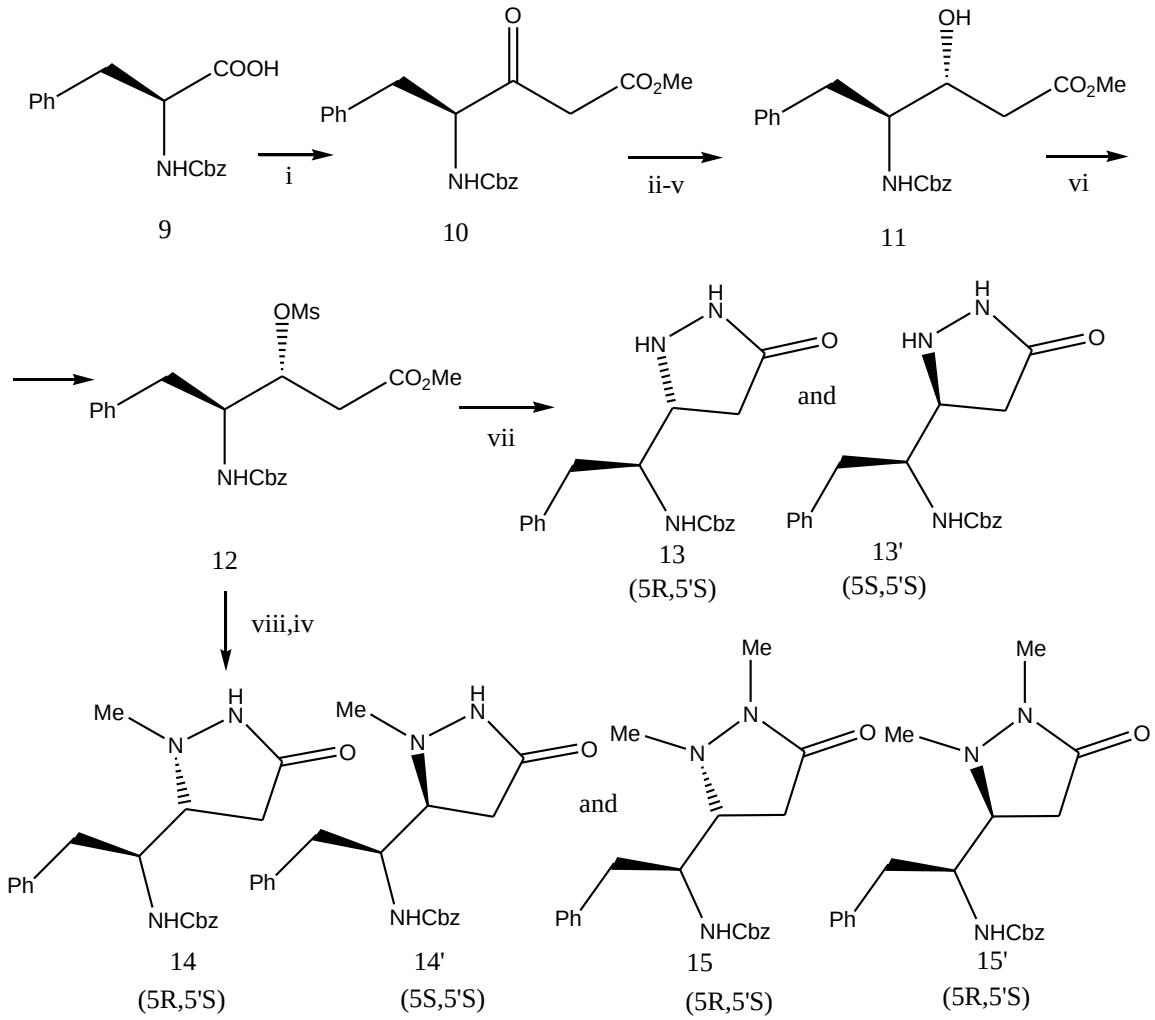

i) CDI, THF, r.t; ii) MeOAc, LDA, THF, -61°C; iii) $NABH_4$, MeOH, -5°C; iv) chromatographic separation
v) re crystallization; vi) MsCI, pyridine, -5°C; vii) N_2H_4 H_2O CH_2Cl_2, r.t ; viii) $MeNHNH_2$, CH_2Cl_2, r.t

Scheme 3-6: synthesis of non-racemic pyrazolidinones 13,13'-15,15

Another example of preparing pyrazolidinones from esters is shown in the scheme below where the pyrazolidinones (23a –c) are prepared starting from methyl acrylate **(16)**; A Michael addition of three amines [24] to **(16)** gives methyl β-alaninates (**17a**–**c)** , which were converted to esters (**18a**–**c)** which in turn hydrolyzed to afford **(19 a-c)** after three steps [23]. The Masamune-Claisen condensation of **(19 a-c)** give the corresponding β-keto esters **(20a–c)** in 87–92% yields. The reduction of this later in NaBH4 afford The pyrazolidinones **(23a-c)** after messalating alcohols (21 a-c) and cyclisation of the mesylates **(22a–c)** [25].

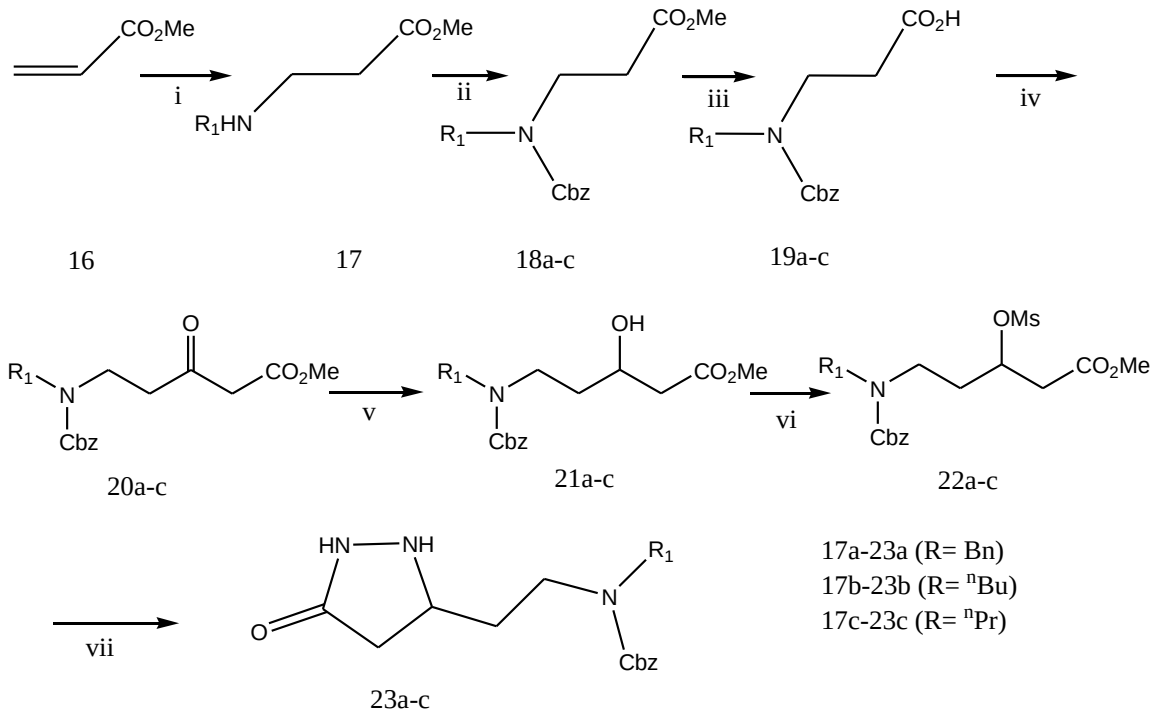

i) R^1NH_2, cat, DBU, r.t; ii) CICOOBn, CH_2Cl_2, Et_3N, 0-20 °C; iii) aq, NaOH, MeOH, r.t; iv) CDI, THF, r.t then potassium monomethyl malonate, $MgCl_2$, r.t; v) $NaBH_4$, MeOH, 0-20 °C; vi) MsCl, pyridine, 0-20 °C; vii) $N_2H_4H_2O$, MeOH, r.t

Scheme 3-7: synthesis of pyrazolidinones 23a-c

3.3.3 Synthesis from cycloaddition reactions of azomethin imines

The 1, 3-dipolar cycloaddition of azomethine imines with alkenes or alkynes is a frequent method for obtaining N,N-bicyclic pyrazolidinone derivatives [26]–[29] Many cycloaddition approaches have been reported and most of them are catalyzed [30]–[37].

A Free catalysed way is also available; Yang and co-workers [38] reported cycloaddition of N'N azomethine imines with trans-β-nitrostyrene **(25)** in different organic solvent and they get a bicyclic pyrazolidinones derivatives in good yield and stereoselectivity and noticed an increase of the yield in accordance with the increase of the temperature of the reaction.

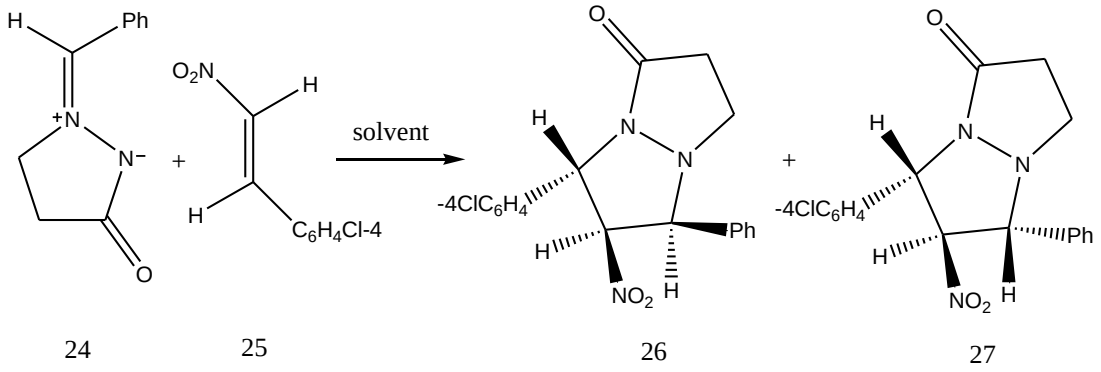

Scheme 3-8: synthesis of pyrazolidinones from azomethine imines

3.3.4 Enantioselective organometallic catalyzed synthesis of pyrazolidinones

Despite the increasing number of applications of pyrazolidinones, very few enantioselective organometallic catalytic syntheses had been cited in literature which push as to mention some related works in what follows:

On 1998 the Kobayashi's group [39] proposed the first enantioselective organometallic catalyzed synthesis of pyrazolidones by adding enantioselective silylated enolate on a hydrazine using a zirconium salt catalyst. The pyrazolidinone is obtained using samarium iodide with good retention of enantiomeric excess.

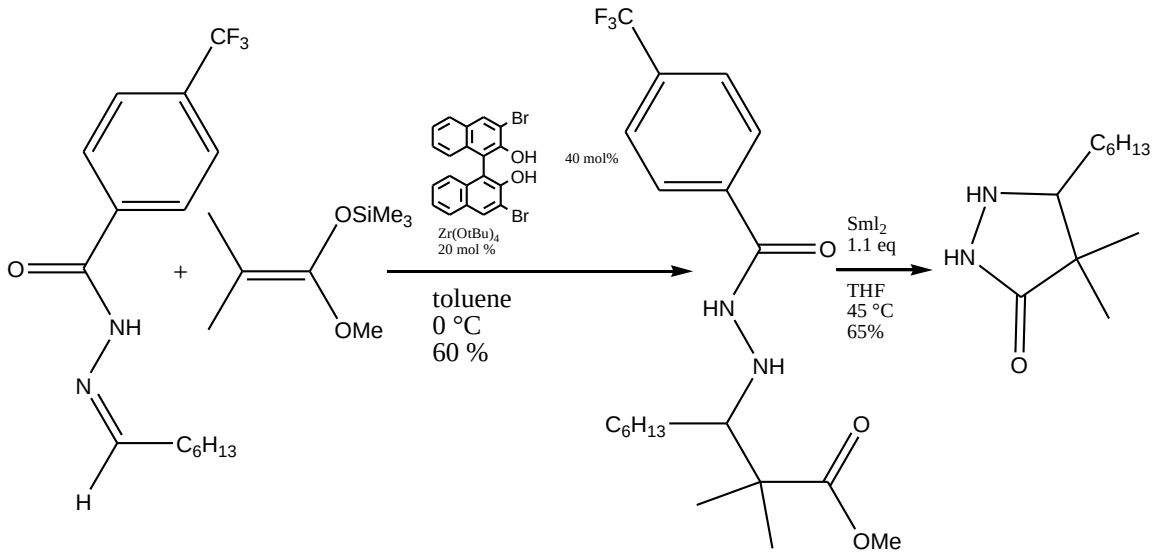

Scheme 3-9: enantioselective synthesis proposed by Kobayashi

Based on the use of magnesium complexed by chiral bis oxazoline, Sibi [35] synthetized with good yields and good enantiomeric excesses chiral pyrazolidinones via aza Michael reaction followed by intramolecular cyclization on an acrylamide; however, the good selectivity of the reaction is limited to the use of aliphatic acrylamides.

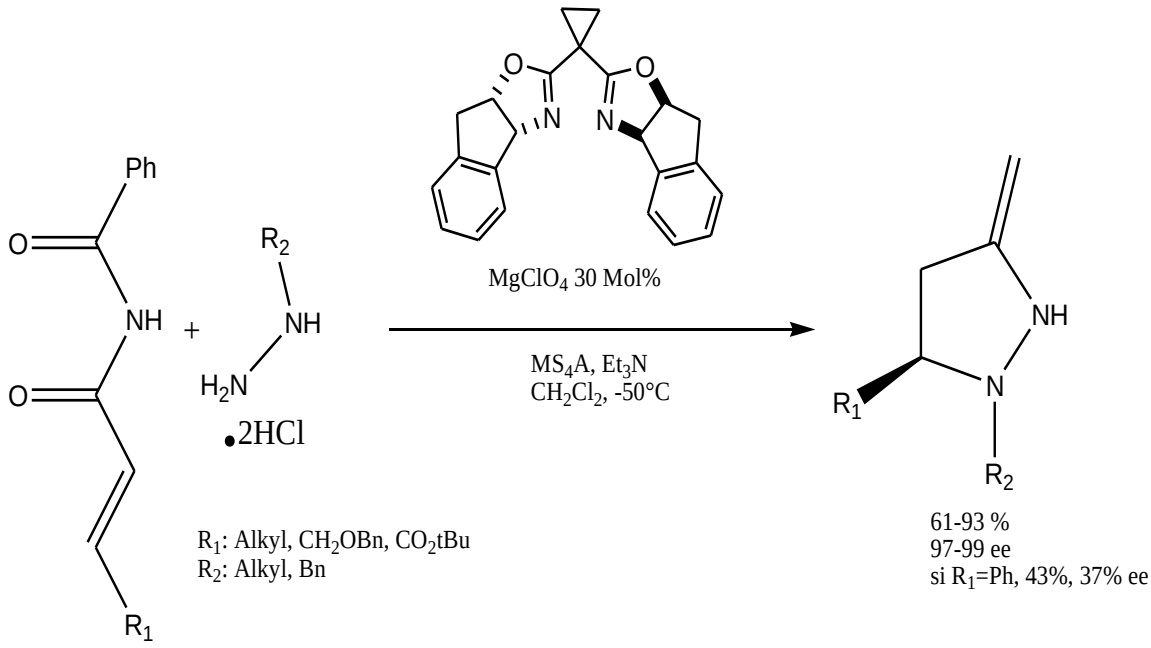

Scheme 3-10: enantioselective synthesis proposed by Sibi

On 2008 the Scheldt's crew published the preparation of a pyrazolidinone by adding an unsaturated aldehyde on a diazene. The reaction is enhanced by carbenes to advance the addition and the pyrazolidinones are obtained with a good yield. [40]

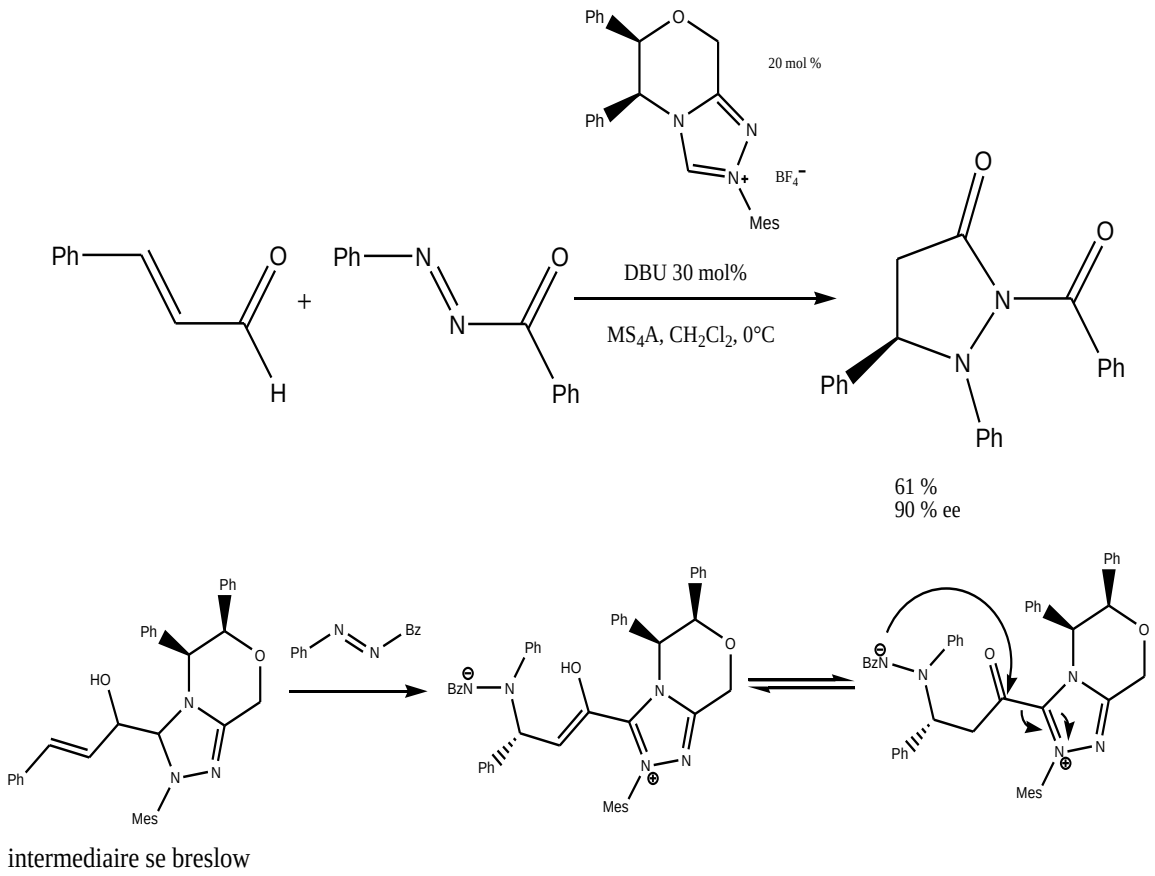

Scheme 3-11: enantioselective synthesis proposed by Scheidt

Another example of enantioselective organocatalyzed synthesis of pyrazolidinones is presented by Vicario's group on 2012 [41] on a aza-Michael reaction between an unsaturated aldehyde and hydrazine and catalyzed by the Jørgensen-Hayashi catalyst, this step is followed by a cyclization leading to the intermediate pyrazolidin-2-ol which is oxygenated later to form the pyrazolidinone. Note that the yield and the enantioselectevity is greatly affected by the groups linked to the N atom such as alkyl, Boc and Nosyl groups.

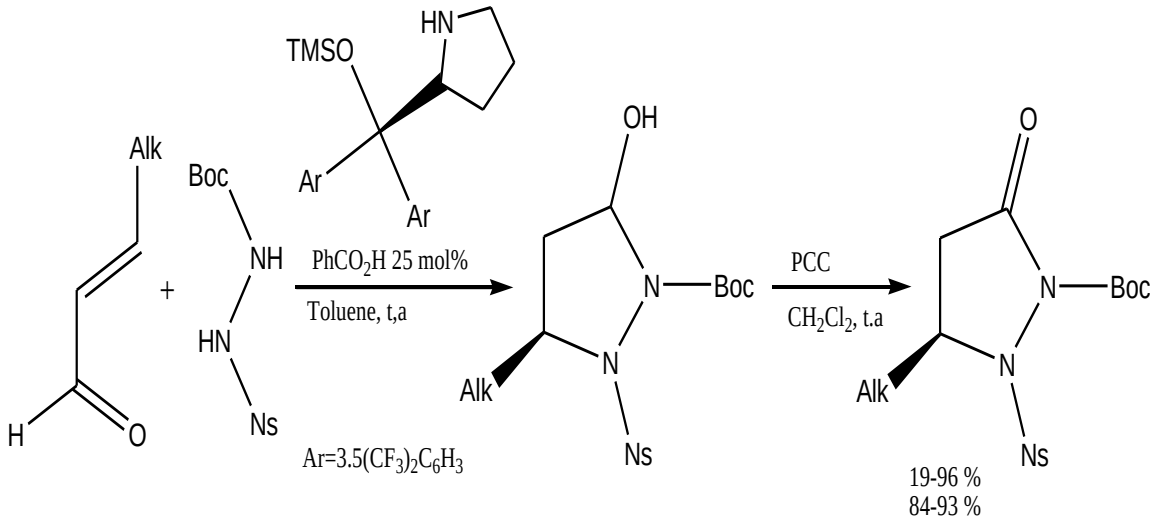

Scheme 3-12: enantioselective synthesis proposed by Vicario

Wang and coworkers [41] proposed another another example of organocatalyzed enantioselective synthesis type of Morita-Baylis-Hillman followed by cyclization in acid medium.

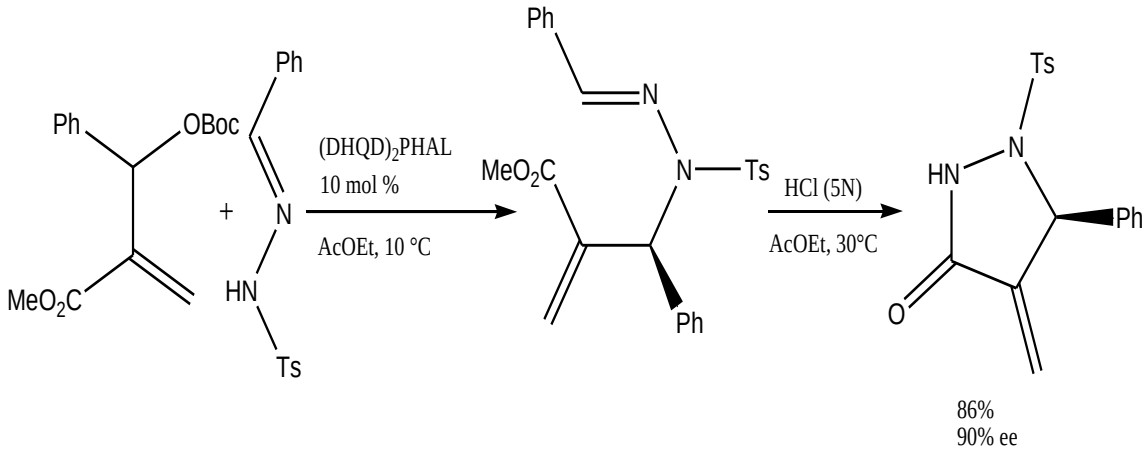

Scheme 3-13: example of enantioselective synthesis proposed by Wang

Gao and coworkers [42] also proposed another alternative using C,N cyclic azomethine imine and α-chlorinated aldehyde catalyzed by carbene; the yield and the enantiomeric of the reaction were good in case of α-aliphatic aldehydes.

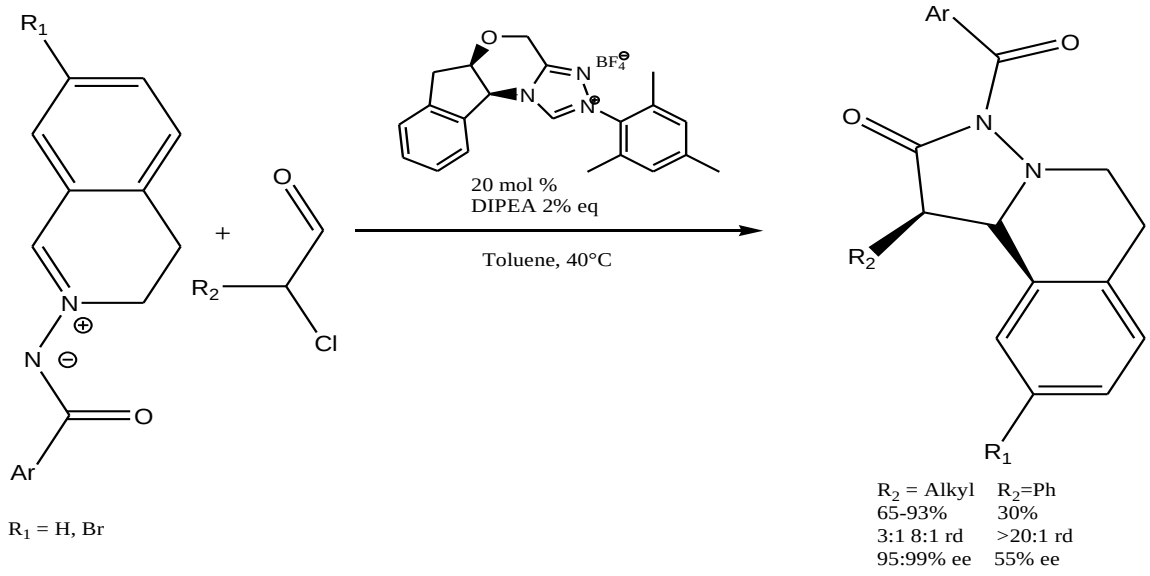

Scheme 3-14: synthesis of pyrazolidinones via azomethine imines by carbene catalysis

Another example was reported by Studier's group; he used C, N cyclic azomethine imines ; the partner here is a carboxylic acid activated in a first time in the form of a mixed anhydride, then by a chiral Lewis base. The better yields and stereoselectivities were obtained with α-substituted carboxylic acid by aromatic or hetero aromatic groups.

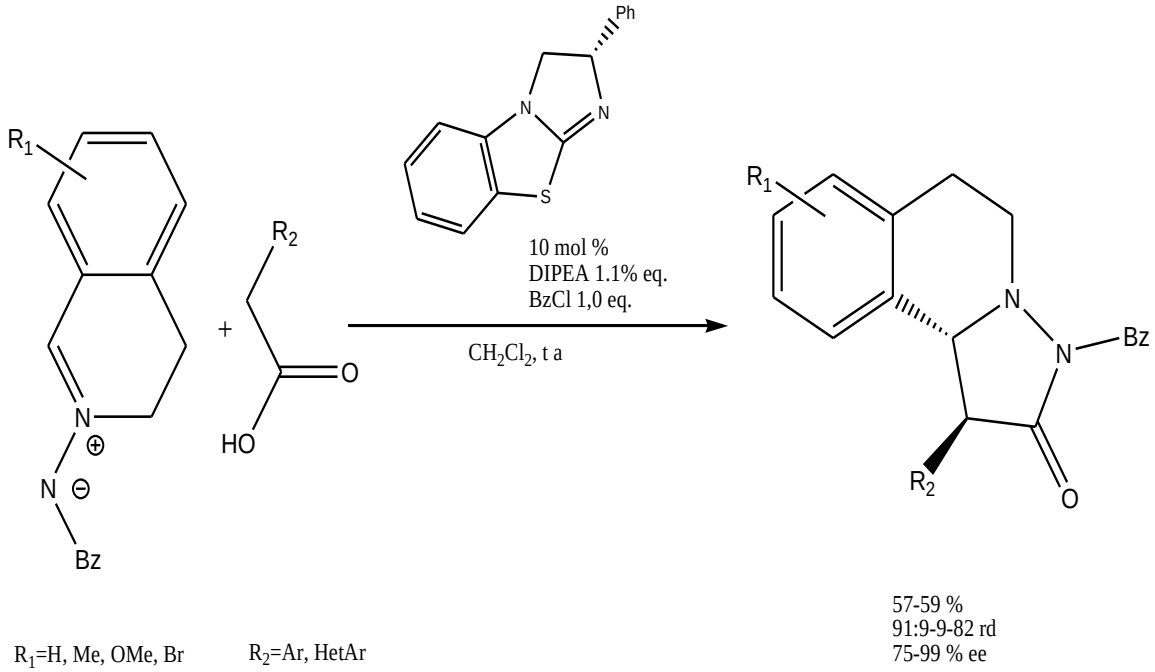

Scheme 3-15: synthesis of pyrazolidinones via azomethine imines by Lewis base catalysis

3.4 Reactivity of pyrazolidinones

3.4.1 Transformation on the ring

It is well known that nitrogen atoms are the favored site where the transformation is likely to occur within pyrazolidinones structure and the reactivity of the two nitrogen atoms differ significantly. The N1 is more basic, more electrophile and thus more reactive, it preferably reacts with SP2 electrophiles, such as carbonyls, electron-deficient alkenes and alkynes, and carbocations (SN1 substrates), whereas reactions with SP3 type of electrophiles (SN2 substrates, such as primary alkyl halides) are usually difficult.

Unsubstituted pyrazolidinones **(10)** react with wide range of electrophiles to afford a variety of compounds such as pyrazolidinones **(29)** where R is NO [43], tosy1 [44], acetyl benzoyl [45],[46] CONHPh, C(NH)OR [46], CSNH2 [47].

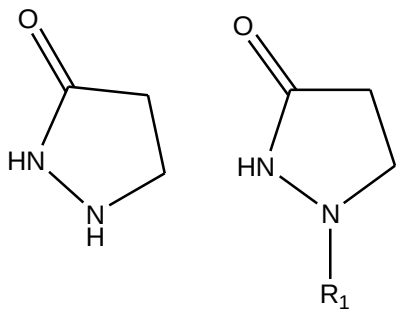

28 29

Scheme 3-16: mono-substituted and un-substituted pyrazolidinone

If N1 is occupied; the N2 react with primary alkyl halides in the presence of a base in polar aprotic solvents to give the 1,2-disubstituted derivatives [48] .

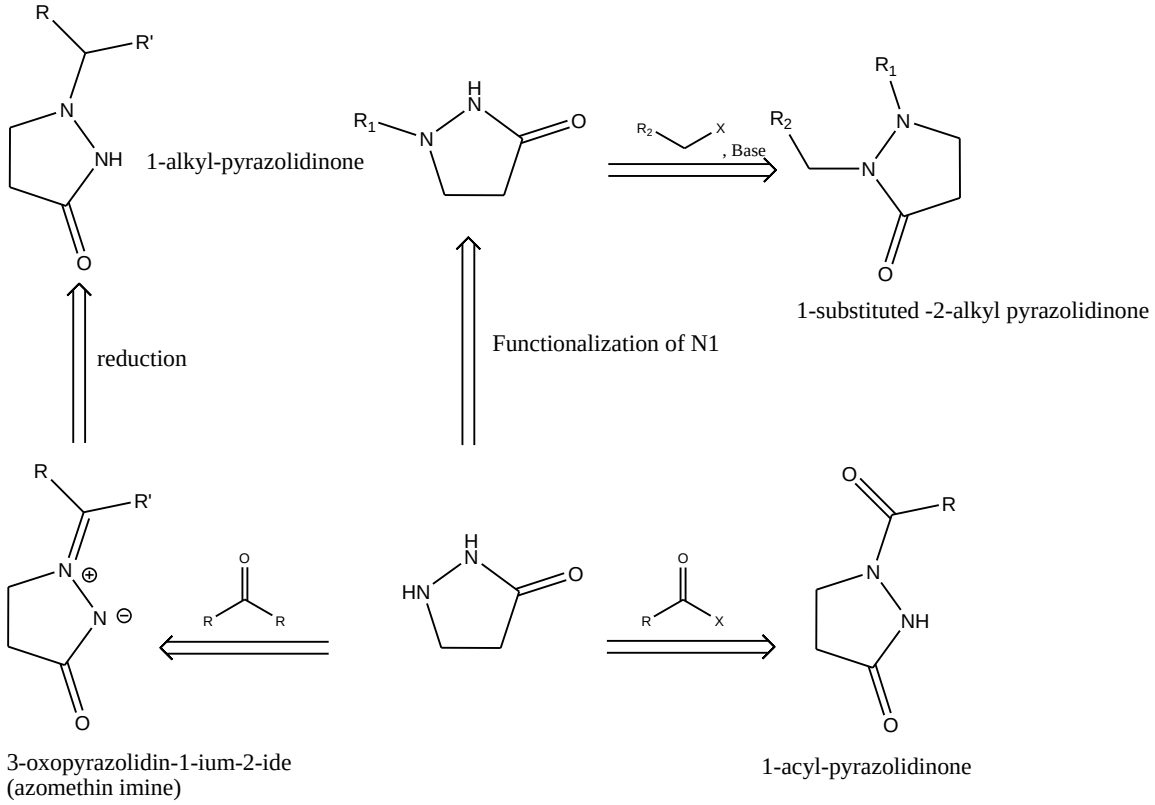

Scheme 3-17: functionalization of ring nitrogene atoms with electrophiles

The reduction of the available azomethine imines with complex hydrides, e.g. with NaBH4 or NaBH3CN gives the corresponding 1-(primary alkyl)-3-pyrazolidinones.

Other transformations on the amino function are studied as well (scheme 3.18) amines (**33), (34), (35)** can be obtained in good yields by hydrogenolytic deprotection of the amino function in the Cbz-protected 4-aminopyrazolidinones **(30)**, **(31)**, and **(32).** Carrying the hydrogenolytic deprotection of the pyrazolidinones **(31)** in aldehyde or a ketone provides the 4-alkylamino-3-pyrazolidinones **(36)** were obtained in 75–100% yields.

Also the N-acyl derivative **(37)** also was obtained in 10% yield by the N-acylation of **(33)** with carboxylic acid in the presence of bis-(pentafluorophenyl) carbonate (BPC) in DMF; also the acylation of di-substituted pyrazolidinones **(34)** and **(35)** smoothly produce the corresponding carboxamides **(38)** and **(39)** in 83% and 82% yield, respectively [19].

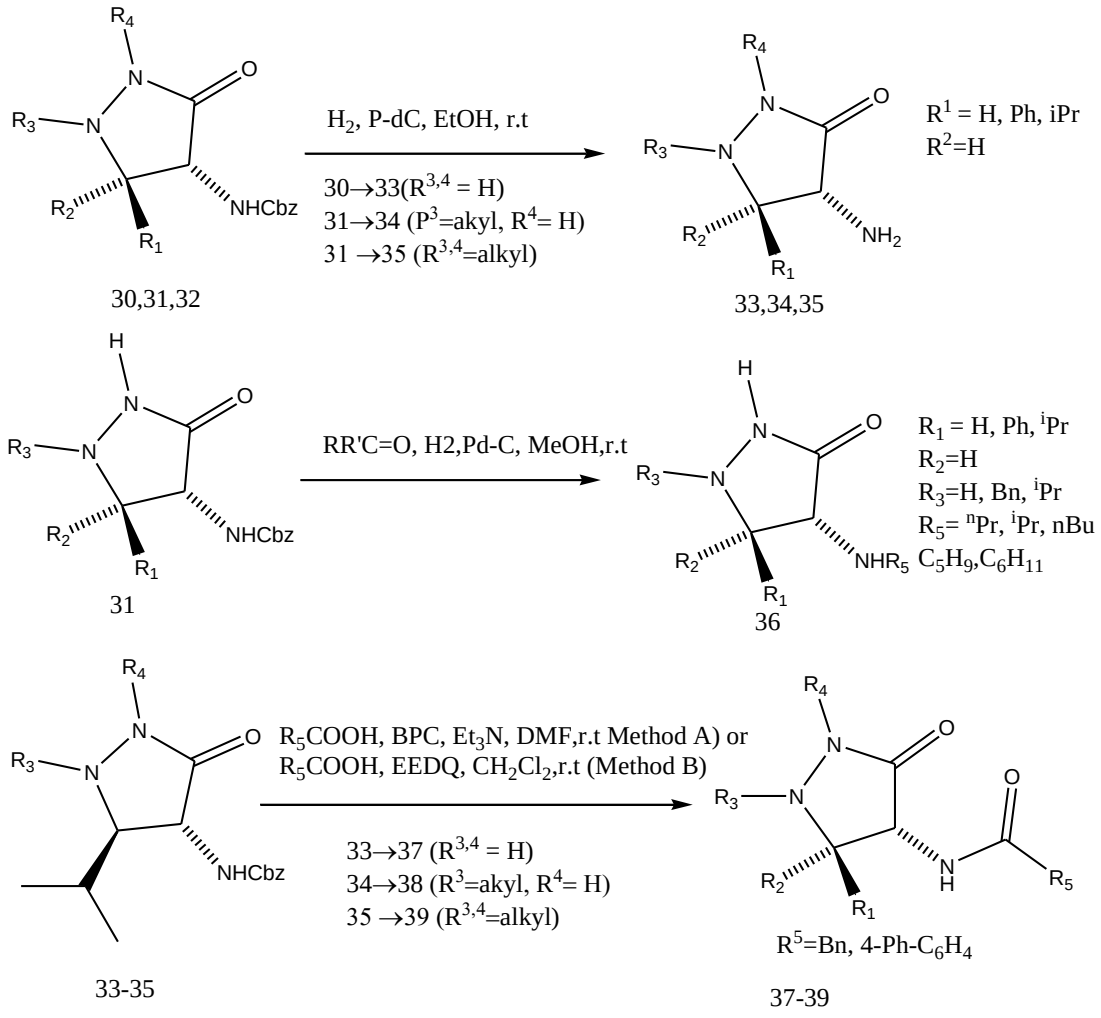

Scheme 3-18: synthesis of poly substituted pyrazolidinones 33-39

3.4.2 Ring switching

This pyrazolidinones reaction was observed in the first time when studying cycloaddition reactions of (1*Z*,4*R**,5*R**)-1-arylmethylidene-4-benzyloxycarbonylamino-3-oxo-5-phenylpyrazolidin-1-ium-2-ides (**40a**,**b)** to *tert*-butyl acrylate in refluxing anisole; is was observed that 25% of the product is the formed benzylideneiminohydantoins **(42)** [49]**.** Heating (**40a**,**b)** alone in anisole under reflux furnished the corresponding *N*-iminohydantoins **(42a,b)** as the sole products in good yields; This ring transformation can be rationalized by thermal cleavage of benzylic-type C–N bond in the enol form of azomethine imine **40'**. The so formed α,β-unsaturated hydrazide (**41)** cyclizes into (**42)** by nucleophilic attack of the amidic nitrogen to the Cbz group (Scheme 8). [18]

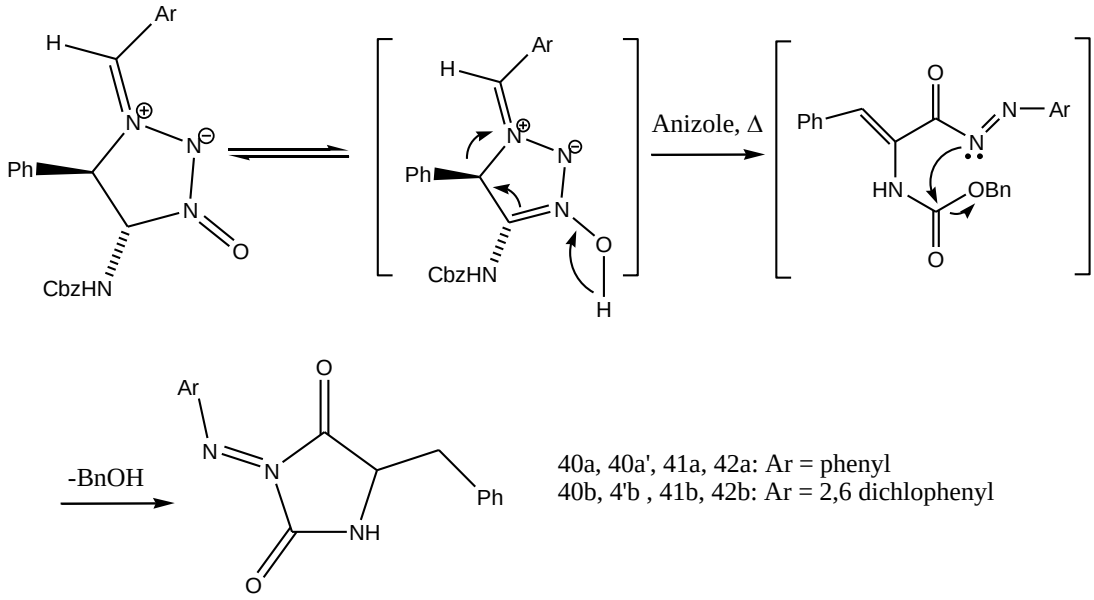

Scheme 3-19: Ring switching transformation of pyrazolidinone derivatives (40a,b) into the N-iminohydantoins (42a,b)

3.5 References

[1] J. M. Indelicato and C. E. Pasini, “The acylating potential of. gamma.-lactam antibacterials: base hydrolysis of bicyclic pyrazolidinones,” *J. Med. Chem.*, vol. 31, no. 6, pp. 1227–1230, 1988.

[2] R. J. Ternansky, S. E. Draheim, A. J. Pike, F. T. Counter, J. A. Eudaly, and J. S. Kasher, “Structure-activity relationship within a series of pyrazolidinone antibacterial agents. 2. Effect of side-chain modification on in vitro activity and pharmacokinetic parameters,” *J. Med. Chem.*, vol. 36, no. 22, pp. 3224–3229, 1993.

[3] C. V Otis, “Standard Quality of Photographic Chemicals,” *J. Soc. Motion Pict. Eng.*, vol. 52, no. 5, pp. 534–539, 1949.

[4] U. Grošelj and J. Svete, “Recent advances in the synthesis of polysubstituted 3-pyrazolidinones,” *Arkivoc*, vol. 2015, pp. 175–205, 2015.

[5] H. Dorn, “Advances in the chemistry of pyrazolidones, iminopyrazolidines, and amino-and hydroxypyrazoles,” *Chem. Heterocycl. Compd.*, vol. 17, pp. 1–24, 1981.

[6] A. Y. Barkov, N. S. Zimnitskiy, I. B. Kutyashev, V. Y. Korotaev, and V. Y. Sosnovskikh, “Highly stereoselective [3+2]-cycloaddition reaction of stabilised N,N’-cyclic azomethine imines with 3-nitro-2-phenyl-2H-chromenes: Synthesis of tetrahydrochromeno[4,3-c]pyrazolo[1,2-a]pyrazol-11-ones,” *Tetrahedron Lett.*, vol. 58, no. 42, 2017, doi: 10.1016/j.tetlet.2017.09.015.

[7] J. Svete, “PYRAZOLIDINONE–AUSEFUL BUILDING BLOCK IN THE SYNTHESIS OF FUNCTIONALIZED PYRAZOLES”.

[8] G. Lukacs and M. Ohno, “Recent progress in the chemical synthesis of antibiotics,” 2012.

[9] L. N. Jungheim, S. K. Sigmund, and J. W. Fisher, “Bicyclic pyrazolidinones, a new class of antibacterial agent based on the β-lactam model,” *Tetrahedron Lett.*, vol. 28, no. 3, pp. 285–288, 1987.

[10] E. M. Kosower, A. E. Radkowsky, A. H. Fairlamb, S. L. Croft, and R. A. Neal, “Bimane cyclic esters, possible stereologues of trypanothione as antitrypanosomal agents. Bimanes 29,” *Eur. J. Med. Chem.*, vol. 30, no. 9, pp. 659–671, 1995.

[11] M. I. Konaklieva and B. J. Plotkin, “Bioisosters of β-lactams as anti-infectives,” *Curr. Med. Chem. Agents*, vol. 2, no. 4, pp. 287–302, 2003.

[12] M. Lemay, L. Aumand, and W. W. Ogilvie, “Design of a conformationally rigid hydrazide organic catalyst,” *Adv. Synth. Catal.*, vol. 349, no. 3, pp. 441–447,

2007.

[13] J. L. Cavill *et al.*, “The α-effect in iminium ion catalysis,” *Tetrahedron*, vol. 62, no. 2–3, pp. 410–421, 2006.

[14] G. Varvounis, Y. Fiamegos, and G. Pilidis, “Pyrazol-3-ones part 1: Synthesis and applications,” 2001.

[15] T. Eicher and S. Hauptmann, “The Chemistry of Heterocycles (2nd Edn), Vols. 1–2.” Wiley-VCH: Weinheim, 2003.

[16] J. Svete, *(4R*, 5R*)-4-benzoylamino-5-phenyl-3-pyrazolidinone: a useful building block in the synthesis of functionalized pyrazoles*. 2008.

[17] U. Schmidt *et al.*, “Diastereoselective formation of (Z)-didehydroamino acid esters,” *Synthesis (Stuttg).*, vol. 1992, no. 05, pp. 487–490, 1992.

[18] A. Novak, J. Bezenšek, U. Grošelj, A. Golobič, B. Stanovnik, and J. Svete, “Serendipity at work: unexpected ring transformations of 4-aminopyrazolidin-3-ones into N-aminohydantoins,” *Arkivoc*, vol. 6, pp. 18–28, 2011.

[19] A. Novak *et al.*, “A Simple Synthesis of Polyfunctionalized 4-Aminopyrazolidin-3-ones as ‘Aza-deoxa’Analogs of D-Cycloserine,” *Helv. Chim. Acta*, vol. 97, no. 2, pp. 245–267, 2014.

[20] J. Bohrisch, H. Faltz, M. Pätzel, and J. Liebscher, “Optically Active 5-(Hydroxyalkyl)-and 5-(Aminoalkyl) pyrazolidin-3-ones by Ring-Chain Transformation of α, β-Unsaturated Lactones or Lactams with Hydrazines,” *Liebigs Ann.*, vol. 1996, no. 10, pp. 1581–1585, 1996.

[21] L. N. Jungheim and S. K. Sigmund, “1, 3-Dipolar cycloaddition reactions of pyrazolidinium ylides with acetylenes. Synthesis of a new class of antibacterial agents,” *J. Org. Chem.*, vol. 52, no. 18, pp. 4007–4013, 1987.

[22] T. S. Mansour and C. A. Evans, “Decarboxylative carbon acylation of malonates with aminoacylimidazolides mediated by Lewis acids,” *Synth. Commun.*, vol. 20, no. 5, pp. 773–781, 1990.

[23] R. M. Devant and H.-E. Radunz, “A novel short and efficient asymmetric synthesis of statine analogues,” *Tetrahedron Lett.*, vol. 29, no. 19, pp. 2307–2310, 1988.

[24] D. Žerovnik *et al.*, “Synthesis of 1, 5, 6, 7-tetrahydro-4H-pyrazolo [4, 3-c] pyridin-4-ones as conformationally constrained pyrazole analogues of histamine,” *Synthesis (Stuttg).*, pp. 3363–3373, 2010.

[25] U. Grošelj *et al.*, “Synthesis of Tetrahydropyrazolo [1, 5-c] pyrimidine-2, 7 (1H, 3H)-diones,” *Synthesis (Stuttg).*, vol. 45, no. 05, pp. 639–650, 2013.

[26] T. Chuang and K. B. Sharpless, “Applications of Aziridinium Ions: Selective Syntheses of Pyrazolidin-3-ones and Pyrazolo [1, 2-a] pyrazoles,” *Helv. Chim. Acta*, vol. 83, no. 8, pp. 1734–1743, 2000.

[27] I. Panfil, Z. Urbańczyk-Lipkowska, K. Suwińska, J. Solecka, and M. Chmielewski, “Synthesis of pyrazolidinone analogs of β-lactam antibiotics,” *Tetrahedron*, vol. 58, no. 6, pp. 1199–1212, 2002.

[28] L. Pezdirc *et al.*, “Stereocontrol in cycloadditions of (1Z, 4R*, 5R*)-1-arylmethylidene-4-benzoylamino-5-phenylpyrazolidin-3-on-1-azomethine imines,” *Tetrahedron*, vol. 61, no. 16, pp. 3977–3990, 2005.

[29] W. Chen *et al.*, “Organocatalytic and Stereoselective [3+ 2] Cycloadditions of Azomethine Imines with α, β-Unsaturated Aldehydes,” *Adv. Synth. Catal.*, vol. 348, no. 14, pp. 1818–1822, 2006.

[30] R. Shintani and G. C. Fu, “A new copper-catalyzed [3+ 2] cycloaddition: Enantioselective coupling of terminal alkynes with azomethine imines to generate five-membered nitrogen heterocycles,” *J. Am. Chem. Soc.*, vol. 125, no. 36, pp. 10778–10779, 2003.

[31] A. Suárez, C. W. Downey, and G. C. Fu, “Kinetic resolutions of azomethine imines via copper-catalyzed [3+ 2] cycloadditions,” *J. Am. Chem. Soc.*, vol. 127, no. 32, pp. 11244–11245, 2005.

[32] W. Chen, W. Du, Y. Duan, Y. Wu, S. Yang, and Y. Chen, “Enantioselective 1, 3-dipolar cycloaddition of cyclic enones catalyzed by multifunctional primary amines: beneficial effects of hydrogen bonding,” *Angew. Chemie*, vol. 119, no. 40, pp. 7811–7814, 2007.

[33] H. Suga, A. Funyu, and A. Kakehi, “Highly enantioselective and diastereoselective 1, 3-dipolar cycloaddition reactions between azomethine imines and 3-acryloyl-2-oxazolidinone catalyzed by binaphthyldiimine− Ni (II) complexes,” *Org. Lett.*, vol. 9, no. 1, pp. 97–100, 2007.

[34] M. P. Sibi, D. Rane, L. M. Stanley, and T. Soeta, “Copper (II)-Catalyzed Exo and enantioselective cycloadditions of azomethine imines,” *Org. Lett.*, vol. 10, no. 14, pp. 2971–2974, 2008.

[35] L. M. Stanley and M. P. Sibi, “Enantioselective copper-catalyzed 1, 3-dipolar cycloadditions,” *Chem. Rev.*, vol. 108, no. 8, pp. 2887–2902, 2008.

[36] M. Keller, A. S. S. Sido, P. Pale, and J. Sommer, “Copper (I) Zeolites as Heterogeneous and Ligand-Free Catalysts:[3+ 2] Cycloaddition of Azomethine Imines,” *Chem. Eur. J.*, vol. 15, no. 12, pp. 2810–2817, 2009.

[37] H. Suga, T. Arikawa, K. Itoh, Y. Okumura, A. Kakehi, and M. Shiro, “Asymmetric 1, 3-dipolar cycloaddition reactions of azomethine imines with acrolein

catalyzed by l-proline and its derivatives." Shinshu University Library, 2010.

[38] D. Yang, M. Fan, H. Zhu, Y. Guo, and J. Guo, "Catalyst-Free and Stereoselective Synthesis of N, N-Bicyclic Pyrazolidinone Derivatives," *Synthesis (Stuttg).*, pp. 1325–1332, 2013.

[39] I. H. Kobayashi Shu, Hasegawa Yoshiki, "Chiral Zirconium-Catalyzed Asymmetric Mannich-Type Reactions Using Acylhydrazones as Imine Equivalents," *Chem. Lett.*, vol. 27, no. 11, pp. 1131–1133, 1998, [Online]. Available: https://doi.org/10.1246/cl.1998.1131

[40] A. Chan and K. A. Scheidt, "Direct amination of homoenolates catalyzed by N-heterocyclic carbenes," *J. Am. Chem. Soc.*, vol. 130, no. 9, pp. 2740–2741, 2008, doi: 10.1021/ja711130p.

[41] M. Fernandez, E. Reyes, J. L. Vicario, D. Badia, and L. Carrillo, "Organocatalytic enantioselective synthesis of pyrazolidines, pyrazolines and pyrazolidinones," *Adv. Synth. Catal.*, vol. 354, no. 2-3, pp. 371–376, 2012.

[42] Z.-H. Gao, X.-Y. Chen, J.-T. Cheng, W.-L. Liao, and S. Ye, "N-Heterocyclic carbene-catalyzed [2+ 3] cyclocondensation of α-chloroaldehydes with azomethine imines," *Chem. Commun.*, vol. 51, no. 45, pp. 9328–9331, 2015.

[43] W. O. Godtfredsen and S. Vangedal, "The reaction of hydrazine with cinnamic acid derivatives," *Acta Chem. Scand*, vol. 9, no. 9, pp. 1498–1509, 1955.

[44] H. Dorn, A. Zubek, and G. Hilgetag, "Synthesis of 5-Pyrazolone and 1-Substituted 5-Pyrazolones," *Angew. Chemie Int. Ed. English*, vol. 5, no. 7, pp. 665–666, 1966.

[45] H. Dorn and A. Zubek, "Synthese von 1-Methyl-pyrazolidon-(5) über N'-acyliertes Pyrazolidon-(3)," *Zeitschrift für Chemie*, vol. 8, no. 6, pp. 218–219, 1968.

[46] M. Neitzel and G. Zinner, "Reaktion von Cyansäureestern mit 3-Pyrazolidinonen," *Liebigs Ann. der Chemie*, vol. 1980, no. 11, pp. 1907–1912, 1980.

[47] A. M. Richter and V. Mojjoukhine, "Synthese und Oxydation von 1-(1, 3-Thiazol-2-yl)-pyrazolid-3-onen," *J. für Prakt. Chemie*, vol. 324, no. 6, pp. 873–881, 1982.

[48] F. P. J. T. Rutjes, H. Hiemstra, F. O. H. Pirrung, and W. N. Speckamp, "Synthesis of bridged bicyclic hydrazines via endocyclic N-acylhydrazonium intermediates: A novel route to the 1-Azatropane skeleton," *Tetrahedron*, vol. 49, no. 44, pp. 10027–10048, 1993.

[49] A. Novak *et al.*, "Synthesis of pyrazolo [1, 2-a] pyrazole-based peptide

mimetics,” *Tetrahedron*, vol. 69, no. 32, pp. 6648–6665, 2013.

Chapter 4: Results and discussion

4.1 Introduction

[3+2] Cycloaddition reactions of is one of the most attractive ways for building heterocyclic compounds [1]. It provides easy access to five-chained heterocycles with several stereogenic centers, usually with excellent and high stereoisomerism [2].

The cycloaddition reaction between alkene derivatives and azomethine imines represent an essential method for construction of pyrazolidinones derivatives; a compounds with high importance in biology and medicines [3] [4] [5]; this reaction typically proceeds according to concerted 1,3-dipolar cycloaddition mechanism in the absence of a catalyst in this case; the charge distribution in the starting reagents determines the regioselectivity while the while the stereoselectivity is determined by secondary orbital and steric interactions, arising in the transition state between substituents of the dipole and dipolarophile molecules.

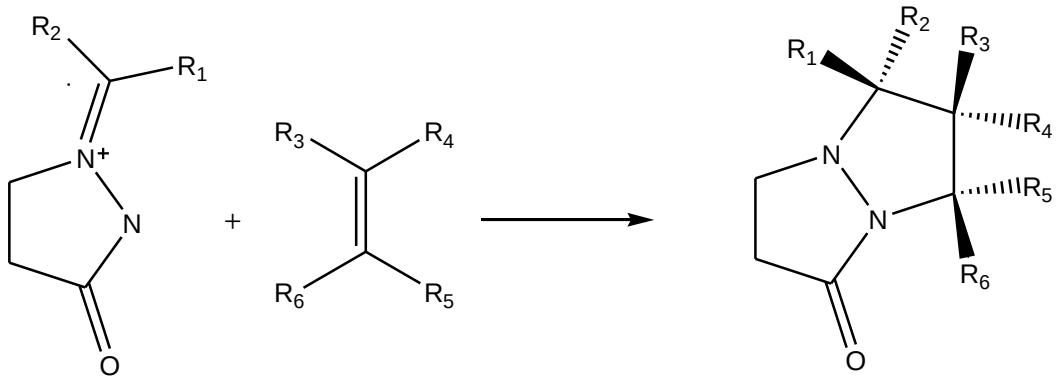

Scheme 4-1: synthesis of pyrazolidinones from azomethine imines and alkene derivatives

On 2017; Alexey Y and coworkers [6] reported the synthesis of the pyrazolidinones derivatives by reacting 3-nitro-2-phenyl-2H-chromenes with 2-arylmethylidene-5-oxopyrazolidin-2-ium-1-ides in isopropanol at 50 °C over 2 days forming tetrahydrochromeno [4,3-c] pyrazolo [1,2-a] pyrazol-11- ones. These reactions proceed with high stereoselectivity and total regioselectivity and 50-81 % yield (Scheme 4.2).

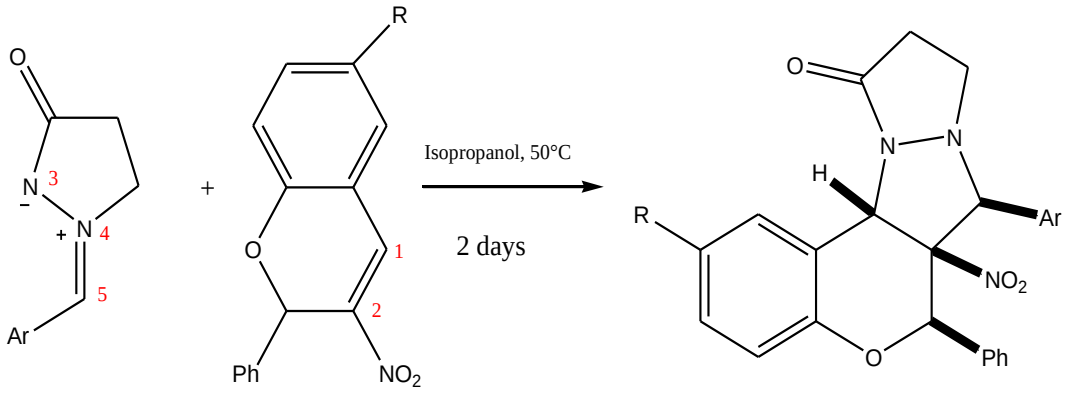

1 2 3

Scheme 4-2: synthesis of tetrahydrochromeno[4,3-c]pyrazolo[1,2-a]pyrazol-11-ones

The main objective of the present study is explore to the mechanism and to shed lights on the factors controlling that influence on the high stereoselectivity of the 32CA reaction between the N,N'-cyclic azomithine imine 5-oxo-2-(phenylmethylidene)pyrazolidin-2-ium-1-ide **(1) (R=H)** and 3-nitro-2-phenyl-2H-chromene **(2) (Ar = Ph)** leading exclusively to the formation of a N,N-bicyclic pyrazolidinone as a single regio- and stereoisomer rel-(6R,6aR,7S,12aS)-6a-nitro-6,7-diphenyl-6a,9,10,12a-tetrahydro-6H,7H,11H-chromeno-[4,3-c]pyrazolo[1,2-a]pyrazol-11-one **(3)** (R=H, Ar=Ph) within MEDT perspective at the B3LYP/6-311G(d,p) computational level.

4.2 ELF topological and NPA analyses of azomethine imine structures

The last decade of the last century knew the appearance of two important theories in computational chemistry allowing the analysis of chemical structure in a very fashionable way: Atoms in Molecules (AIM) and Electron Localization Function (ELF) [7].

While AIM permits a partition of the electron density within the molecular space into basins associated with atoms; the ELF measures the electron pair localization and characterizes the corresponding electron density. Later Silvi and Savin [8] used the ELF as an appealing model for chemical bonding.

ELF is a dimensionless, empirical function in 3-space; it constitutes a useful relative estimation of the electron pair localization characterizing the corresponding electron density of a chemical system. Within the DFT context and based on the positive-definite local Pauli and Thomas Fermi kinetic energy densities in the given system, ELF was valued between [0-1]. Thus; highest values are related to highest relative spatial position of electron localization [7]. The spatial points with maximal gradient values of ELF are designated as basin of attractors. Furthermore ELF basins are classified as core basins C(…) and valence basins V(…). The latter are characterized by the synaptic order, i.e., the number of atomic valence shells in which they participate. While Lone pairs or non-bonding regions are labelled by monosynaptic basins V (A), bonding regions A-B are labelled by disynaptic basin V(A,B) which connects two nuclei A and B [8],[9]. This description recovers the Lewis bonding model [10], providing a very suggestive graphical representation of the molecular system.

Many studies have been reported to understand the reactivity of TACs participating in CA32 reactions have made it possible to establish a very good link between their electronic structures and their reactivity. Indeed, using ELF the electronic structure of the TACs are classified into four types: pseudodiradical (pdr), pseudomonoradical (pmr), carbenoid (cb), and zwitterionic (zw) type [11]. (Figure 4-1)

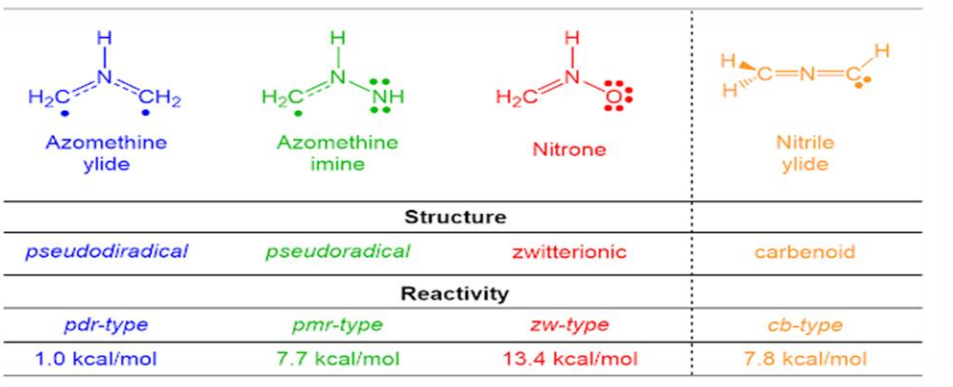

Figure 4-1: Classification of TAC participating in 32CA

The molecular electron density theory (MEDT) [12] proposed by Domingo as a new theory of reactivity model states that: the reactivity in organic chemistry cannot be characterized neither by a static energy nor by a geometrical study of the corresponding stationary points, including the transition state structures, but by a rigorous analysis of the molecular electron density changes along the reaction path, as well as of the changes in energies required to reach the transition state geometry in order to explain experimental activation energies Thus, based on this theory, several studies [13],[14] have been performed in order to understand the reactivity and the mechanism of some cycloaddition reactions.

Based on MEDT; the 32CA reactions involving TAC were classified in:

- Cb-type (carbenoid 32CA reactions): These reactions take place depending on their polar of the nucleophilic character of the carbenoid TAC and the electrophilic character of the ethylene derivative.
- Pr-type (Pseudodiradical 32CA reactions type): These reactions are characterized by the very low activation energy and a very low global electron density transfer (GEDT) at the transition state structure (TS).
- Pmr-type (Pseudo mono radical 32CA reactions): These reactions are characterized by the low activation energy and a low global electron density transfer (GEDT) at the transition state structure (TS).
- Zw-type (Zwitterionic 32CA reactions): Like cb-type reactions, the feasibility of these reactions depends on the nucleophilic character of the zwitterionic TAC and the electrophilic character of the ethylene derivative or vice versa [11], [15], [16]

In the aim of defining the structure of the azomithine imine (1) and knowing its participation in the 32CA reaction with chromene (2); an analysis of its structure as well as the simplest azomithine imine shown in the figure 4.1 is carried out (Figure 4.2 below):

The simplest azomethine imine 4 can participate in the 32CA reactions as a pseudomonoradical TAC. In fact its structure shows one monosynaptic basin integrating 3.05 e corresponds to the N3 two lone pairs, two disynaptic basins V(C1,N2) and V(N2,N3) integrating a population of 3.01 and 1.96 e accounting for the C1=N2 double bond and the N2−N3 single bond respectively and two monosynaptic basins V(C1) and V'(C1) integrating a total electron population 0.57 e corresponding to the C1 pseudoradical center.

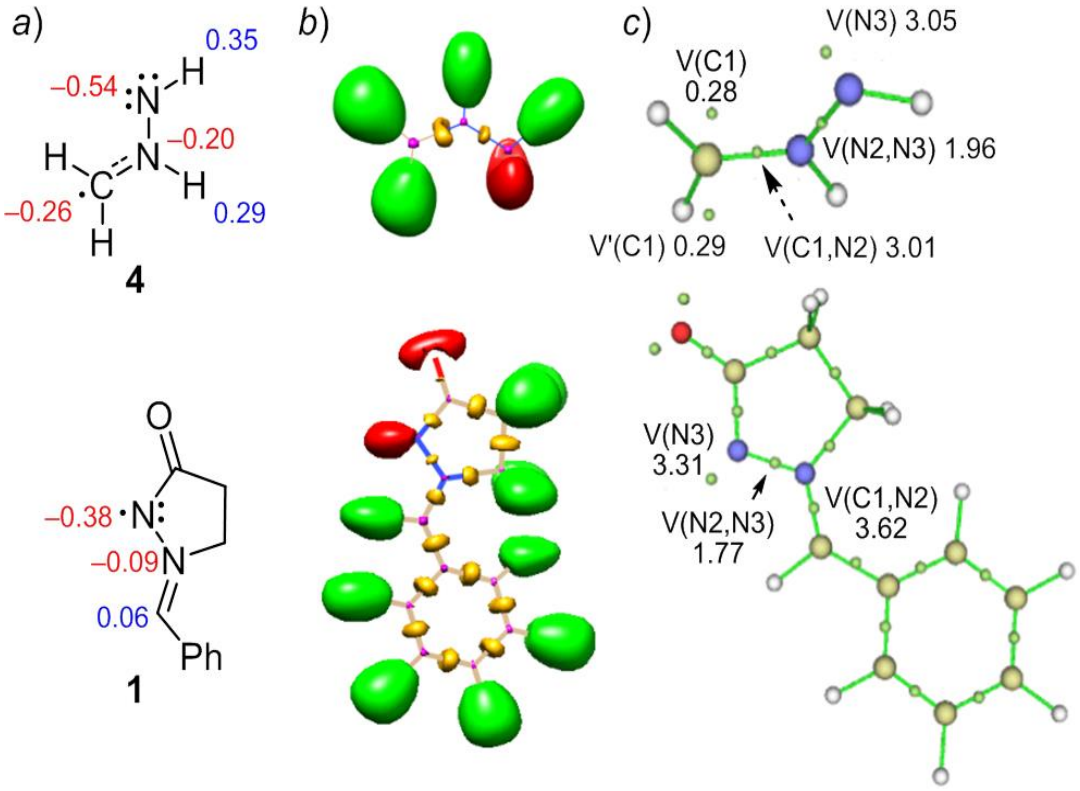

Figure 4-2: a) The proposed ELF-based Lewis structures of azomithine imines 1 and 4 together with the natural atomic charges given in average number of electrons of the most relevant atoms. b) ELF localization domains represented with an isosurface value of 0.83.

c) ELF basin attractor positions, together with the most representative valence basin populations in e

Like the structure of azomithine 4; azomithine 1 (E-isomer was used in the calculations), presents one monosynaptic basin integrating 3.31 e corresponding to the lone pair on N3 atom, two disynaptic basins V(C1,N2), integrating a population of 3.62 e that obviously describes the C1=N2 double bond, and V(N2,N3), integrating

1.77 e corresponding to the N2−N3 single bond. On the other hand, the substitution on the terminal atoms carbon C1 and nitrogen N3 make the azomithine imine (1) different than that of the azomithine imine (4) in ELF electronic structure (Figure 4.2). In the ELF electronic structure of azomethine imine 1 (E-isomer was used in the calculations), there are no monosynaptic basins corresponding to pmr, pdr, or cb center, which corresponds to a zwitterionic electronic structure that permits its participation in 32CA reaction as zw TAC [17].

Figure 4-2 depicts also the proposed Lewis-like structures based on the ELF study and the natural atomic charges, obtained by NPA [18],[19] . The formal charges on the core framework C5–N4–N3 atoms of azomithine imine (1) (see atom numbring in scheme 4-2) are –0.26, –0.20, and –0.54 e, respectively, and for azomithine Imine (4) are –0.26, –0.20, and –0.54 e, respectively. While the three atoms of TAC (4) are negatively charged, the C1 of azomithine imine (1) presents a negligible positive charge. However, the azomethine imine framework of TAC (1) has been depopulated by 0.59 e, which may be due to the withdrawing nature of the carbonyl and phenyl groups attached to its structure. In this regard, it is very important to emphasize that the NPA charge distribution is the result of the delocalization of electron density generated by the nuclei in the respective molecule and not the consequence of resonance Lewis structures [20] and, therefore, ignores the 1,3-zwitterionic Lewis structure proposed by Huisgen [18].

4.3 Analysis of CDFT reactivity indices of azomethine imines (1) and (4) and chromene (2)

4.3.1 Global reactivity indices

The analysis of CDFT indices [21] [22] is a very effective tool to predict the reactivity of organic molecules participating in 32CA reactions and Diels–Alder reactions. [23] [24] Therefore, in order to set the relationship between the electronic structure of the reagents and the polar or nonpolar character of the 32CA between azomithine imine (1) and the chromene (2), the CFDT of these species as well as of the simplest azomethine imine (4) were computed at the B3LYP/6-31G(d) level and

collected in table 4-1. The B3LYP/6-31G(d) theoretical level was employed to compute the global CDFT indices because it was used to set the electrophilicity scales of organic molecules. [25]

The chemical potential μ values of chromene (2) is lower than of that the azomethine imines (1) and (4) indicating that in a polar process, the GEDT [15] will occur from azomethine imines (1), (4) that will act as nucleophiles toward chromene (2) which will act as an electrophile [25] until the equalization of the chemical potential between the two reacting species according to the equalization principle. [26] while compound (1) with nucleophilicity index value of 3.57 eV and electrophilicity index of 2.06 eV is classified as strong nucleophile but weaker nucleophile than its analog (4) which is characterized by a nucleophilicity index of 4.09 eV and electrophilicity index of 0.68 eV and this due to the electron-withdrawing effect of carbonyl group and the phenyl ring. Compound (4) with nucleophilicity index of 4.09 eV and electrophilicity index of 0.68 eV can be classified as a marginal electrophile and strong nucleophile, in addition, compound (1) may be classified as a strong electrophile according to the electrophilicity scale. [25] This high electrophilicity behavior is also due to the electron-accepting properties of carbonyl and phenyl groups.

Both azomethine imine (1) and (4) present lower values electrophilicity index than chromene (2) (2.74 eV) and higher values of nucleophilicity index than Chromene (2) (2.85eV) thus; chromene (2) can be classified as strong electrophile and moderate nucleophile (See values in table 4-1). In addition, the 32CA reaction between chromene (2) and azomethine imine (4) will be more feasible than the reaction between chromene (2) and azomethine imine (**1)**. Consequently, the presence of a carbonyl function and a phenyl ring in azomithine imine (**1)** slightly decreases its nucleophilicity but increases its electrophilicity, compound (**1)** still remaining a strong nucleophile. Consequently, due to the strong nucleophilic character of azomethine imine (**1)** and the strong electrophilic character of chromene (**2)**, it is expected that the 32CA reaction between these species will have a *zwitterionic* (*zw*) character with high GEDT value (polar character).

Table 4-1: The B3LYP/6-31G(d) theoretical level was employed to compute the global

Reagent	*μ*	*η*	*ω*	*N*
1	*-3.79*	*3.49*	*2.06*	*3.57*
2	*-4.45*	*3.61*	*2.74*	*2.85*
4	*-2.58*	*4.78*	*0.68*	*4.09*

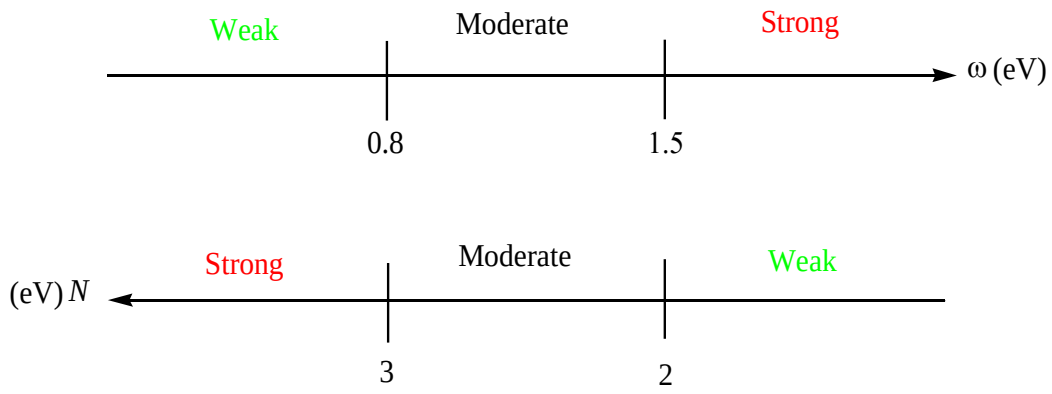

Figure 4-3: The electrophilicity and nucleophilicity scales [25] [22]

4.3.2 Local reactivity indices

While The global reactivity indices are used for the prediction or interpretation of the reactivity of the reagents in their ground states, the local reactivity indices are used for the prediction or investigation of regioselectivity. Thus, during a polar process, the regioselectivity is predicted from the most favoured interaction that will occur between the most nucleophilic center of the nucleophile framework and the most electrophilic center of the electrophile framework. In this context, the analysis of the atomic spin density (ASD) of the radical cations and radical

anions using nucleophilic (P_k^-) and electrophilic (P_k^+) Parr functions, introduced in 2013 by Domingo and co-workers [27] to reveal the most electrophilic and nucleophilic centers (k) in organic molecules has been demonstrated to be an efficient tool for predicting and interpreting the regioselectivity of organic reactions, especially cycloaddition reactions. [28] [29] The obtained three-dimensional (3D) representation of the Mulliken ASD of azomethine imine radical cation $1^{\cdot +}$ and chromene radical anion $2^{\cdot -}$ together with the values of the local Parr functions of the pertinent reactive centers are given in Figure 4-4.

As can be seen in the figure 4-4 below, the most nucleophilic reactive center in azomethine imine (1) is N3 atom with (P_{N3}^- 0.55), which is higher than that of C1 atom (P_{C1}^- 0.14). on the other side; the most electrophilic reactive center in chromene (2) is the C1 atom (P_{C1}^+ 0.29), thus its local electrophilic power is significantly higher than that of C2 atom (P_{C2}^+ 0.07) (see for atom numbering on scheme 4-2 above), indicating that the most favored regioisomeric interaction will occur between N3 nitrogen atom of azomithine imine (1) and C1 carbon atom of chromene (2), giving ortho-regioisomeric cycloadducts 3, in clear agreement with experimental findings.[6]

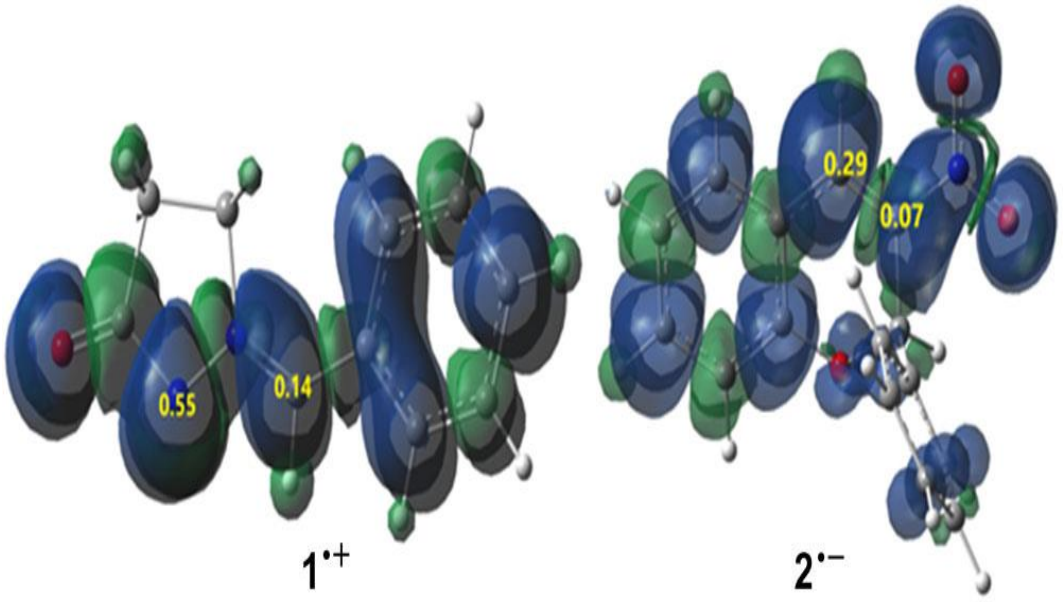

Figure 4-4: 3D representation of ASD of radical cation 1·+ and radical anion 2·–, together with the values of Parr functions Pk + and Pk– of the most reactive atoms

4.4 Analysis of energetic profiles of the 32CA reaction of azomethine imine (1) with chromene (2)

The 32CA reaction between azomethine imine (1) with chromene (2) can take place through two regioisomeric pathways, namely, the ortho and the meta channels as a result of the non-symmetry of the two reagents (1) and (2), in which the meta channel corresponds to the C1−C5 and N3−C2 interactions toward the formation of the regioisomeric structure and the ortho channel is related to the C1−N3 and C2−C5 interactions toward the formation of structure (3) (for atom numbering, see Scheme 4-2). In addition, each regioisomeric path can lead to two possible cycloadducts, associated with two stereoisomeric approaches, namely, exo and endo, according to the orientation of the phenyl ring of reactant (1) toward the planar structure of chromene (2). Note that the phenyl ring of the imine (1) and the nitro group of chromene (2) are oriented to the same side in the exo approach and in an opposite side in the endo approach. Consequently, four TSs are associated with this 32CA reaction that are TS-ox (ortho-exo), TS-on (ortho-endo), TS-mn (meta-endo), and TS-mx (meta-exo), and four corresponding cycloadducts (3ox), (3on), (3mn), and (3mx) (Scheme 4-5)

Table 4-2: relative energies in gas phase and in isopropanol of stationary points involved in the 32CA reaction of azomithine imine (1) and chromene (2)

Structure	Gas phase		Isopropanol, 50 °C	
	Energy (a.u)	**ΔE(kcal.mol^{-1})**	**Energy (a.u)**	**ΔE(kcal.mol^{-1})**
Azomithine imine (1)	-858.743772		-858.7538373	
Chromene (2)	-571.908046		-571.926000	
TS-ox	-1430.63884	**8.138922**	-1430.66001	**12.442193**
TS-on	-1430.62862	**14.556460**	-1430.650963	**18.119396**
TS-mn	-1430.56559	**54.108879**	-1430.584528	**59.807857**
TS-mx	-1430.62305	**18.049931**	-1430.642416	**23.482530**
P-ox	-1430.66445	**-7.927326**	-1430.679159	**0.426204**
P-on	-1430.67198	**-12.652158**	-1430.686535	**- 4.202367**
P-mn	-1430.67162	**-12.427133**	-1430.685198	**-3.363387**
P-mx	-1430.65346	**-1.035578**	-1430.667409	**7.799000**

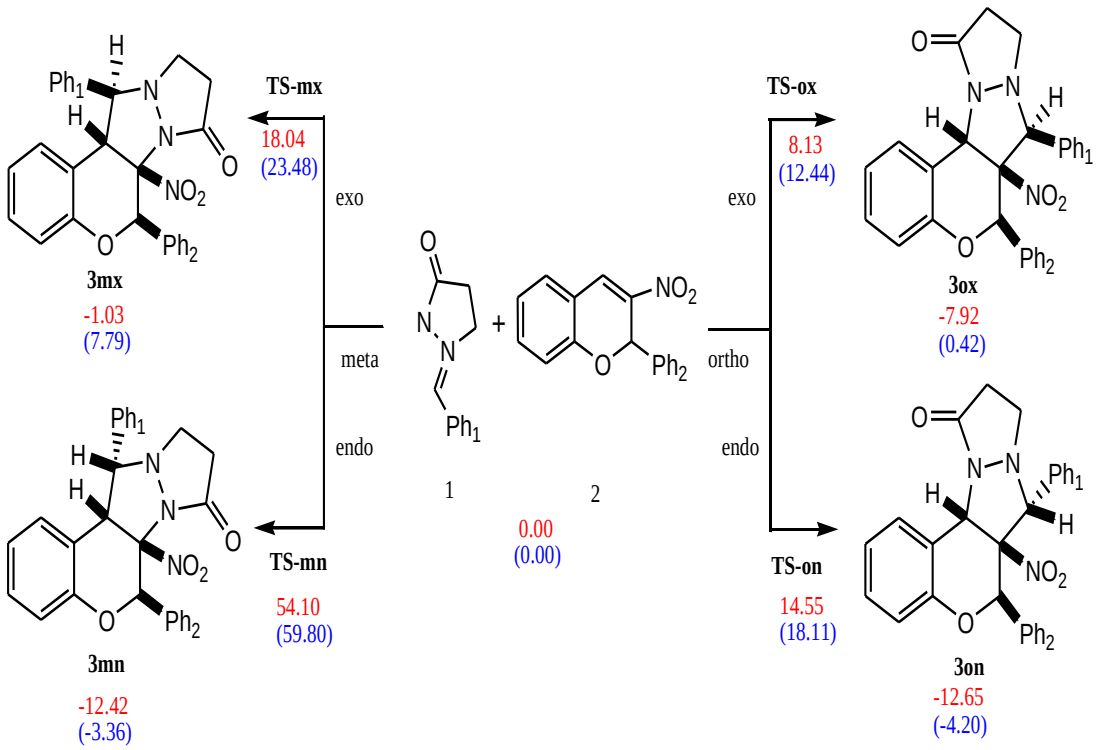

Scheme 4-3: The possible reactive pathways involved in the 32CA reaction of azomethine imine 1 with chromene 2 together with B3LYP/6-311G(d,p) relative energies (kcal·mol–1) in gas phase (red) and in i-PrOH solvent (blue)

The obtained relative energy values in gas phase and in solvent (isopropanol) are given in Scheme 4.5, while the respective total energies are collected in the Table 4-2.

A quick look at the relative energies shown in scheme 4-5 we can conclude that the 32CA reaction between azomethine imine (1) and chromene (2) is completely orthoregioselective due to the high difference in energetic barrier (9.91 kcal.mol^{-1}) between the two regioisomeric channels ortho-exo and meta-exo. Furthermore, the comparison between the two activation barriers of the ortho pathways shows that the (ortho-exo) is lower than (ortho-endo) pathway by 6.42 kcal.mol^{-1}. Thus, the 32CA reaction is highly ortho-exo-stereoselective, therefore the cycloadduct (3-ox) is kinetically favored, while cycloadduct (3-on) is the thermodynamic product. In addition; this 32CA reaction is irreversible in which all

possible reaction pathways are exothermic and the most favoured (ortho-exo) path is exothermic by –7.92 kcal.mol^{-1}. Therefore, this 32CA reaction is only under kinetic control, leading to the favorable formation of cycloadduct (3-ox) generated from the ortho-exo approach, as observed experimentally.

As the reaction proceeded in isopropanol and 50° Celsius, the inclusion of the solvent effect and temperature on calculation shows that despite it affects the activation energies and the exothermic character of this 32CA reaction, the same stereoselectivity is predicted for reaction both in gas phase and in isopropanol. [6] Indeed, the solvent increases the activation energies by 5.70 kcal.mol^{-1} for TS-mn, 5.44 kcal.mol^{-1} for TS-mx, 3.56 kcal.mol^{-1} for TS-on and 4.31 kcal.mol^{-1} for the most favored TS-ox on the other hand, a decrease in the stability of the all cycloadducts is noticed by 6.76 kcal.mol^{-1} for cycloadduct (3-mx), 9.06 kcal.mol^{-1} for cycloadduct (3-mn), 8.45 kcal.mol^{-1} for cycloadduct (3-on) and 7.50 kcal.mol^{-1} for experimentally obtained cycloadduct (3-ox)

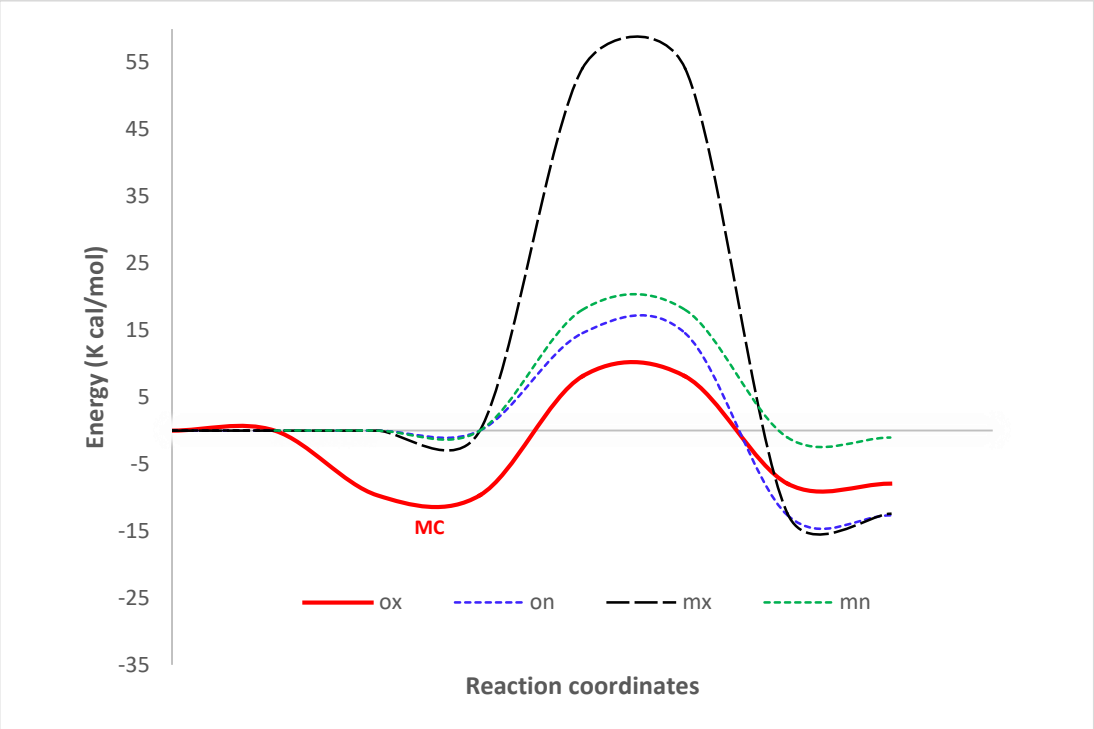

Figure 4-5: Energy profile of the reaction of azomithine imine (1) and the chromene (2)

4.5 Thermodynamic data

Total (u.a) and relative (kcal.mol^{-1}), enthalpies, total (u.a) and relative (kcal.mol^{-1}) Gibbs free energies (kcal.mol^{-1}) and tatal and relative entropy (cal/mol.K) of stationary points of to the 32CA reaction of azomethine imine (1) and chromene (2) are presented in table 4.3

Table 4-3: thermodynamic parameters of stationary points of to the 32CA reaction of azomethine imine (1) and chromene (2) are presented in table 4.3

	H	ΔH	G	ΔG	S	ΔS
AI (1)	-858.49997		-858.5588		123.96	
Chromene (2)	-571.71246		-571.7616		103.5	
TS-ox	-1430.1980	9.02	-1430.2811	24.68	174.93	-52.537
TS-on	-1430.1879	15.3	-1430.2711	31.00	175.00	-52.46
TS-mn	-1430.1269	53.64	-1430.2122	67.96	179.43	-48.03
TS-mx	-1430.1826	18.70	-1430.2650	34.80	173.47	-53.99
P-ox	-1430.2206	-5.14	-1430.3022	11.43	171.84	-55.62
P-on	-1430.2282	-9.91	-1430.3107	6.12	173.68	-53.77
P-mn	-1430.2285	-10.08	-1430.3097	6.77	170.92	-56.53
P-mx	-1430.2102	1.37	-1430.2903	18.92	168.59	-58.87

We notice that the enthalpy of the most favoured transition state TS-ox is less than its competitive ortho endo pathway by 6.28 kcal.mol−1 while the products are presenting negative enthalpy which account for an exothermic character for all the possible paths.

The inclusion of the term TΔS to the enthalpy increases the free energy considerably by values varies from 12.6 to15.8 kcal.mol^{-1}; indeed, these high free energy and entropy values are associated to these two bimolecular process and well explain the experimental condition of this 32CA reaction which are 50 degrees Celsius and two days' reaction time.

4.6 Analysis of TSs geometries and reaction polarity

Figure 4-6 depicts the optimized geometries of TSs of all possible reaction pathways of the reaction between the azomethine imine (1) and the chromene (2). The TS were obtained starting from the optimized structure of the corresponding cycloadducts and confirmed by frequency calculation.

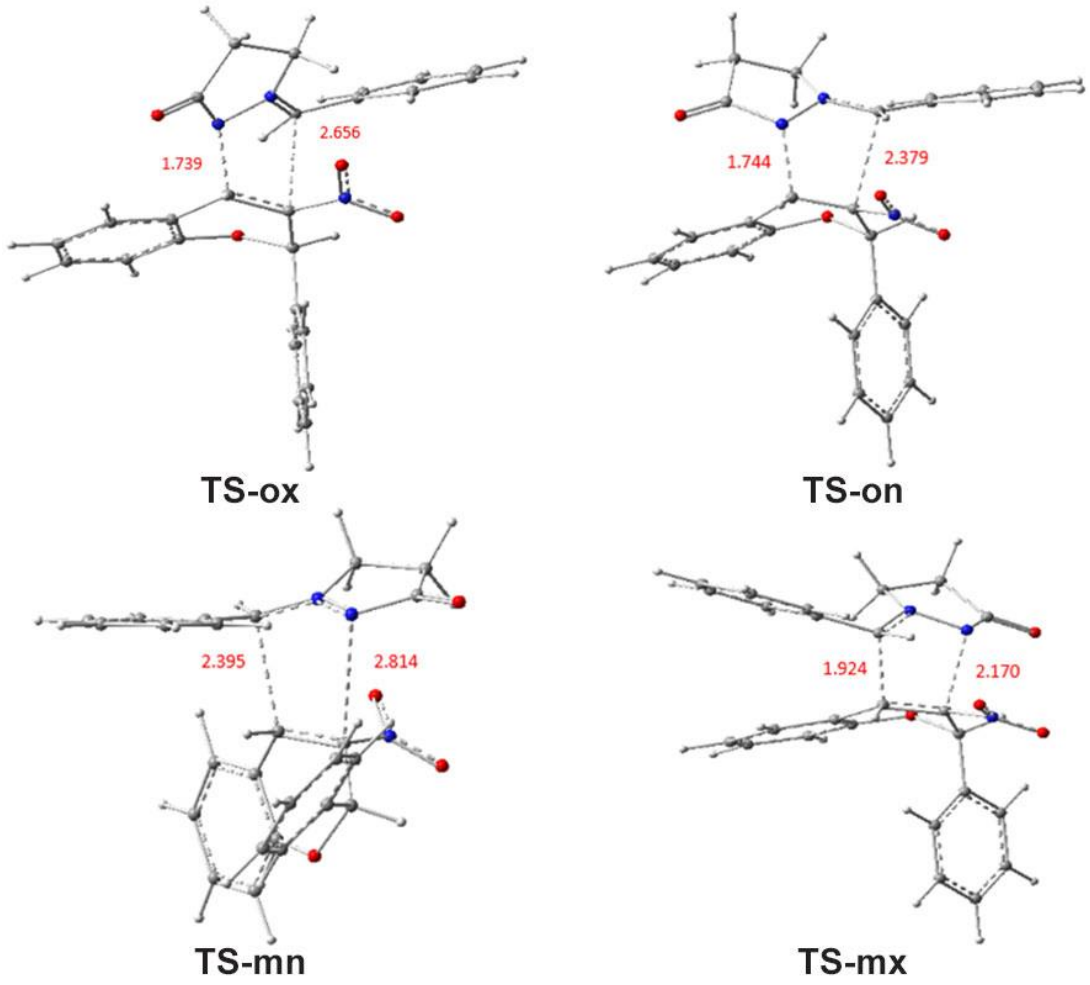

Figure 4-6: Gas phase optimized TSs geometries of the possible reaction pathways for 32CA between azomethine imine (1) and chromene (2)

The lengths of the newly formed bonds of the ortho channel are 1.739 (C1−N3) and 2.656 Å (C2−C5) for TS-ox and 1.744 and 2.379 Å for the respective bonds of TS-on, while those of the meta channel are 2.395 (C1−C5) and 2.814 Å (C2−N3) for TS-mn and 1.924 and 2.170 Å for the respective bonds of TS-mx.

Based on the calculated geometries of TSs and starting from the fact that the C−C bond lengths are in the range 1.90 to 2.0 Å and while the C−N bonds are 1.70 to 1.92 Å. [11],[30], [31] we can note that, firstly, a highly asynchronous bond formation is observed in all pathways of this 32CA reaction but the ortho pathways are more asynchronous than the meta ones and (TS-ox) is the most asynchronous one, while the asynchronicity decreases in the in the following order: 0.92 (TS-ox), 0.64 (TS-on), 0.42 (TS-mn) and 0.25 for the (TS-mx), secondly, in the meta pathways, the C−N bond formation is less advanced than the C−C bonds, inversely, the C−C bond formation is less advanced than the formation of C−N bonds in the ortho pathways. It is also worth to mention that along the most favorable (ortho-exo) pathway the formation of the new C−N bond is almost completed while that of the C−C bond is not yet begun. Such very large asynchronicity comes from the high polar character of this 32CA reaction between the zwitterionic azomithine imine (1) and chromene (2) and may be indicating for the two-stage one-step mechanism that has been observed for similar 32CA reactions. [30]

Calculation of the GEDT at the TSs [32] permits the analysis of the polar character of the 32CA, Indeed, the highest value of GEDT (0.35 e) has been recorded at the most favorable pathway (ortho-exo) with a negative sign in excellent agreement with CDFT analysis that expected an electron flux from the azomithine imine (1) toward the chromene (2).

Note that the values of GEDT above 0.2 e are considered characteristic for polar and values near 0 e for nonpolar reactions. Therefore, the obtained GEDT value allows to classify the 32CA reaction between azomithine imine (1) and chromene (2) as *polar zwitterionic*.

4.7 Origin of the ortho-exo stereoselectivity

Many studies have been reported that the noncovalent interactions (NCI) such as O···H, N···H and X···H are generally the origin of the stability of the major product. Thus, due to the structure of the cycloadducts (3) of the reaction between azomethine imine (1) and chromene (2) which contains nitro group, heteroatoms (oxygen and nitrogen) as well as close phenyl rings; we have performed an investigation with some quantum tools to confirm and to determine the presence and the nature of these interactions at the most favourable transition states (TS-ox) and (TS-on).

4.7.1 Analysis of noncovalent interactions

Many published researches proved that NCI [33] are the origin of stability of most molecular structures especially in cycloaddition reactions. [34],[35] to this end; the evaluation of the low reduced density gradient isosurface permits the visualisation of the formation of non-covalent interactions [36] figure 4-6 shows the reduced density gradient isosurface of TS-ox and TS-on.

We clearly remark that the two structures contain some noncovalent interactions of hydrogen bond between the ethylenic carbon of the methine CH group of the azomethine imine moiety and the nitro group of the chromene framework and a van der Waals type between the different ring systems. In addition, by comparison between the gradient isosurfaces of TS-ox and TS-on, it is clear that TS-ox structure contains two wider, more coherent, and more widely spread green surfaces between the phenyl ring of azomethine imine (1), the pyrazolidinone ring, and the chromene moiety, which accounts for the existence of stronger noncovalent interactions in TS-ox compared to TS-on and, therefore, an enhanced stability of the former.

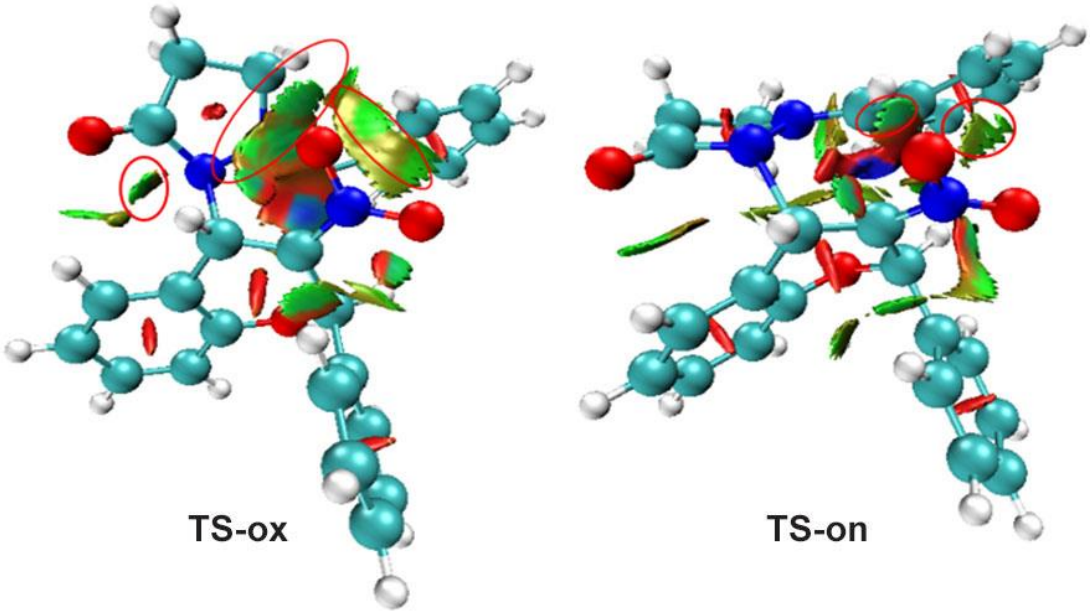

Figure 4-7: Noncovalent interactions in TS-ox and TS-on visualized by low reduced density gradient isosurfaces at isosurface value of 0.5 au. Blue color indicates a hydrogen bonding interaction, green color indicates favorable noncovalent interaction

Red color indicates steric non favorable interaction

4.7.2 Quantum theory of atoms in molecules analysis

Further analysis using the quantum theory of atoms in molecules (QTAIM) method proposed by Bader and coworkers [37],[38]. is used with the goal of deeply understanding the parameters controlling the stereoselectivity of the 32CA reaction between azomethine imine (1) and chromene (2) and to identify the kind of non-covalent interactions stabilizing the ortho-exo approach. This theory provides access to and classification of atomic interactions within a chemical system based on the bond critical point (BCP) and their associated features, such as the energy density (H_{bcp}), the gradient of the electronic density (ρ_{bcp}), and its Laplacian ($\nabla^2\rho_{bcp}$). [38] Table 4-4 compiles the (3,–1) BCPs parameters of TS-ox and TS-on. Figure 4-7 displays the molecular graphs of TS-ox and TS-on, which were produced using QTAIM analysis of electron density (estimated at the B3LYP/6 311G(d,p) level) in conjunction with (3,−1) BCPs.

Table 4-4: QTAIM (3,–1) bond critical points parameters (au) of TS-ox and TS-on

Interaction	Type	BCP label	ρ_{bcp}	$\nabla^2\rho_{bcp}$	H_{bcp}
		TS-ox			
H···O	Intermolecular	134	0.007613	0.024344	0.0007850
H···O	Intermolecular	86	0.010358	0.033725	0.000958
H···O	Intermolecular	74	0.005926	0.022041	0.000856
H···O	Intermolecular	89	0.007433	0.023378	0.000598
H···O	Intermolecular	108	0.013409	0.050485	0.001733
N···O	Intermolecular	106	0.013522	0.049892	0.001251
H···H	Intramolecular	96	0.008618	0.032067	0.001588
N···C	New bond	117	0.137999	–0.043831	–0.073049
C···C	New bond	92	0.025301	0.05090	–0.000763
		TS-on			
H···O	Intermolecular	106	0.005618	0.019345	0.000664
H···O	Intermolecular	91	0.003213	0.012579	0.000637
H···C	Intermolecular	110	0.009553	0.037380	0.001840
H···C	Intramolecular	117	0.009271	0.032245	0.001203
N···C	New bond	101	0.138558	–0.053689	–0.072079
C···C	New bond	84	0.043109	0.052933	–0.006540

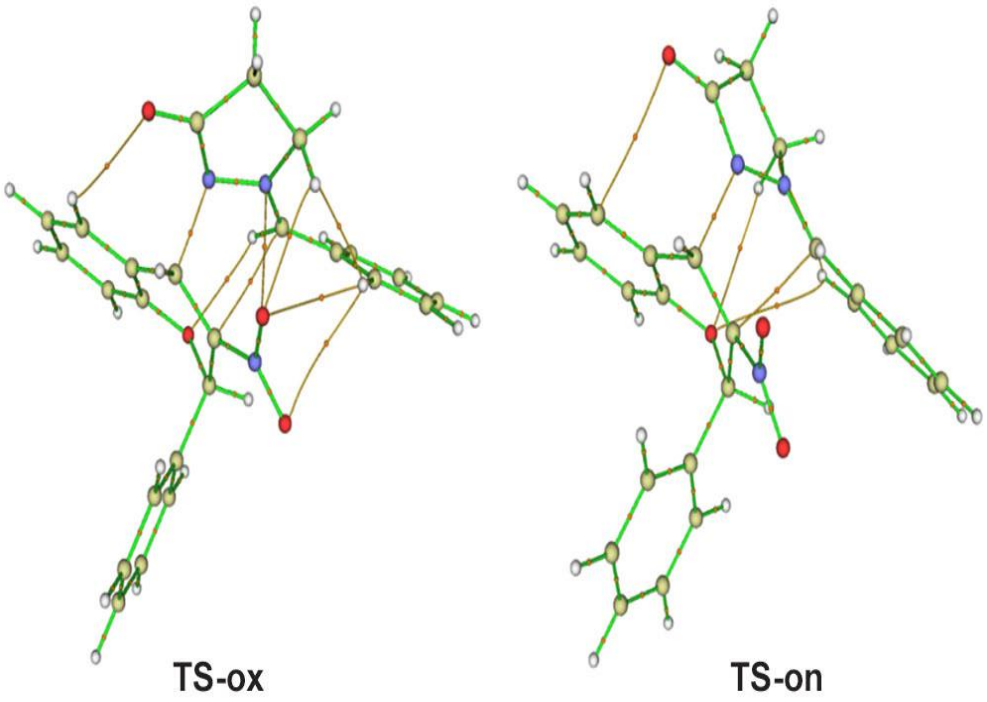

Figure 4-8: Molecular graphs of TS-ox and TS-on obtained by QTAIM analysis of B3LYP/6-311G(d,p) electron density, with (3, −1) bond critical points (orange spheres), bond paths (brown lines)

There are six H···O, one N···O, and one H···H intramolecular noncovalent interactions shown on the QTAIM molecular graph of TS-ox. However, for TS-on, only one C···H and three H···O intramolecular noncovalent interactions can be found. As a result, TS-ox is more stable and kinetically preferred than TS-on due to the greater amount of stabilized noncovalent contacts in this system.

The two TSs structures exhibit a strong N-C interaction, which is corresponding to the newly formed bond represented by a negative Laplacian of energy density. [39] Notably, the formation of the new C-C bond began at the TS due to its solely negative energy density, which is in line with the examination of TS geometries and the independent gradient model derived from the Hirshfeld partition (IGMH) (refer below).

Five intermolecular weak noncovalent hydrogen bonds (HB) are present in TS-ox, according to a study of its BCP features (Table 4-4). These HBs correspond to the BCP number 134, 86, 74, 89, and 108. An N···O interaction that is weak and

noncovalent is represented by the BCP number 106. Moreover, BCP number 96 is associated with the presence of a single intramolecular H···H interaction, it is worth to mention that the positive Laplacian of energy density for each of these BCPs indicates that they are weak HBs and van der Waals type interactions. Furthermore, due to their greater energy density values, the interactions associated with BCP number 108, 106, and 96 are weaker than the rest.

Three weak noncovalent HBs that are intermolecular and correspond to BCP numbers 106, 91, and 110 as well as one intramolecular H···C interaction that corresponds to BCP number 117 are visible according the parameters of TS-on. Positive Laplacian of electron density and positive energy density values are associated to all these BCPs. It's also important to note that because BCPs 106 and 91 have lower energy density values than BCPs 110 and 117, thus, their corresponding interactions are stronger. This demonstrates that TS-ox is preferred comparing to TS-on due to weaker van der Waals and HB bonds that contains.

4.7.3 IGMH analysis

One of the most effective methods for examining weak and covalent interactions is the Independent Gradient Model (IGM). [40] Hénon and colleagues first presented it in 2018, and it was further developed using three different axes: promolecular density, gradient-based partitioning (GBP), and Hirshfeld partition (IGMH). IGM is an effective tool because it can quantify intra- and inter-fragment interaction strengths using the internal bond strength index for weak interactions (IBSIW), which can be calculated using the following formula:

$$\boldsymbol{IBSIW(i,j) = 100\,x\ \frac{\delta G_{i,j}^{pair}}{d(i,j)^2}} \qquad \textbf{Eq. 56}$$

Where d(i,j) is the distance between atoms i and j and $\delta G_{i,j}^{pair}$ is atomic pair contribution to interfragment interaction.

With the exception of the interacting atoms of TS-ox (C1−N3 and C2−C5), the total IBSIW of all atoms is 16.31, which is more than the corresponding value of TS-on, which is 15.94. This suggests that compared to TS-on, the weak interactions in TS-ox are stronger. The reason behind that is; in TS-ox, the pyrazolidinone and pyrazolidinones are oriented toward the O2N−C−C atoms of the chromene framework creating a boat shap that lead to the formation of more weak interactions. However, in the TS-on the ring pyrazolidinone is oriented away from the chromene moiety, thus less and weaker interactions.

4.8 BET study of the 32CA reaction between azomethine imine (1) and chromene (2).

We have conducted a BET [41] study based on ELF topological analysis of some selected points along the intrinsic reaction coordinate (IRC) curve of the most favorable pathway (ortho-exo) in order to get a detailed view of changes of the electron density as well as the bond forming/breaking pattern and thus elucidate the type of reaction mechanism applicable to the 32CA reaction under study. Scheme 4-6 provides a schematic representation of the bond forming and breaking pattern of the 32CA reaction between azomithine imine (1) and chromene (2).

A molecular complex (MC) is formed as the separated reagents gradually approach each other. The MC is 9.67 kcal.mol^{-1} more stable than the separated reagents, with interacting atoms (C1,N3) and (C2,C5) have a distance of 2.58 and 3.11 Å, respectively (Table 4-5). At this moment, there is a slight difference is noticed in in molecular electron density between separated reagents and the molecular complex.

The MC structure displays three disynaptic basins, V(C1,C2), V(N3,N4), and V(N4,C5), with populations of 3.45, 1.74, and 3.68 e, respectively, associated with the C1=C2 double bond of the chromene (2) molecule, the N3−N4 single bond, and the N4=C5 double bond of the azomethine imine (1) moiety. One monosynaptic basin, V(N3), integrating a population of 3.31 e, which corresponds to the N3 lone pair of azomethine imine (1). Just a small amount of electron density (~0.06 e) has moved between the two frameworks at this stage.

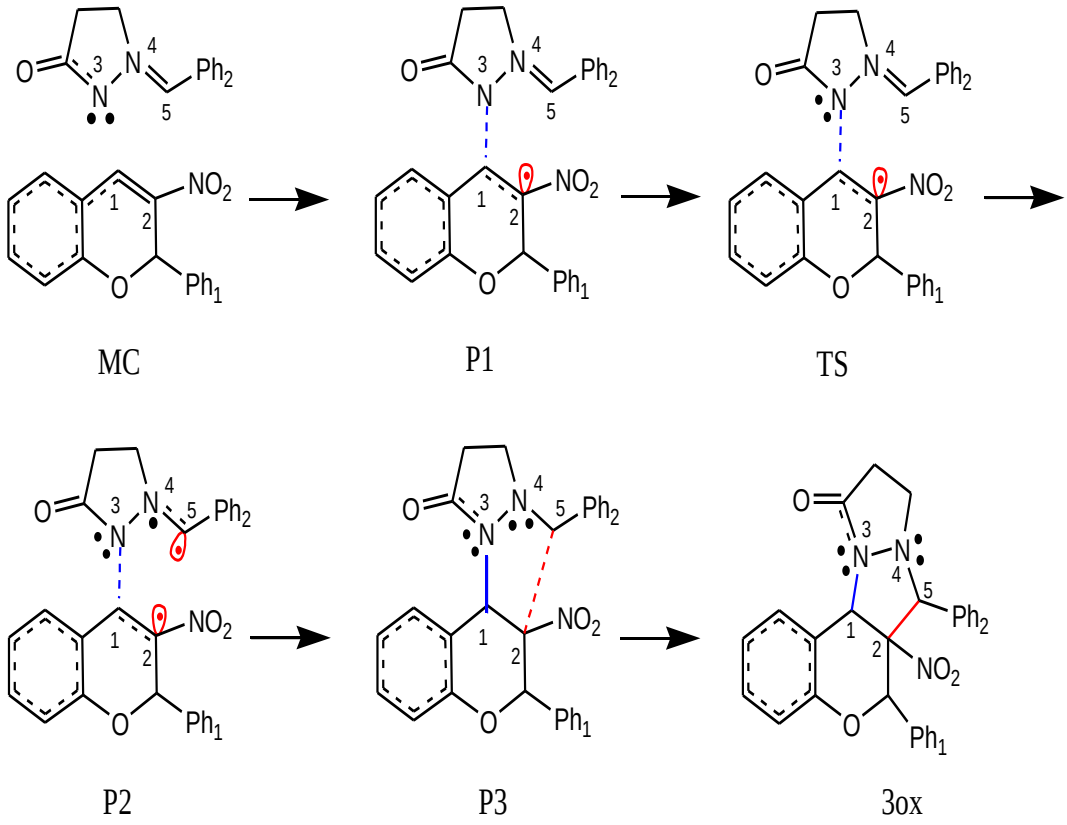

Scheme 4-4: Schematic explanation of the bond breaking/forming pattern of the 32CA reaction of azomithine imine (1) with chromene (2)

There is an apparent changes with regard to MC at point P1 on the IRC curve, where the distance d(C1,N3) and d(C2,C5) are 1.80 and 2.68 Å, respectively. These changes are due to full depopulation of the N3 lone pair valence basin V(N3), which results in the formation of a disynaptic basin V(C1,N3) integrating 3.33 e. the second topological change is the apparition of a monosynaptic basin at the C2 atom integrating a population of 0.52 e as a result of the depopulation of the V(C1,C2) by 0.64 e. Additionally, we can observe that the disynaptic basin V(N3,N4) is depopulated by 0.16 e toward the C5 atom. On the other side, the V(N4,C5) is slightly populated by 0.18 e. Thus, these topological changes suggest that the first new bond formation is thus caused by the donation of a portion of the N3 non-bonding electron density of the azomithine imine (1) to the C1 atom of the chromene (2) moiety and the double bond between C1 and C2 has already ruptured giving rise to the formation of the C2 pseudoradical center. This accounts for the donation bond formation model [15] that costs 8.01 kcal.mol^{-1} and occurs at 0.32 e of GEDT.

Table 4-5: ELF valence basin populations (in e), ΔE (kcal·mol–1), GEDT (e) along the IRC of TS (ortho-exo) of the 32CA reaction of azomethine imine (1) with chromene (2)

Parameter	MC	P1	TS	P2	P3	3ox
V(C1,C2)	3.45	2.81	2.71	2.31	2.06	2.03
V(C2)		0.52	0.56	0.79	2.09	
V(N3)	3.31		2.17	1.92	1.84	1.79
V(N3,N4)	1.74	1.58	1.54	1.45	1.33	1.32
V(N4,C5)	3.68	3.86	3.88	2.79	2.20	1.98
V(N4)				1.27	1.96	2.05
V(C5)				0.15		
V(C1,N3)		3.33	1.19	1.50	1.59	1.61
V(C2,C5)					1.66	1.75
d(N1,N3)	2.58	1.80	1.73	1.56	1.50	1.49
d(C2,C5)	3.11	2.68	2.65	2.33	1.82	1.73
ΔE	-3.09	8.01	8.14	7.50	1.34	-0.83
GEDT	-0.06	-0.32	-0.35	-0.29	-0.31	0.05

The most significant change at TS where the distances d(C1,N3) and d(C2,C5) are 1.73 and 2.65 Å; is the reappearance of the V(N3) with 2.17 e population corresponding to the N3 lone pair and the severe depopulation of the disynaptic basin V(C1,N3) created at point P1 by 2.14 e. the depopulation of the V(C1,C2) disynaptic basin at this point reaches 2.71 e, which in turn slightly populate the pseudoradical center V(C2) by 0.04 e. it is important to mention that the first new bond C1−N3 is not formed yet and the GEDT reaches its maximum value of 0.35 e, indicating the polar character of this zwitterionic 32CA reaction with an energy barrier of 8.13 kcal.mol^{-1} .

The populations of the monosynaptic basin V(C2) and the disynaptic basin V(C1,N3) are increased by 0.23 and 0.31 e, respectively, at the reaction point P2, where d(C1,N3) and d(C2,C5) are 1.56 and 2.33 Å, respectively. Also the populations

of the disynaptic basin V(N3,N4) and the non-bonding electron of the N3 lone pair and are decreased by 0.0.09 and 0.0.25 e, respectively. Around 1.09 e are extracted from the population of the disynaptic basin V(N4,C5), resulting in the formation of the V(C5) pseudoradical center. This center is necessary for the subsequent formation of the C2−C5 disynaptic basin and the V(N4) monosynaptic basins, which account for the formation of N4 lone pairs with initial populations of 0.15 and 1.27 e, respectively.

The most significant topological change at P3 where the distances of newly formed bonds (C1,N3) and d(C2,C5) decreases to 1.50 and 1.82 Å, respectively, is the appearance of the disynaptic basin V(C2,C5) with an initial population of 1.66 e and the vanish of the pseudoradical center V(C5) recently created at P2. We remark also the depopulation of V(N4,C5) makes an increase of the population of the monosynaptic basin V(N4). Also an increase by 1.59 e on the population of the disynaptic basin V(C1,N3) is noticeable at this stage.

The pseudoradical center V(C2) merges into the disynaptic basin V(C2,C5) during the production of cycloadduct 3ox, the last point on the IRC curve. This basin reaches its final population of 1.75 e, which is approximately 0.14 e more populated than the V(C1,N3) of the first new bond. However, the populations of the N3 lone pair drops to 1.79 e, while the new lone pair of the N4 increases to 2.05 e. In contrast, the populations of the initial double bonds of the two reagents, V(C1,C2) and V(N4,C5), reach 2.03 and 1.98 e, respectively.

From the ELF topological analysis we can conclude that the first new bond, C1−N3, forms via a donation bond formation model and begins after the TS point with d(C1,N3) 1.73 Å. This is consistent with earlier research that found that the formation of C−N bonds begins at approximately 1.70 Å, due to the donation of a portion of the non-bonding electron density of the azomethine imine N3 atom to the chromene (C1) atom. This finding is in excellent agreement with the Parr function analysis. Additionally, the coupling of the C2 and C5 pseudoradical centers results in the production of the second C2−C5 single bond in the late stage of the process (P3), with

a length of 1.82 Å. The chromene moiety's C=C double bond must be broken homolytically for the creation of the first new bond (C1−N3), whereas the imine C=N double bond must be broken heterolytically for creation of the second single bond (C2−C5). When the population of the first single bond (C1−N3) reaches 98% of its final value, the production of the second single bond (C2−C5) begins, suggesting a two-stage one-step mechanism.

4.9 Computational details

DFT calculations were carried out using the hybrid functional B3LYP [42] combined with the 6-311G(d,p) basis set. [43] in which the d-type polarization for second row elements and p-type polarization functions for hydrogen atoms were incorporated. For the optimization process, Berny's analytical gradient method was employed. It is demonstrated that the B3LYP/6-311G(d,p) level is appropriate for Diels-Alder cycloaddition processes and 32CA reactions' geometry optimization and electronic property characterization. [44] In order to verify the nature of the optimized stationary points, a supplementary frequency calculation was performed at the same level of theory, in which the reactants, the products, and the intermediates should not present any imaginary frequency, while the TSs structures should exhibit only one imaginary frequency. Solvent effects were taken in consideration by single point calculation over the optimized gas phase geometries by using the polarizable continuum model developed by Tomasi's group [45] in the framework of the self-consistent reaction field. [46]

The minimum energy path which connects TS to the two linked minima was found by tracing the IRC [47] By calculating the GEDT at the TS within the NBO technique [19] the polarity of the reaction was assessed. A GEDT value above 0.2 e indicates a polar nature of the reaction, while a value near 0.0 e corresponds to a nonpolar process. [32] It is important to note in this context that the term of GEDT refers to the global, not local, transfer of electron density between reagents.

Using the Multiwfn program [48] ELF and NPA examined the electronic structures of the simplest azomethine imine and N,N'-cyclic azomethine imine (1)

across the B3LYP/6-311G(d,p) monodeterminantal wave functions. The results were displayed using the UCSF Chimera software.[49] The Gaussian suite of programs optimized all the structures examined in this work, while the CFDT indices were calculated from the energies of the frontier molecular orbitals.

4.10 References

[1] A. Padwa, *1, 3-Dipolar cycloaddition chemistry*. Wiley-interscience, 1984.

[2] A. Padwa and W. H. Pearson, *Synthetic Applications of 1, 3-Dipolar Cycloaddition Chemistry Toward Heterocycles and Natural Products, Volume 59*, vol. 59. John Wiley & Sons, 2003.

[3] R. S. Kumar, M. Moydeen, S. S. Al-Deyab, A. Manilal, and A. Idhayadhulla, "Synthesis of new morpholine-connected pyrazolidine derivatives and their antimicrobial, antioxidant, and cytotoxic activities," *Bioorg. Med. Chem. Lett.*, vol. 27, no. 1, pp. 66–71, 2017.

[4] Y. R. Prasad, A. L. Rao, L. Prasoona, K. Murali, and P. R. Kumar, "Synthesis and antidepressant activity of some 1, 3, 5-triphenyl-2-pyrazolines and 3-(2 ''-hydroxy naphthalen-1 ''-yl)-1, 5-diphenyl-2-pyrazolines," *Bioorg. Med. Chem. Lett.*, vol. 15, no. 22, pp. 5030–5034, 2005.

[5] J. R. Goodell, F. Puig-Basagoiti, B. M. Forshey, P.-Y. Shi, and D. M. Ferguson, "Identification of compounds with anti-West Nile virus activity," *J. Med. Chem.*, vol. 49, no. 6, pp. 2127–2137, 2006.

[6] A. Y. Barkov, N. S. Zimnitskiy, I. B. Kutyashev, V. Y. Korotaev, and V. Y. Sosnovskikh, "Highly stereoselective [3+2]-cycloaddition reaction of stabilised N,N'-cyclic azomethine imines with 3-nitro-2-phenyl-2H-chromenes: Synthesis of tetrahydrochromeno[4,3-c]pyrazolo[1,2-a]pyrazol-11-ones," *Tetrahedron Lett.*, vol. 58, no. 42, 2017, doi: 10.1016/j.tetlet.2017.09.015.

[7] A. D. Becke and K. E. Edgecombe, "A simple measure of electron localization in atomic and molecular systems," *J. Chem. Phys.*, vol. 92, no. 9, pp. 5397–5403, 1990, doi: 10.1063/1.458517.

[8] B. Silvi and A. Savin, "Classification of chemical bonds based on topological analysis of electron localization functions," *Nature*, vol. 371, no. 6499, pp. 683–686, 1994.

[9] B. Silvi, "The synaptic order: a key concept to understand multicenter bonding," *J. Mol. Struct.*, vol. 614, no. 1–3, pp. 3–10, 2002.

[10] G. N. Lewis, *Valence and the Structure of Atoms and Molecules*, no. 14. Chemical Catalog Company, Incorporated, 1923.

[11] L. R. Domingo and M. Ríos-Gutiérrez, "A Molecular Electron Density Theory study of the reactivity of azomethine imine in [3+2] cycloaddition reactions," *Molecules*, vol. 22, no. 5, 2017, doi: 10.3390/molecules22050750.

[12] L. R. Domingo, "Molecular electron density theory: A modern view of reactivity in organic chemistry," *Molecules*, vol. 21, no. 10, pp. 1–15, 2016, doi:

10.3390/molecules21101319.

[13] F. Chafaa, A. Khorief Nacereddine, and A. Djerourou, “Unravelling the mechanism and the origin of the selectivity of the [3 + 2] cycloaddition reaction between electrophilic nitrone and nucleophilic alkene,” *Theor. Chem. Acc.*, vol. 138, no. 12, pp. 1–11, 2019, doi: 10.1007/s00214-019-2510-6.

[14] M. Ríos-Gutiérrez, L. Nasri, A. Khorief Nacereddine, A. Djerourou, and L. R. Domingo, “A molecular electron density theory study of the [3 + 2] cycloaddition reaction between an azomethine imine and electron deficient ethylenes,” *J. Phys. Org. Chem.*, vol. 31, no. 6, 2018, doi: 10.1002/poc.3830.

[15] L. R. Domingo, M. Ríos-Gutiérrez, and P. Pérez, “A new model for C–C bond formation processes derived from the molecular electron density theory in the study of the mechanism of [3+ 2] cycloaddition reactions of carbenoid nitrile ylides with electron-deficient ethylenes,” *Tetrahedron*, vol. 72, no. 12, pp. 1524–1532, 2016, doi: 10.1016/j.tet.2016.01.061.

[16] L. R. Domingo and S. R. Emamian, “Understanding the mechanisms of [3+ 2] cycloaddition reactions. The pseudoradical versus the zwitterionic mechanism,” *Tetrahedron*, vol. 70, no. 6, pp. 1267–1273, 2014.

[17] L. Nasri, M. Ríos-Gutiérrez, A. K. Nacereddine, A. Djerourou, and L. R. Domingo, “A molecular electron density theory study of [3 + 2] cycloaddition reactions of chiral azomethine ylides with β-nitrostyrene,” *Theor. Chem. Acc.*, vol. 136, no. 9, pp. 1–12, 2017, doi: 10.1007/s00214-017-2133-8.

[18] A. E. Reed, R. B. Weinstock, and F. Weinhold, “Natural population analysis,” *J. Chem. Phys.*, vol. 83, no. 2, pp. 735–746, 1985, doi: 10.1063/1.449486.

[19] A. E. Reed, L. A. Curtiss, and F. Weinhold, “Intermolecular interactions from a natural bond orbital, donor-acceptor viewpoint,” *Chem. Rev.*, vol. 88, no. 6, pp. 899–926, 1988.

[20] l R. Huisgen, “Kinetik und Mechanismus 1.3-Dipolarer Cycloadditionen,” *Angew. Chemie*, vol. 75, no. 16-17, pp. 742–754, 1963.

[21] P. Geerlings, F. De Proft, and W. Langenaeker, “Conceptual density functional theory,” *Chem. Rev.*, vol. 103, no. 5, pp. 1793–1874, 2003.

[22] L. R. Domingo, M. Ríos-Gutiérrez, and P. Pérez, “Applications of the conceptual density functional theory indices to organic chemistry reactivity,” *Molecules*, vol. 21, no. 6, p. 748, 2016.

[23] L. R. Domingo, M. Ríos-Gutiérrez, and P. Pérez, “A Molecular Electron Density Theory Study of the Reactivity and Selectivities in [3 + 2] Cycloaddition Reactions of C,N-Dialkyl Nitrones with Ethylene Derivatives,” *J. Org. Chem.*, vol. 83, no. 4, pp. 2182–2197, 2018, doi: 10.1021/acs.joc.7b03093.

[24] P. Pérez, L. R. Domingo, M. J. Aurell, and R. Contreras, “Quantitative characterization of the global electrophilicity pattern of some reagents involved in 1,3-dipolar cycloaddition reactions,” *Tetrahedron*, vol. 59, no. 17, pp. 3117–3125, 2003, doi: 10.1016/S0040-4020(03)00374-0.

[25] L. R. Domingo *et al.*, “Quantitative characterization of the global electrophilicity power of common diene/dienophile pairs in Diels–Alder reactions,” *Tetrahedron*, vol. 58, no. 22, pp. 4417–4423, 2002.

[26] R. T. Sanderson, “Partial charges on atoms in organic compounds,” *Science (80-.).*, vol. 121, no. 3137, pp. 207–208, 1955.

[27] L. R. Domingo, P. Pérez, and J. A. Sáez, “Understanding the local reactivity in polar organic reactions through electrophilic and nucleophilic Parr functions,” *RSC Adv.*, vol. 3, no. 5, pp. 1486–1494, 2013, doi: 10.1039/c2ra22886f.

[28] W. Yahia, A. Khorief Nacereddine, M. Liacha, and A. Djerourou, “A quantum-chemical DFT study of the mechanism and regioselectivity of the 1, 3-dipolar cycloaddition reaction of nitrile oxide with electron-rich ethylenes,” *Int. J. Quantum Chem.*, vol. 118, no. 11, p. e25540, 2018.

[29] S. Sadi, A. Khorief Nacereddine, and A. Djerourou, “The effects of solvent nature and steric hindrance on the reactivity, mechanism and selectivity of the cationic imino-Diels–Alder cycloaddition reaction between cationic 2-azadienes and arylpropene,” *J. Phys. Org. Chem.*, vol. 35, no. 4, p. e4311, 2022.

[30] M. Ríos-Gutiérrez, L. Nasri, A. Khorief Nacereddine, A. Djerourou, and L. R. Domingo, “A molecular electron density theory study of the [3+ 2] cycloaddition reaction between an azomethine imine and electron deficient ethylenes,” *J. Phys. Org. Chem.*, vol. 31, no. 6, p. e3830, 2018.

[31] M. Ríos-Gutiérrez and L. R. Domingo, “Unravelling the Mysteries of the [3+2] Cycloaddition Reactions,” *European J. Org. Chem.*, vol. 2019, no. 2, pp. 267–282, 2019, doi: 10.1002/ejoc.201800916.

[32] L. R. Domingo, “A new C-C bond formation model based on the quantum chemical topology of electron density,” *RSC Adv.*, vol. 4, no. 61, pp. 32415–32428, 2014, doi: 10.1039/c4ra04280h.

[33] E. R. Johnson, S. Keinan, P. Mori-Sánchez, J. Contreras-García, A. J. Cohen, and W. Yang, “Revealing noncovalent interactions,” *J. Am. Chem. Soc.*, vol. 132, no. 18, pp. 6498–6506, 2010.

[34] A. K. Nacereddine, C. Sobhi, A. Djerourou, M. Ríos-Gutiérrez, and L. R. Domingo, “Non-classical CH⋯ O hydrogen-bond determining the regio-and stereoselectivity in the [3+ 2] cycloaddition reaction of (Z)-C-phenyl-N-methylnitrone with dimethyl 2-benzylidenecyclopropane-1, 1-dicarboxylate. A topological electron-density study,” *RSC Adv.*, vol. 5, no. 120, pp. 99299–

99311, 2015.

[35] M. Ríos-Gutiérrez, P. Pérez, and L. R. Domingo, “A bonding evolution theory study of the mechanism of [3+2] cycloaddition reactions of nitrones with electron-deficient ethylenes,” *RSC Adv.*, vol. 5, no. 72, pp. 58464–58477, 2015, doi: 10.1039/c5ra10458k.

[36] J. R. Lane, J. Contreras-García, J.-P. Piquemal, B. J. Miller, and H. G. Kjaergaard, “Are bond critical points really critical for hydrogen bonding?,” *J. Chem. Theory Comput.*, vol. 9, no. 8, pp. 3263–3266, 2013.

[37] R. F. W. Bader, “A quantum theory,” *Clarendon Oxford, UK*, 1990.

[38] R. F. W. Bader and H. Essén, “The characterization of atomic interactions,” *J. Chem. Phys.*, vol. 80, no. 5, pp. 1943–1960, 1984.

[39] A. Khorief Nacereddine, “A MEDT computational study of the mechanism, reactivity and selectivity of non-polar [3+2] cycloaddition between quinazoline-3-oxide and methyl 3-methoxyacrylate,” *J. Mol. Model.*, vol. 26, no. 11, 2020, doi: 10.1007/s00894-020-04585-0.

[40] C. Lefebvre, H. Khartabil, J. Boisson, J. Contreras-García, J. Piquemal, and E. Hénon, “The independent gradient model: a new approach for probing strong and weak interactions in molecules from wave function calculations,” *ChemPhysChem*, vol. 19, no. 6, pp. 724–735, 2018.

[41] X. Krokidis, S. Noury, and B. Silvi, “Characterization of elementary chemical processes by catastrophe theory,” *J. Phys. Chem. A*, vol. 101, no. 39, pp. 7277–7282, 1997.

[42] P. J. Stephens, F. J. Devlin, C. F. Chabalowski, and M. J. Frisch, “Ab initio calculation of vibrational absorption and circular dichroism spectra using density functional force fields,” *J. Phys. Chem.*, vol. 98, no. 45, pp. 11623–11627, 1994.

[43] J. A. Pople, P. V. Schleyer, W. J. Hehre, and L. Radom, *AB INITIO molecular orbital theory*. John Wiley & Sons, Incorporated, 1986. doi: 10.1016/s0022-328x(00)99651-7.

[44] C. X. Cui and Y. J. Liu, “A DFT study on Diels-Alder cycloadditions of trans-1,3-butadiene to C60 and C70,” *J. Phys. Org. Chem.*, vol. 28, no. 4, pp. 281–289, 2015, doi: 10.1002/poc.3408.

[45] V. Barone, M. Cossi, and J. Tomasi, “Geometry optimization of molecular structures in solution by the polarizable continuum model,” *J. Comput. Chem.*, vol. 19, no. 4, pp. 404–417, 1998, doi: 10.1002/(SICI)1096-987X(199803)19:4<404::AID-JCC3>3.0.CO;2-W.

[46] E. Cances *et al.*, “A new integral equation formalism for the polarizable continuum model: Theoretical background and applications to isotropic and anisotropic dielectrics,” *J. Chem. Phys.*, vol. 107, no. 8, pp. 3032–3041, Aug. 1997, doi: 10.1063/1.474659.

[47] K. Fukui, “A formulation of the reaction coordinate,” *Journal of Physical Chemistry*, vol. 74, no. 23. p. 4161, 1970. doi: 10.1021/j100717a029.

[48] T. Lu and F. Chen, “Multiwfn: a multifunctional wavefunction analyzer,” *J. Comput. Chem.*, vol. 33, no. 5, pp. 580–592, 2012.

[49] E. F. Pettersen *et al.*, “UCSF Chimera—a visualization system for exploratory research and analysis,” *J. Comput. Chem.*, vol. 25, no. 13, pp. 1605–1612, 2004.

General conclusion

In this work, we conducted a computational study using the DFT quantum chemistry method at the DFT/ B3LYP/6-311G(d,p) theoretical level of the [3+2] cycloaddition reactions between N,N'-cyclic azomethine imine and 3-nitro-2-phenyl-2H-chromene.

The ELF and NPA analysis showed that while the simplest azomethine imine is a pmr-type TAC, the structural changes on its terminal atoms, makes the N,N'-cyclic azomethine imine zw-type TAC. The strong nucleophilic character of the azomithine imine reactant and the strong electrophilic character of the chromene reactant shown by CDFT indices point to a high polar zw-type molecule, which is confirmed by the high value of GEDT in the most favorable TS (0.35 e).

Despite the presence of electron-withdrawing groups, such as carbonyl function and phenyl ring, in the N,N'-cyclic azomethine imine structure, this species remain a strong nucleophile and can participate in a polar 32CA reaction with a strong electrophile. The total ortho regioselectivity observed experimentally is explained with success using the analysis of the Parr function local reactivity indices.

Analysis of the PES shows that the reaction takes place along a very asynchronous two-stage one-step mechanism to give exclusively the kinetically favored ortho-exo cycloadduct with low activation energy of 8.14 kcal.mol^{-1} in gas phase.

Analysis of TSs structures using NCI, QTAIM, and IGMH techniques allows to explain the high stereoselectivity observed experimentally by the presence of several stabilized intermolecular noncovalent interactions of hydrogen bond and van der Waals type in both ortho TSs.

The BET study using ELF topological analysis of pertinent points along the IRC of the most favorable reactive pathway indicates a two-stage one-step mechanism, in which the C−N bond is formed first by donation of part of the non-bonding electron density of the most nucleophilic center of the azomethine imine molecule to the most electrophilic center of the chromene molecule and the C−C bond is formed afterward by carbon–carbon coupling of two pseudoradical centers.

In addition to this work, we plan to study the molecular mechanism and the selectivity of other cycloaddition reactions involving other 1,3-dipoles for the synthesis of other biologically active heterocycles. In addition, we are trying to deepen the study of the influence of the nature of the solvent and the catalyst on the nature of the mechanism and on the selectivity of this type of reactions as well as other Diels-Alder cycloaddition reactions.

Appendix A: supplementary information

1. Table S1: Total energies (a.u) of the stationary points involved in the reaction of and chromene 8a with the azomethine imine AI 9a.

	Gas phase	Isopropanol @ 50 °C
Chromene 8a	-858.743772	-858.7538373
Azomethine imine 9a	-571.9080461	-571.9260006
TS-ox	-1430.638848	-1430.66001
TS-on	-1430.628621	-1430.650963
TS-mn	-1430.56559	-1430.584528
TS-mx	-1430.623054	-1430.642416
P-ox	-1430.664451	-1430.679159
P-on	-1430.671981	-1430.686535
P-mn	-1430.671622	-1430.685198
P-mx	-1430.653468	-1430.667409

2. Table S2: B3LYP/6-311G (d,p) gas phase enthalpy H (a.u), Gibbs free energy G (a.u) and entropy S (cal/mol.K) of the stationary points involved in the reaction of and chromene 8a with the azomethine imine AI 9a.

	Enthalpy H	Free energy G	entropy
Chromene 8a	-858.499971	-858.558871	123.967
AI 9a	-571.712469	-571.761645	103.5
Ts ox	-1430.198064	-1430.281179	174.93
TS on	-1430.187951	-1430.271102	175.007
TS-mn	-1430.126954	-1430.21221	179.437
TS-mx	-1430.182635	-1430.265058	173.474
P ox	-1430.220647	-1430.302295	171.843
P on	-1430.228235	-1430.31076	173.688
P-mn	-1430.228512	-1430.309726	170.929
P-mx	-1430.210252	-1430.290357	168.595

3. Table S3: B3LYP/6-311G (d,p) In isopropanol at 50°C enthalpy H (a.u), Gibbs free energy G (a.u) and entropy S (cal/mol.K) and of the stationary points involved in the reaction of and chromene 8a and the azomethine imine AI 9a.

	Enthalpy H	free energy G	entropy
Chromene 8a	-858.507582	-858.574613	130.165
AI 9a	-571.73023	-571.779511	103.722
TS-ox	-1430.215994	-1430.307742	178.162
TS-on	-1430.20598	-1430.300809	184.144
TS-mn	-1430.142728	-1430.238937	186.825
TS-mx	-1430.198863	-1430.289939	176.857
P-ox	-1430.232143	-1430.321951	174.393
P-on	-1430.239664	-1430.330511	176.412
TS-mn	-1430.237979	-1430.331687	181.968
TS-mx	-1430.22005	-1430.31186	178.281

4. Cartesian coordinates of the chromene 8a

C	-1.177009	1.515036	0.446993
C	0.01583	1.544032	-0.1647
C	0.536782	0.391277	-0.982377
O	-0.580336	-0.400157	-1.489347
C	-1.680023	-0.572671	-0.713282
C	-2.03566	0.366685	0.27743
N	0.874887	2.715898	-0.046795
O	0.510192	3.644015	0.666324
O	1.927037	2.6909	-0.682031
C	-3.222197	0.177773	1.002619
C	-4.035509	-0.917691	0.754485
C	-3.673139	-1.832488	-0.239412
C	-2.504448	-1.664916	-0.974471
H	-1.492083	2.361045	1.045822
H	-3.493971	0.904683	1.760517
H	-4.307226	-2.68834	-0.441094
H	-2.214017	-2.364031	-1.748464
H	-4.947484	-1.060237	1.320879
H	1.012796	0.775332	-1.882764
C	1.525896	-0.5076	-0.258166
C	2.512092	-1.157038	-1.006369

C	1.451185	-0.746095	1.116366
C	3.405559	-2.030965	-0.396009
H	2.580348	-0.971543	-2.073111
C	2.344255	-1.622229	1.729287
H	0.701254	-0.242878	1.715184
C	3.321953	-2.266349	0.975374
H	4.169744	-2.522591	-0.987236
H	2.278296	-1.797497	2.797101
H	4.0196	-2.943861	1.45455

5. Cartesian coordinates of the Azomethine imine 9a

C	0.018222	-0.913021	-0.088252
N	-1.153839	-0.321998	-0.060714
N	-2.28132	-1.045023	-0.122883
C	-3.360415	-0.203624	0.00498
C	-2.888469	1.254345	0.206014
C	-1.385383	1.166771	0.044286
O	-4.523387	-0.544821	-0.019416
C	1.359347	-0.364557	-0.04898
C	1.742474	0.990202	-0.148461
C	3.082699	1.356067	-0.097681
C	4.081502	0.396475	0.049163
C	3.725638	-0.948865	0.137546
C	2.391422	-1.321236	0.085833
H	-3.192207	1.588702	1.199368
H	-3.368829	1.898359	-0.530077
H	-0.809864	1.54473	0.888062
H	-1.02331	1.625443	-0.876026
H	-0.071722	-1.990985	-0.133493
H	1.009281	1.769548	-0.282729
H	3.347451	2.404193	-0.17923
H	5.12315	0.692352	0.088385
H	4.490297	-1.70943	0.245501
H	2.126741	-2.370535	0.154048

6. Cartesian coordinates of the TS-ox

C	3.470565	2.277483	2.348066
C	2.818258	1.049916	2.406584
C	1.884923	0.723825	1.426308
C	1.586381	1.619479	0.39205
C	2.258051	2.843657	0.343578
C	3.199885	3.172766	1.312675
H	4.201996	2.530183	3.107566
H	3.025314	0.332672	3.191233
C	0.516228	1.261467	-0.584844
H	2.005168	3.545228	-0.442679
H	3.71513	4.124773	1.265907
C	0.250079	-0.150857	-0.649565
C	0.965712	-1.12927	0.240625
C	-1.930513	0.261221	0.80987
H	-1.113382	0.263909	1.520188
C	-2.895018	-0.826291	0.855917
C	-3.557825	-1.308063	-0.287001
C	-3.101991	-1.469116	2.090247
C	-4.439337	-2.377044	-0.177975
H	-3.329382	-0.898277	-1.261809
C	-3.994566	-2.526983	2.191688
H	-2.563787	-1.125815	2.966916
C	-4.670986	-2.978193	1.057825
H	-4.930476	-2.755205	-1.066636
H	-4.156584	-3.006706	3.149769
H	-5.360317	-3.811222	1.134399
C	-1.247715	3.244553	-0.832794
C	-2.764765	3.266426	-1.01739
H	-3.206377	3.946666	-0.283905
H	-3.00429	3.627166	-2.015986
C	-3.163618	1.812507	-0.778986
H	-4.086649	1.66944	-0.21967
H	-3.184075	1.250541	-1.70812
O	1.228461	-0.481736	1.520538
O	-0.448375	4.036089	-1.266897
N	-0.908009	2.118996	-0.073857
N	-2.024646	1.334777	0.06136
N	-0.559522	-0.640314	-1.656904
O	-0.679848	-1.871787	-1.804083
H	0.604502	1.756755	-1.548486
O	-1.202623	0.187998	-2.362114
C	2.259581	-1.73458	-0.303824
C	2.70206	-1.513318	-1.606619

C	3.009391	-2.569036	0.532809
C	3.879102	-2.104673	-2.064757
H	2.128343	-0.879026	-2.271142
C	4.184451	-3.15772	0.079077
H	2.671249	-2.745171	1.548025
C	4.623749	-2.926186	-1.224451
H	4.210572	-1.92247	-3.080964
H	4.757081	-3.799245	0.739968
H	5.538719	-3.386028	-1.58103
H	0.289056	-1.948724	0.488041

7. Cartesian coordinates of the TS-on

C	-3.643492	1.767569	-1.814709
C	-2.577218	0.907952	-2.071751
C	-1.641967	0.66824	-1.072121
C	-1.741861	1.291261	0.180104
C	-2.830888	2.131381	0.427262
C	-3.780029	2.367213	-0.563814
H	-4.379627	1.952437	-2.588923
H	-2.469877	0.401257	-3.02296
C	-0.663747	1.038683	1.182734
H	-2.913063	2.62057	1.389794
H	-4.617766	3.024016	-0.362635
C	-0.009771	-0.248201	1.005003
C	-0.292943	-1.088372	-0.216706
C	2.136974	0.710169	0.635329
C	0.161135	3.547737	0.527637
C	1.040849	3.90254	-0.680275
H	0.426063	4.365982	-1.450506
H	1.81119	4.615336	-0.37422
C	1.635995	2.551755	-1.085086
H	1.013913	2.039509	-1.824573
H	2.666366	2.593319	-1.434083
O	-0.586586	-0.178086	-1.324901
O	-0.727796	4.211112	0.995461
N	0.545387	2.282988	0.998025
N	1.583149	1.839777	0.209273
N	0.481631	-0.919482	2.138874
O	0.806837	-2.111983	2.013773
H	-0.937516	1.246343	2.210605
O	0.664678	-0.269053	3.187722

C	-1.39798	-2.133899	-0.106794
C	-2.345009	-2.139006	0.916777
C	-1.476858	-3.111947	-1.10345
C	-3.355543	-3.098438	0.941821
H	-2.293687	-1.399637	1.706874
C	-2.484645	-4.070072	-1.082706
H	-0.740851	-3.118073	-1.900917
C	-3.429473	-4.064715	-0.057177
H	-4.081832	-3.092053	1.746788
H	-2.529751	-4.824443	-1.860464
H	-4.213389	-4.813464	-0.034583
H	0.617363	-1.596591	-0.535082
C	3.027999	-0.163163	-0.109489
C	3.049613	-0.276237	-1.512691
C	3.867925	-1.002134	0.647365
C	3.919211	-1.165586	-2.131023
H	2.365736	0.298901	-2.120455
C	4.734612	-1.888594	0.022182
H	3.824784	-0.957437	1.728957
C	4.769772	-1.966311	-1.36869
H	3.924189	-1.244708	-3.211946
H	5.375253	-2.525391	0.620446
H	5.444628	-2.659435	-1.857538
H	2.143675	0.627703	1.717411

8. Cartesian coordinates of the TS-mn

C	1.497117	3.721864	-2.371463
C	0.286172	4.413794	-2.315747
C	1.577266	2.438148	-1.842937
C	0.46053	1.833707	-1.275926
C	-0.783749	2.538107	-1.232557
C	-0.843568	3.835496	-1.749825
C	0.291622	0.572367	-0.524902
C	-0.886921	-0.0725	-0.912966
C	-2.069907	0.600868	-0.301395
O	-1.922889	2.052617	-0.653901
N	0.305898	-2.491417	-0.107486
N	1.370019	-2.039131	-0.722655
C	2.08755	-0.994856	-0.287897
C	-0.288832	-3.478246	-0.919929
C	0.463635	-3.579341	-2.254259

C	1.694492	-2.725455	-2.02988
O	-1.264906	-4.10336	-0.592801
H	0.216915	5.415026	-2.725737
H	2.508295	1.885181	-1.88317
H	-1.788069	4.363694	-1.711001
H	2.840588	-0.688396	-1.004047
H	-0.177784	-3.17317	-3.039123
H	0.681959	-4.622113	-2.48114
H	1.870445	-1.968906	-2.787683
H	2.599043	-3.311514	-1.854668
N	-1.032981	-0.384356	-2.321216
O	0.007515	-0.603039	-2.961555
O	-2.157692	-0.523724	-2.799014
H	-2.973761	0.304728	-0.831515
C	-2.251066	0.434386	1.19377
C	-2.359813	1.529177	2.051082
C	-2.582594	1.333019	3.413973
C	-2.70532	0.045444	3.927266
C	-2.600959	-1.050683	3.070917
C	-2.37443	-0.860789	1.711318
H	-2.278141	2.529703	1.647837
H	-2.664424	2.191287	4.071624
H	-2.883753	-0.105309	4.986147
H	-2.696614	-2.058056	3.460387
H	-2.278837	-1.718835	1.055461
H	0.360459	0.702581	0.553103
C	2.361428	-0.657128	1.113006
C	3.44817	0.204393	1.351812
C	1.636614	-1.149767	2.21185
C	3.808861	0.554574	2.645809
H	4.015963	0.594285	0.51337
C	2.010836	-0.798856	3.505228
H	0.78609	-1.793518	2.04277
C	3.091196	0.05141	3.730301
H	4.651133	1.217186	2.8085
H	1.442546	-1.186778	4.342614
H	3.369291	0.324957	4.741577
H	2.368195	4.179883	-2.824068

9. Cartesian coordinates of the TS-mx

C	1.812797	3.459857	-0.474753
C	0.758809	3.863619	-1.2934
C	1.895905	2.134233	-0.057557
C	0.935272	1.195355	-0.449025
C	-0.141644	1.633534	-1.236937
C	-0.227147	2.953712	-1.66749
C	1.006616	-0.237127	-0.06259
C	-0.222306	-0.951185	-0.205728
C	-1.486782	-0.256367	-0.644162
O	-1.118045	0.75196	-1.631876
N	0.314168	-2.114992	-1.956944
N	1.457996	-1.489143	-2.276551
C	2.230632	-1.231578	-1.164815
C	-0.566395	-1.980959	-3.050821
C	0.174107	-1.315955	-4.213812
C	1.377603	-0.683696	-3.528164
O	-1.718036	-2.336263	-3.033281
H	0.688376	4.894087	-1.622524
H	2.718627	1.815065	0.57244
H	-1.076315	3.250014	-2.271054
H	-0.482976	-0.599754	-4.703605
H	0.460517	-2.08138	-4.940151
H	1.197771	0.36785	-3.296769
H	2.317846	-0.780156	-4.069178
N	-0.39711	-2.140164	0.60906
O	0.608028	-2.637054	1.124575
O	-1.527832	-2.599909	0.705751
H	-2.110747	-0.954649	-1.199885
C	-2.33247	0.364194	0.459893
C	-1.807059	0.813177	1.673256
C	-2.631378	1.41749	2.620534
C	-3.989877	1.580634	2.365091
C	-4.52388	1.132143	1.157992
C	-3.699914	0.526784	0.215389
H	-0.753526	0.68864	1.891831
H	-2.210032	1.757469	3.559886
H	-4.630906	2.047299	3.104574
H	-5.582993	1.245419	0.955573
H	-4.11798	0.170185	-0.719861
H	1.544781	-0.446287	0.856407
H	2.566489	4.173109	-0.162986
C	3.588794	-0.635004	-1.261671
C	4.595682	-1.225876	-0.481613

C	3.922198	0.488437	-2.0331
C	5.894704	-0.729861	-0.487825
H	4.353546	-2.088346	0.129862
C	5.225169	0.979139	-2.044976
H	3.168642	1.003103	-2.611013
C	6.215768	0.372877	-1.276453
H	6.655586	-1.207504	0.118641
H	5.462023	1.846732	-2.650208
H	7.22818	0.760029	-1.28778
H	2.203151	-2.099995	-0.511881

10. Cartesian coordinates of the P-ox

C	3.640224	2.031151	2.438677
C	2.917366	0.848166	2.518104
C	1.92261	0.586483	1.575906
C	1.642795	1.496606	0.557691
C	2.386763	2.678278	0.484965
C	3.381179	2.947805	1.417244
H	4.41422	2.235152	3.169807
H	3.104642	0.114944	3.292831
C	0.529778	1.244333	-0.445863
H	2.160467	3.386627	-0.305171
H	3.950278	3.867356	1.351109
C	-0.161841	-0.122443	-0.233524
C	0.697559	-1.174682	0.508843
C	-1.424595	0.28823	0.642582
H	-0.981839	0.339343	1.640574
C	-2.601852	-0.660909	0.755794
C	-3.377959	-1.097962	-0.327304
C	-2.942762	-1.109576	2.03838
C	-4.458287	-1.951765	-0.124957
H	-3.149263	-0.790294	-1.338368
C	-4.023099	-1.963632	2.241383
H	-2.355076	-0.779085	2.888106
C	-4.786517	-2.386036	1.157115
H	-5.041964	-2.281534	-0.976645
H	-4.266479	-2.295171	3.244285
H	-5.62927	-3.051007	1.307912
C	-0.841925	3.18718	-1.246237
C	-2.351476	3.409804	-1.160584
H	-2.557965	4.214384	-0.448028

H	-2.747419	3.688798	-2.135392
C	-2.848016	2.052756	-0.646422
H	-3.78793	2.102985	-0.098415
H	-2.953488	1.365012	-1.489889
O	1.200948	-0.576357	1.722173
O	-0.025457	3.727983	-1.963954
N	-0.558888	2.214023	-0.322335
N	-1.754524	1.676963	0.285631
N	-0.632891	-0.70371	-1.555365
O	-0.743595	-1.915849	-1.620203
H	0.914894	1.340855	-1.463331
O	-0.95041	0.076145	-2.44565
C	1.818857	-1.862266	-0.255743
C	2.617259	-1.238223	-1.218663
C	2.096222	-3.191526	0.081536
C	3.663768	-1.9286	-1.827491
H	2.440886	-0.211257	-1.508655
C	3.141509	-3.881474	-0.522198
H	1.48153	-3.690153	0.823296
C	3.930161	-3.249706	-1.481565
H	4.2696	-1.42857	-2.574423
H	3.335671	-4.91254	-0.249315
H	4.743031	-3.785031	-1.958882
H	0.021392	-1.949072	0.86812

11. Cartesian coordinates of the P-on

C	1.500542	2.923775	2.982728
C	1.33317	1.552864	2.830501
C	0.853881	1.0504	1.62139
C	0.537973	1.903906	0.565199
C	0.72664	3.280364	0.727886
C	1.20423	3.791058	1.929824
H	1.874264	3.315593	3.921972
H	1.571012	0.856387	3.625022
C	-0.050682	1.360627	-0.725576
H	0.463477	3.944724	-0.087699
H	1.342646	4.859305	2.045939
C	-0.062919	-0.193241	-0.796402
C	0.879238	-0.888109	0.221272
C	-1.607729	-0.595562	-0.66561
C	-2.163377	2.797074	-1.127825

C	-3.617972	2.454083	-0.783217
H	-3.857379	2.947734	0.163732
H	-4.300703	2.826734	-1.545693
C	-3.607584	0.924819	-0.6441
H	-4.32447	0.533776	0.076377
H	-3.790955	0.455349	-1.622653
O	0.674906	-0.30715	1.521452
O	-1.706954	3.849432	-1.530401
N	-1.46493	1.661269	-0.85751
N	-2.227899	0.647564	-0.190402
N	0.358977	-0.69037	-2.195856
O	0.32059	-1.902702	-2.343103
H	0.464638	1.773183	-1.591559
O	0.680645	0.109908	-3.053
C	2.357793	-0.963615	-0.130425
C	3.093672	0.09207	-0.680318
C	3.023451	-2.158356	0.167028
C	4.45913	-0.047239	-0.920221
H	2.618257	1.031612	-0.92565
C	4.38661	-2.298239	-0.070153
H	2.463668	-2.986794	0.587601
C	5.109326	-1.239564	-0.615705
H	5.012466	0.780095	-1.349405
H	4.881767	-3.233486	0.165001
H	6.171209	-1.345072	-0.806802
H	0.51956	-1.907559	0.339037
C	-1.968955	-1.78512	0.197278
C	-2.195484	-1.646247	1.570743
C	-2.100085	-3.048103	-0.390361
C	-2.544483	-2.753567	2.339311
H	-2.097087	-0.669543	2.02476
C	-2.44139	-4.155356	0.381847
H	-1.923133	-3.163665	-1.453362
C	-2.665756	-4.010161	1.749156
H	-2.720318	-2.633928	3.402496
H	-2.538373	-5.128374	-0.086248
H	-2.93743	-4.870411	2.350651
H	-1.945081	-0.802176	-1.692228

12. Cartesian coordinates of the P-mn

C	2.438953	3.711122	0.152883

C	1.371782	4.56379	0.431319
C	2.209843	2.346454	-0.004819
C	0.923027	1.82606	0.118665
C	-0.144782	2.698247	0.386153
C	0.078588	4.064449	0.541954
C	0.522019	0.386305	0.013954
C	-0.797969	0.289198	-0.780479
C	-1.9264	1.020594	-0.019703
O	-1.431275	2.253001	0.553992
N	-0.885895	-1.09602	-1.03804
N	0.370107	-1.792314	-0.760846
C	1.392206	-0.730475	-0.604319
C	-1.668885	-1.757644	-1.956032
C	-0.935001	-3.059616	-2.258416
C	0.518563	-2.722445	-1.900456
O	-2.721528	-1.346062	-2.394461
H	1.543692	5.627122	0.553469
H	3.038271	1.679741	-0.208201
H	-0.767119	4.710493	0.741287
H	1.7727	-0.402786	-1.579308
H	-1.085322	-3.34672	-3.297722
H	-1.339738	-3.847135	-1.61468
H	1.010221	-2.229394	-2.749941
H	1.107943	-3.585897	-1.5928
N	-0.618754	1.03446	-2.199862
O	0.069792	0.461274	-3.028
O	-1.168973	2.103137	-2.358618
H	-2.693799	1.307754	-0.738439
C	-2.555896	0.180276	1.077957
C	-2.155443	0.302739	2.410088
C	-2.753368	-0.477306	3.398836
C	-3.759967	-1.379502	3.066551
C	-4.172283	-1.494411	1.739809
C	-3.577686	-0.716734	0.750803
H	-1.399787	1.029897	2.678855
H	-2.438044	-0.369206	4.43061
H	-4.228862	-1.981149	3.837076
H	-4.965548	-2.184254	1.474524
H	-3.900156	-0.808748	-0.280252
H	0.246496	0.03142	1.015752
C	2.546777	-1.216061	0.248948
C	3.862134	-1.03087	-0.182983
C	2.320501	-1.862193	1.469019
C	4.935056	-1.460369	0.59678
H	4.049152	-0.552333	-1.139172

C	3.390169	-2.292728	2.24762
H	1.30266	-2.045638	1.792195
C	4.700799	-2.089424	1.816131
H	5.95019	-1.309099	0.247515
H	3.201542	-2.79247	3.1912
H	5.532749	-2.42678	2.42385
H	3.443981	4.104771	0.060542

13. Cartesian coordinates of the P-mx

C	-1.435838	4.082999	-0.701254
C	-0.483333	4.686156	0.119901
C	-1.366223	2.71455	-0.942897
C	-0.355181	1.938192	-0.374733
C	0.605677	2.561126	0.437527
C	0.533214	3.931345	0.691059
C	-0.121008	0.482409	-0.640306
C	0.514125	-0.242064	0.564579
C	1.838507	0.47332	0.955148
O	1.65867	1.901342	1.009616
N	0.546985	-1.567847	0.100505
N	-0.381438	-1.798601	-1.013256
C	-1.142386	-0.519829	-1.23565
C	0.816728	-2.726255	0.798037
C	0.046486	-3.826456	0.078537
C	-1.066641	-3.054105	-0.640989
O	1.540382	-2.803995	1.76695
H	-0.532278	5.750594	0.319311
H	-2.107173	2.24102	-1.57574
H	1.281032	4.377232	1.334797
H	-0.312676	-4.564334	0.793958
H	0.721929	-4.319293	-0.62837
H	-1.906798	-2.882265	0.040439
H	-1.428384	-3.553622	-1.540211
N	-0.430803	-0.203608	1.867244
O	-1.094931	-1.194117	2.105065
O	-0.428321	0.819545	2.526943
H	2.099843	0.182194	1.97296
C	3.000653	0.134916	0.032634
C	3.340748	0.96474	-1.038894
C	4.416893	0.643737	-1.864506
C	5.169157	-0.501974	-1.621289

C	4.84376	-1.323553	-0.543515
C	3.768814	-1.006731	0.281612
H	2.786643	1.87852	-1.213961
H	4.672314	1.297966	-2.690511
H	6.009978	-0.747576	-2.260203
H	5.432443	-2.210671	-0.338592
H	3.514924	-1.651533	1.114815
H	0.705066	0.431865	-1.36283
H	-2.227813	4.672033	-1.147606
H	-1.137011	-0.374685	-2.319295
C	-2.614918	-0.498971	-0.82856
C	-3.507245	-1.156037	-1.689335
C	-3.142896	0.141468	0.296574
C	-4.871199	-1.205305	-1.422344
H	-3.125622	-1.633592	-2.586734
C	-4.511142	0.10303	0.561733
H	-2.512036	0.706039	0.966848
C	-5.378747	-0.575632	-0.288002
H	-5.536098	-1.724664	-2.10329
H	-4.894548	0.610836	1.43922
H	-6.441369	-0.604318	-0.075436